

# MECHANICAL PROPERTIES OF MATERIALS

David Roylance

2008



# Contents

<b>1 Uniaxial Mechanical Response</b>	<b>5</b>
1.1 Tensile Strength and Tensile Stress . . . . .	5
1.2 Stiffness in Tension - Young's Modulus . . . . .	8
1.3 The Poisson Effect . . . . .	12
1.4 Shearing Stresses and Strains . . . . .	13
1.5 Stress-Strain Curves . . . . .	16
1.6 Problems . . . . .	23
<b>2 Thermodynamics of Mechanical Response</b>	<b>25</b>
2.1 Enthalpic Response . . . . .	25
2.2 Entropic Response . . . . .	32
2.3 Viscoelasticity . . . . .	37
2.4 Problems . . . . .	41
<b>3 Composites</b>	<b>43</b>
3.1 Materials . . . . .	43
3.2 Stiffness . . . . .	44
3.3 Strength . . . . .	47
3.4 Problems . . . . .	48
<b>4 General Concepts of Stress and Strain</b>	<b>51</b>
4.1 Kinematics: the Strain–Displacement Relations . . . . .	51
4.2 Equilibrium: the Stress Relations . . . . .	55
4.3 Transformation of Stresses and Strains . . . . .	59
4.4 Constitutive Relations . . . . .	71
4.5 Problems . . . . .	78
<b>5 Yield and Plastic Flow</b>	<b>79</b>
5.1 Multiaxial Stress States . . . . .	80
5.2 Effect of Hydrostatic Pressure . . . . .	84
5.3 Effect of Rate and Temperature . . . . .	86
5.4 Continuum Plasticity . . . . .	88
5.5 The Dislocation Basis of Yield and Creep . . . . .	89
5.6 Kinetics of Creep in Crystalline Materials . . . . .	100
5.7 Problems . . . . .	102

<b>6 Fracture</b>	<b>105</b>
6.1 Atomistics of Creep Rupture . . . . .	105
6.2 Fracture Mechanics - the Energy-Balance Approach . . . . .	106
6.3 The Stress Intensity Approach . . . . .	112
6.4 Fatigue . . . . .	121
6.5 Problems . . . . .	128

# Chapter 1

## Uniaxial Mechanical Response

This chapter is intended as a review of certain fundamental aspects of mechanics of materials, using the material's response to unidirectional stress to provide an overview of mechanical properties without addressing the complexities of multidirectional stress states. Most of the chapter will restrict itself to small-strain behavior, although the last section on stress-strain curves will preview material response to nonlinear, yield and fracture behavior as well.

### 1.1 Tensile Strength and Tensile Stress

Perhaps the most natural test of a material's mechanical properties is the *tension test*, in which a strip or cylinder of the material, having length  $L$  and cross-sectional area  $A$ , is anchored at one end and subjected to an axial load  $P$  – a load acting along the specimen's long axis – at the other. (See Fig. 1.1). As the load is increased gradually, the axial deflection  $\delta$  of the loaded end will increase also. Eventually the test specimen breaks or does something else catastrophic, often fracturing suddenly into two or more pieces. (Materials can fail mechanically in many different ways; for instance, recall how blackboard chalk, a piece of fresh wood, and Silly Putty break.) As engineers, we naturally want to understand such matters as how  $\delta$  is related to  $P$ , and what ultimate fracture load we might expect in a specimen of different size than the original one. As materials technologists, we wish to understand how these relationships are influenced by the constitution and microstructure of the material.

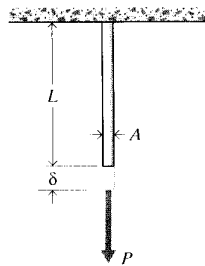


Figure 1.1: The tension test.

One of the pivotal historical developments in our understanding of material mechanical properties was the realization that the strength of a uniaxially loaded specimen is related to the magnitude of its *cross-sectional area*. This notion is reasonable when one considers the strength to arise from

the number of chemical bonds connecting one cross section with the one adjacent to it as depicted in Fig. 1.2, where each bond is visualized as a spring with a certain stiffness and strength. Obviously, the number of such bonds will increase proportionally with the section's area<sup>1</sup>. The axial strength of a piece of blackboard chalk will therefore increase as the *square* of its diameter. In contrast, increasing the *length* of the chalk will not make it stronger (in fact it will likely become weaker, since the longer specimen will be statistically more likely to contain a strength-reducing flaw.)

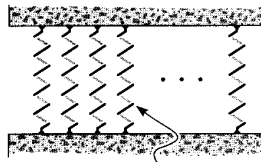


Figure 1.2: Interplanar bonds (surface density approximately  $10^{19} \text{ m}^{-2}$ ).

When reporting the strength of materials loaded in tension, it is customary to account for the effect of area by dividing the breaking load by the cross-sectional area:

$$\boxed{\sigma_f = \frac{P_f}{A_0}} \quad (1.1)$$

where  $\sigma_f$  is the *ultimate tensile stress*, often abbreviated as UTS,  $P_f$  is the load at fracture, and  $A_0$  is the original cross-sectional area. (Some materials exhibit substantial reductions in cross-sectional area as they are stretched, and using the original rather than final area gives the so-call *engineering* strength.) The units of stress are obviously load per unit area,  $\text{N/m}^2$  (also called Pascals, or Pa) in the SI system and  $\text{lb/in}^2$  (or psi) in units still used commonly in the United States.

### Example 1.1

In many design problems, the loads to be applied to the structure are known at the outset, and we wish to compute how much material will be needed to support them. As a very simple case, let's say we wish to use a steel rod, circular in cross-sectional shape as shown in Fig. 1.3, to support a load of 10,000 lb. What should the rod diameter be?

Directly from Eqn. 1.1, the area  $A_0$  that will be just on the verge of fracture at a given load  $P_f$  is

$$A_0 = \frac{P_f}{\sigma_f}$$

All we need do is look up the value of  $\sigma_f$  for the material, and substitute it along with the value of 10,000 lb for  $P_f$ , and the problem is solved.

A number of materials properties are listed in the *Materials Properties*<sup>2</sup> module, where we find the UTS of carbon steel to be 1200 MPa. We also note that these properties vary widely for given materials depending on their composition and processing, so the 1200 MPa value is only a preliminary design estimate. In light of that uncertainty, and many other potential ones, it is common to include a “factor of safety” in the

<sup>1</sup>The surface density of bonds  $N_S$  can be computed from the material's density  $\rho$ , atomic weight  $W_a$  and Avogadro's number  $N_A$  as  $N_S = (\rho N_A / W_a)^{2/3}$ . Illustrating for the case of iron (Fe):

$$N_S = \left( \frac{7.86 \frac{\text{g}}{\text{cm}^3} \cdot 6.023 \times 10^{23} \frac{\text{atoms}}{\text{mol}}}{55.85 \frac{\text{g}}{\text{mol}}} \right)^{\frac{2}{3}} = 1.9 \times 10^{15} \frac{\text{atoms}}{\text{cm}^2}$$

$N_S \approx 10^{15} \frac{\text{atom}}{\text{cm}^2}$  is true for many materials.

<sup>2</sup><http://web.mit.edu/course/3/3.11/www/modules/props.html>

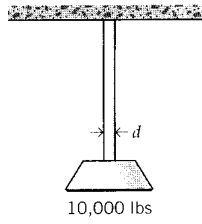


Figure 1.3: Steel rod supporting a 10,000 lb weight.

design. Selection of an appropriate factor is an often-difficult choice, especially in cases where weight or cost restrictions place a great penalty on using excess material. But in this case steel is relatively inexpensive and we don't have any special weight limitations, so we'll use a conservative 50% safety factor and assume the ultimate tensile strength is  $1200/2 = 600$  MPa.

We now have only to adjust the units before solving for area. Engineers must be very comfortable with units conversions, especially given the mix of SI and older traditional units used today. Eventually, we'll likely be ordering steel rod using inches rather than meters, so we'll convert the MPa to psi rather than convert the pounds to Newtons. Also using  $A = \pi d^2/4$  to compute the diameter rather than the area, we have

$$d = \sqrt{\frac{4A}{\pi}} = \sqrt{\frac{4P_f}{\pi\sigma_f}} = \left[ \frac{4 \times 10000(\text{lb})}{\pi \times 600 \times 10^6(\text{N/m}^2) \times 1.449 \times 10^{-4} \left( \frac{\text{lb/in}^2}{\text{N/m}^2} \right)} \right]^{\frac{1}{2}} = 0.38 \text{ in}$$

We probably wouldn't order rod of exactly 0.38 in, as that would be an oddball size and thus too expensive. But 3/8" (0.375 in) would likely be a standard size, and would be acceptable in light of our conservative safety factor.

---

If the specimen is loaded by an axial force  $P$  less than the breaking load  $P_f$ , the *tensile stress* is defined by analogy with Eqn. 1.1 as

$$\boxed{\sigma = \frac{P}{A_0}} \quad (1.2)$$

The tensile stress, the force per unit area acting on a plane transverse to the applied load, is a fundamental measure of the internal forces within the material. Much of Mechanics of Materials is concerned with elaborating this concept to include higher orders of dimensionality, working out methods of determining the stress for various geometries and loading conditions, and predicting what the material's response to the stress will be.

---

### Example 1.2

Many engineering applications, notably aerospace vehicles, require materials that are both strong and lightweight. One measure of this combination of properties is provided by computing how long a rod of the material can be that when suspended from its top will break under its own weight (see Fig. 1.4). Here the stress is not uniform along the rod: the material at the very top bears the weight of the entire rod, but that at the bottom carries no load at all.

To compute the stress as a function of position, let  $y$  denote the distance from the bottom of the rod and let the weight density of the material, for instance in  $\text{N/m}^3$ , be denoted by  $\gamma$ . (The weight density is related to the mass density  $\rho$  [ $\text{kg/m}^3$ ] by  $\gamma = \rho g$ , where  $g = 9.8 \text{ m/s}^2$  is the acceleration due to gravity.) The weight supported by the cross-section at  $y$  is just the weight density  $\gamma$  times the volume of material  $V$  below  $y$ :

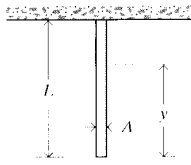


Figure 1.4: Circular rod suspended from the top and bearing its own weight.

$$W(y) = \gamma V = \gamma A y$$

The tensile stress is then given as a function of  $y$  by Eqn. 1.2 as

$$\sigma(y) = \frac{W(y)}{A} = \gamma y$$

Note that the area cancels, leaving only the material density  $\gamma$  as a design variable.

The length of rod that is just on the verge of breaking under its own weight can now be found by letting  $y = L$  (the highest stress occurs at the top), setting  $\sigma(L) = \sigma_f$ , and solving for  $L$ :

$$\sigma_f = \gamma L \Rightarrow L = \frac{\sigma_f}{\gamma}$$

In the case of steel, we find the mass density  $\rho$  in Appendix A to be  $7.85 \times 10^3 \text{ (kg/m}^3)$ ; then

$$L = \frac{\sigma_f}{\rho g} = \frac{1200 \times 10^6 \text{ (N/m}^2)}{7.85 \times 10^3 \text{ (kg/m}^3) \times 9.8 \text{ (m/s}^2)} = 15.6 \text{ km}$$

This would be a long rod indeed; the purpose of such a calculation is not so much to design superlong rods as to provide a vivid way of comparing material.

---

## 1.2 Stiffness in Tension - Young's Modulus

It is important to distinguish *stiffness*, which is a measure of the *load* needed to induce a given *deformation* in the material, from the *strength*, which usually refers to the material's resistance to failure by fracture or excessive deformation. The stiffness is usually measured by applying relatively small loads, well short of fracture, and measuring the resulting deformation. Since the deformations in most materials are very small for these loading conditions, the experimental problem is largely one of measuring small changes in length accurately.

Hooke<sup>3</sup> made a number of such measurements on long wires under various loads, and observed that to a good approximation the load  $P$  and its resulting deformation  $\delta$  were related linearly as long as the loads were sufficiently small. This relation, generally known as *Hooke's Law*, can be written algebraically as

$$P = k\delta \quad (1.3)$$

where  $k$  is a constant of proportionality called the *stiffness* and having units of lb/in or N/m. The stiffness as defined by  $k$  is not a function of the material alone, but is also influenced by the

<sup>3</sup>Robert Hooke (1635–1703) was a contemporary and rival of Isaac Newton. In the style of his time, Hooke originally published his observation as a Latin anagram *ceiiinosssttuu* from *ut tensio, sic vis* - As the extension, so the force.

specimen shape. A wire gives much more deflection for a given load if coiled up like a watch spring, for instance.

A useful way to adjust the stiffness so as to be a purely materials property is to normalize the load by the cross-sectional area; i.e. to use the tensile stress rather than the load. Further, the deformation  $\delta$  can be normalized by noting that an applied load stretches all parts of the wire uniformly, so that a reasonable measure of “stretching” is the deformation per unit length:

$$\epsilon = \frac{\delta}{L_0} \quad (1.4)$$

Here  $L_0$  is the original length and  $\epsilon$  is a dimensionless measure of stretching called the *strain*. Using these more general measures of load per unit area and displacement per unit length<sup>4</sup>, Hooke's Law becomes:

$$\frac{P}{A_0} = E \frac{\delta}{L_0} \quad (1.5)$$

or

$$\sigma = E\epsilon \quad (1.6)$$

The constant of proportionality  $E$ , called *Young's modulus*<sup>5</sup> or the *modulus of elasticity*<sup>6</sup>, is one of the most important mechanical descriptors of a material. It has the same units as stress, Pa or psi. As shown in Fig. 1.5, Hooke's law can refer to either of Eqns. 1.3 or 1.6.

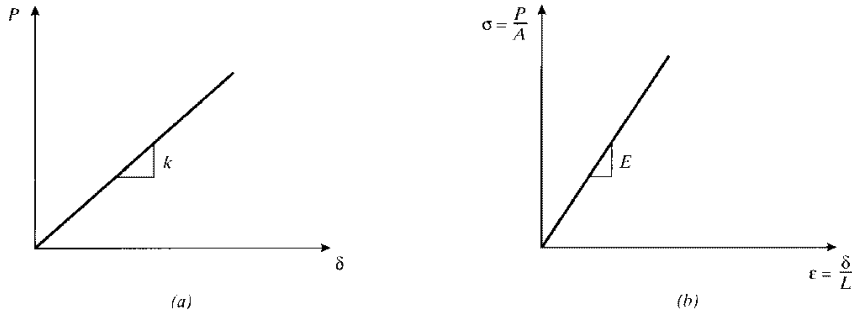


Figure 1.5: Hooke's law in terms of (a) load-displacement and (b) stress-strain.

The Hookean stiffness  $k$  is now recognizable as being related to the Young's modulus  $E$  and the specimen geometry as

$$k = \frac{AE}{L} \quad (1.7)$$

---

<sup>4</sup>It was apparently the Swiss mathematician Jakob Bernoulli (1655-1705) who first realized the correctness of this form, published in the final paper of his life.

<sup>5</sup>After the English physicist Thomas Young (1773–1829), who also made notable contributions to the understanding of the interference of light as well as being a noted physician and Egyptologist.

<sup>6</sup>*Elasticity* is a form of materials response that refers to immediate and time-independent deformation upon loading, and complete and instant recovery of the original geometry upon removal of the load. A material is elastic or it is not, one material cannot be “more elastic” than another, and a material can be elastic without obeying the linear relation given by Hooke's law.

where here the 0 subscript is dropped from the area  $A$ ; it will be assumed from here on (unless stated otherwise) that the change in area during loading can be neglected. Another useful relation is obtained by solving Eqn. 1.5 for the deflection in terms of the applied load as

$$\boxed{\delta = \frac{PL}{AE}} \quad (1.8)$$

Note that the stress  $\sigma = P/A$  developed in a tensile specimen subjected to a fixed load is independent of the material properties, while the deflection depends on the material property  $E$ . Hence the stress  $\sigma$  in a tensile specimen at a given load is the same whether it's made of steel or polyethylene, but the strain  $\epsilon$  would be different: the polyethylene will exhibit much larger strain and deformation, since its modulus is two orders of magnitude less than steel's.

### Example 1.3

In Example 1.1, we found that a steel rod 0.38" in diameter would safely bear a load of 10,000 lb. Now let's assume we have been given a second design goal, namely that the geometry requires that we use a rod 15 ft in length but that the loaded end cannot be allowed to deflect downward more than 0.3" when the load is applied. Replacing  $A$  in Eqn. 1.8 by  $\pi d^2/4$  and solving for  $d$ , the diameter for a given  $\delta$  is

$$d = 2\sqrt{\frac{PL}{\pi\delta E}}$$

From Appendix A, the modulus of carbon steel is 210 GPa; using this along with the given load, length, and deflection, the required diameter is

$$d = 2\sqrt{\frac{10^4(\text{lb}) \times 15(\text{ft}) \times 12(\text{in}/\text{ft})}{\pi \times 0.3(\text{in}) \times 210 \times 10^9(\text{N}/\text{m}^2) \times 1.449 \times 10^{-4} \left(\frac{\text{lb/in}^2}{\text{N/m}^2}\right)}} = 0.5 \text{ in}$$

This diameter is larger than the 0.38" computed earlier; therefore a larger rod must be used if the deflection as well as the strength goals are to be met. Clearly, using the larger rod makes the tensile stress in the material less and thus lowers the likelihood of fracture. This is an example of a *stiffness-critical* design, in which deflection rather than fracture is the governing constraint. As it happens, many structures throughout the modern era have been designed for stiffness rather than strength, and thus wound up being "overdesigned" with respect to fracture. This has undoubtedly lessened the incidence of fracture-related catastrophes, which will be addressed in the chapters on fracture.

### Example 1.4

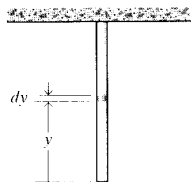


Figure 1.6: Deformation of a column under its own weight.

When very long columns are suspended from the top, as in a cable hanging down the hole of an oil well, the deflection due to the weight of the material itself can be important. The solution for the total deflection

is a minor extension of Eqn. 1.8, in that now we must consider the increasing weight borne by each cross section as the distance from the bottom of the cable increases. As shown in Fig. 1.6, the total elongation of a column of length  $L$ , cross-sectional area  $A$ , and weight density  $\gamma$  due to its own weight can be found by considering the incremental deformation  $d\delta$  of a slice  $dy$  a distance  $y$  from the bottom. The weight borne by this slice is  $\gamma Ay$ , so

$$d\delta = \frac{(\gamma Ay) dy}{AE}$$

$$\delta = \int_0^L d\delta = \frac{\gamma}{E} \left. \frac{y^2}{2} \right|_0^L = \frac{\gamma L^2}{2E}$$

Note that  $\delta$  is independent of the area  $A$ , so that finding a fatter cable won't help to reduce the deformation; the critical parameter is the *specific modulus*  $E/\gamma$ . Since the total weight is  $W = \gamma AL$ , the result can also be written

$$\delta = \frac{WL}{2AE}$$

The deformation is the same as in a bar being pulled with a tensile force equal to half its weight; this is just the average force experienced by cross sections along the column.

In Example 2, we computed the length of a steel rod that would be just on the verge of breaking under its own weight if suspended from its top; we obtained  $L = 15.6\text{km}$ . Were such a rod to be constructed, our analysis predicts the deformation at the bottom would be

$$\delta = \frac{\gamma L^2}{2E} = \frac{7.85 \times 10^3(\text{kg/m}^3) \times 9.8(\text{m/s}^2) \times [15.6 \times 10^3(\text{m})]^2}{2 \times 210 \times 10^9(\text{N/m}^2)} = 44.6 \text{ m}$$

However, this analysis assumes Hooke's law holds over the entire range of stresses from zero to fracture. This is not true for many materials, including carbon steel, and later chapters will address materials response at high stresses.

A material that obeys Hooke's Law (Eqn. 1.6) is called *Hookean*. Such a material is *elastic* according to the description of elasticity given earlier (immediate response, full recovery), and it is also *linear* in its relation between stress and strain (or equivalently, force and deformation). Therefore a Hookean material is *linear elastic*, and materials engineers use these descriptors interchangeably. It is important to keep in mind that not all elastic materials are linear (rubber is elastic but nonlinear), and not all linear materials are elastic (viscoelastic materials can be linear in the mathematical sense, but do not respond immediately and are thus not elastic).

The linear proportionality between stress and strain given by Hooke's law is not nearly as general as, say, Einstein's general theory of relativity, or even Newton's law of gravitation. It's really just an approximation that is observed to be reasonably valid for many materials as long the applied stresses are not too large. As the stresses are increased, eventually more complicated material response will be observed. Some of these effects will be outlined in the later section on stress-strain curves, which introduces the experimental measurement of the strain response of materials over a range of stresses up to and including fracture.

If we were to push on the specimen rather than pulling on it, the loading would be described as *compressive* rather than tensile. In the range of relatively low loads, Hooke's law holds for this case as well. By convention, compressive stresses and strains are negative, so the expression  $\sigma = E\epsilon$  holds for both tension and compression.

### 1.3 The Poisson Effect

A positive (tensile) strain in one direction will also contribute a negative (compressive) strain in the other direction, just as stretching a rubber band to make it longer in one direction makes it thinner in the other directions (see Fig. 1.7). This lateral contraction accompanying a longitudinal extension is called the *Poisson effect*,<sup>7</sup> and the *Poisson's ratio* is a material property defined as

$$\nu = \frac{-\epsilon_{\text{lateral}}}{\epsilon_{\text{longitudinal}}} \quad (1.9)$$

where the minus sign accounts for the sign change between the lateral and longitudinal strains. The stress-strain, or “constitutive,” law of the material must be extended to include these effects, since the strain in any given direction is influenced by not only the stress in that direction, but also by the Poisson strains contributed by the stresses in the other two directions.

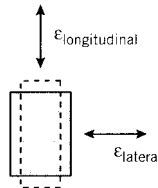


Figure 1.7: The Poisson effect.

A material subjected only to a stress  $\sigma_x$  in the  $x$  direction will experience a strain in that direction given by  $\epsilon_x = \sigma_x/E$ . A stress  $\sigma_y$  acting alone in the  $y$  direction will induce an  $x$ -direction strain given from the definition of Poisson's ratio of  $\epsilon_x = -\nu\epsilon_y = -\nu(\sigma_y/E)$ . If the material is subjected to both stresses  $\sigma_x$  and  $\sigma_y$  at once, the effects can be superimposed (since the governing equations are *linear*) to give:

$$\epsilon_x = \frac{\sigma_x}{E} - \frac{\nu\sigma_y}{E} = \frac{1}{E} (\sigma_x - \nu\sigma_y) \quad (1.10)$$

Similarly for a strain in the  $y$  direction:

$$\epsilon_y = \frac{\sigma_y}{E} - \frac{\nu\sigma_x}{E} = \frac{1}{E} (\sigma_y - \nu\sigma_x) \quad (1.11)$$

The material is in a state of *plane stress* if no stress components act in the third dimension (the  $z$  direction, here). This occurs commonly in thin sheets loaded in their plane. The  $z$  components of stress vanish at the surfaces because there are no forces acting externally in that direction to balance them, and these components do not have sufficient specimen distance in the thin through-thickness dimension to build up to appreciable levels. However, a state of plane stress is *not* a state of plane strain. The sheet will experience a strain in the  $z$  direction equal to the Poisson strain contributed by the  $x$  and  $y$  stresses:

$$\epsilon_z = -\frac{\nu}{E} (\sigma_x + \sigma_y) \quad (1.12)$$

---

<sup>7</sup>After the French mathematician Simeon Denis Poisson, (1781–1840).

The Poisson's ratio is a dimensionless parameter that provides a good deal of insight into the nature of the material. The major classes of engineered structural materials fall neatly into order when ranked by Poisson's ratio:

Material Class	Poisson's Ratio $\nu$
Ceramics	0.2
Metals	0.3
Plastics	0.4
Rubber	0.5

(The values here are approximate.) It will be noted that the most brittle materials have the lowest Poisson's ratio, and that the materials appear to become generally more flexible as the Poisson's ratio increases. The ability of a material to contract laterally as it is extended longitudinally is related directly to its molecular mobility, with rubber being liquid-like and ceramics being very tightly bonded.

The Poisson's ratio is also related to the compressibility of the material. The *bulk modulus*  $K$ , also called the modulus of compressibility, is the ratio of the hydrostatic pressure  $p$  needed for a unit relative decrease in volume  $\Delta V/V$ :

$$K = \frac{-p}{\Delta V/V} \quad (1.13)$$

where the minus sign indicates that a compressive pressure (traditionally considered positive) produces a negative volume change. It can be shown that for isotropic materials the bulk modulus is related to the elastic modulus and the Poisson's ratio as

$$K = \frac{E}{3(1 - 2\nu)} \quad (1.14)$$

This expression becomes unbounded as  $\nu$  approaches 0.5, so that rubber is essentially incompressible. Further,  $\nu$  cannot be larger than 0.5, since that would mean volume would *increase* on the application of positive pressure. A ceramic at the lower end of Poisson's ratios, by contrast, is so tightly bonded that it is unable to rearrange itself to "fill the holes" that are created when a specimen is pulled in tension; it has no choice but to suffer a volume increase. Paradoxically, the tightly bonded ceramics have lower bulk moduli than the very mobile elastomers.

## 1.4 Shearing Stresses and Strains

Not all deformation is elongational or compressive, and we need to extend our concept of strain to include "shearing," or "distortional," effects. To illustrate the nature of shearing distortions, first consider a square grid inscribed on a tensile specimen as depicted in Fig. 1.8(a). Upon uniaxial loading, the grid would be deformed so as to increase the length of the lines in the tensile loading direction and contract the lines perpendicular to the loading direction. However, the lines remain perpendicular to one another. These are termed *normal* strains, since planes normal to the loading direction are moving apart.

Now consider the case illustrated in Fig. 1.8(b), in which the load  $P$  is applied *transversely* to the specimen. Here the horizontal lines tend to *slide* relative to one another, with line lengths of the originally square grid remaining unchanged. The vertical lines tilt to accommodate this motion, so

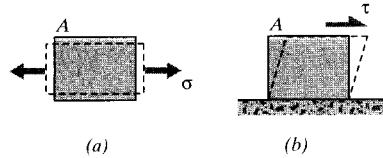


Figure 1.8: (a) Normal and (b) shearing deformations.

the originally right angles between the lines are distorted. Such a loading is termed *direct shear*. Analogously to our definition of normal stress as force per unit area, or  $\sigma = P/A$ , we write the *shear stress*  $\tau$  as

$$\tau = \frac{P}{A}$$

This expression is identical to the expression for normal stress, but the different symbol  $\tau$  reminds us that the loading is transverse rather than extensional.

### Example 1.5

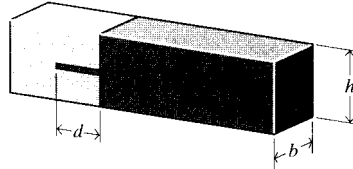


Figure 1.9: Tongue-and-groove adhesive joint.

Two timbers, of cross-sectional dimension  $b \times h$ , are to be glued together using a tongue-and-groove joint as shown in Fig. 1.9, and we wish to estimate the depth  $d$  of the glue joint so as to make the joint approximately as strong as the timber itself.

The axial load  $P$  on the timber acts to shear the glue joint, and the shear stress in the joint is just the load divided by the total glue area:

$$\tau = \frac{P}{2bd}$$

If the bond fails when  $\tau$  reaches a maximum value  $\tau_f$ , the load at failure will be  $P_f = (2bd)\tau_f$ . The load needed to fracture the timber in tension is  $P_f = bh\sigma_f$ , where  $\sigma_f$  is the ultimate tensile strength of the timber. Hence if the glue joint and the timber are to be equally strong we have

$$(2bd)\tau_f = bh\sigma_f \rightarrow d = \frac{h\sigma_f}{2\tau_f}$$

Normal stresses act to pull parallel planes within the material apart or push them closer together, while shear stresses act to slide planes along one another. Normal stresses promote crack formation and growth, while shear stresses underlie yield and plastic slip. The shear stress can be depicted on the stress square as shown in Fig. 1.10(a); it is traditional to use a half-arrowhead to distinguish

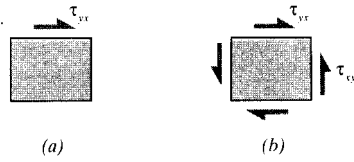


Figure 1.10: Shear stress.

shear stress from normal stress. The  $yx$  subscript indicates the stress is on the  $y$  plane in the  $x$  direction.

The  $\tau_{yx}$  arrow on the  $+y$  plane must be accompanied by one in the opposite direction on the  $-y$  plane, in order to maintain horizontal equilibrium. But these two arrows by themselves would tend to cause a clockwise rotation, and to maintain moment equilibrium we must also add two vertical arrows as shown in Fig. 1.10(b); these are labeled  $\tau_{xy}$ , since they are on  $x$  planes in the  $y$  direction. For rotational equilibrium, the magnitudes of the horizontal and vertical stresses must be equal:

$$\tau_{yx} = \tau_{xy} \quad (1.15)$$

Hence any shearing that tends to cause tangential sliding of horizontal planes is accompanied by an equal tendency to slide vertical planes as well. These stresses are positive by a sign convention of + arrows on + faces being positive. A positive state of shear stress, then, has arrows meeting at the upper right and lower left of the stress square. Conversely, arrows in a negative state of shear meet at the lower right and upper left.

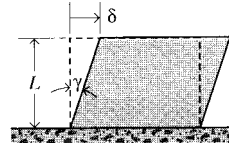


Figure 1.11: Shear strain.

The strain accompanying the shear stress  $\tau_{xy}$  is a *shear strain* denoted  $\gamma_{xy}$ . This quantity is a deformation per unit length just as was the normal strain  $\epsilon$ , but now the displacement is transverse to the length over which it is distributed (see Fig. 1.11). This is also the distortion or change in the right angle:

$$\frac{\delta}{L} = \tan \gamma \approx \gamma \quad (1.16)$$

This angular distortion is found experimentally to be linearly proportional to the shear stress at sufficiently small loads, and the shearing counterpart of Hooke's Law can be written as

$$\boxed{\tau_{xy} = G\gamma_{xy}} \quad (1.17)$$

where  $G$  is a material property called the *shear modulus*. For *isotropic* materials (properties same in all directions), there is no Poisson-type effect to consider in shear, so that the shear strain is not influenced by the presence of normal stresses. Similarly, application of a shearing stress

has no influence on the normal strains. For plane stress situations (no normal or shearing stress components in the  $z$  direction), the constitutive equations as developed so far can be written:

$$\boxed{\begin{aligned}\epsilon_x &= \frac{1}{E}(\sigma_x - \nu\sigma_y) \\ \epsilon_y &= \frac{1}{E}(\sigma_y - \nu\sigma_x) \\ \gamma_{xy} &= \frac{1}{G}\tau_{xy}\end{aligned}} \quad (1.18)$$

It will be shown later that for isotropic materials, only two of the material constants here are independent, and that

$$\boxed{G = \frac{E}{2(1 + \nu)}} \quad (1.19)$$

Hence if any two of the three properties  $E$ ,  $G$ , or  $\nu$ , are known, the other is determined.

## 1.5 Stress-Strain Curves

Stress-strain curves are an extremely important graphical measure of a material's mechanical properties, and all students of Mechanics of Materials will encounter them often. However, they are not without some subtlety, especially in the case of ductile materials that can undergo substantial geometrical change during testing. This section will provide an introductory discussion of several points needed to interpret these curves, and in doing so will also provide a preliminary overview of several aspects of a material's mechanical properties. However, this section will not attempt to survey the broad range of stress-strain curves exhibited by modern engineering materials (the atlas by Boyer cited in the References section can be consulted for this). Several of the topics mentioned here — especially yield and fracture — will appear with more detail in later chapters.

### 1.5.1 “Engineering” Stress-Strain Curves

Perhaps the most important test of a material's mechanical response is the tensile test<sup>8</sup>, in which one end of a rod or wire specimen is clamped in a loading frame and the other subjected to a controlled displacement  $\delta$  (see Fig. 1.1). A transducer connected in series with the specimen provides an electronic reading of the load  $P(\delta)$  corresponding to the displacement. Alternatively, modern servo-controlled testing machines permit using load rather than displacement as the controlled variable, in which case the displacement  $\delta(P)$  would be monitored as a function of load.

The engineering measures of stress and strain, denoted in this section as  $\sigma_e$  and  $\epsilon_e$  respectively, are determined from the measured load and deflection using the original specimen cross-sectional area  $A_0$  and length  $L_0$  as

$$\sigma_e = \frac{P}{A_0}, \quad \epsilon_e = \frac{\delta}{L_0} \quad (1.20)$$

When the stress  $\sigma_e$  is plotted against the strain  $\epsilon_e$ , an *engineering stress-strain curve* such as that shown in Fig. 1.12 is obtained.

In the early (low strain) portion of the curve, many materials obey Hooke's law to a reasonable approximation, so that stress is proportional to strain with the constant of proportionality being the modulus of elasticity or Young's modulus  $E$ :

---

<sup>8</sup>Stress-strain testing, as well as almost all experimental procedures in mechanics of materials, is detailed by standards-setting organizations, notably the American Society for Testing and Materials (ASTM). Tensile testing of metals is prescribed by ASTM Test E8, plastics by ASTM D638, and composite materials by ASTM D3039.

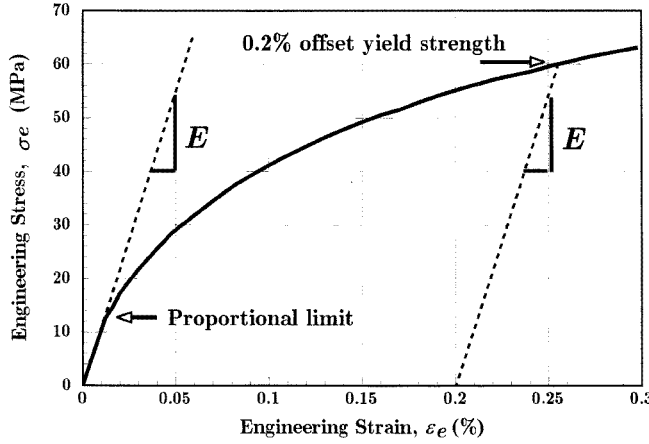


Figure 1.12: Low-strain region of the engineering stress-strain curve for annealed polycrystalline copper; this curve is typical of that of many ductile metals.

$$\sigma_e = E\epsilon_e \quad (1.21)$$

As strain is increased, many materials eventually deviate from this linear proportionality, the point of departure being termed the proportional limit. This nonlinearity is usually associated with stress-induced “plastic” flow in the specimen. Here the material is undergoing a rearrangement of its internal molecular or microscopic structure, in which atoms are being moved to new equilibrium positions. This plasticity requires a mechanism for molecular mobility, which in crystalline materials can arise from dislocation motion (discussed further in a later chapter.) Materials lacking this mobility, for instance by having internal microstructures that block dislocation motion, are usually brittle rather than ductile. The stress-strain curve for brittle materials are typically linear over their full range of strain, eventually terminating in fracture without appreciable plastic flow.

Note in Fig. 1.12 that the stress needed to increase the strain beyond the proportional limit in a ductile material continues to rise beyond the proportional limit; the material requires an ever-increasing stress to continue straining, a mechanism termed *strain hardening*.

These microstructural rearrangements associated with plastic flow are usually not reversed when the load is removed, so the proportional limit is often the same as or at least close to the material’s *elastic limit*. Elasticity is the property of complete and immediate recovery from an imposed displacement on release of the load, and the elastic limit is the value of stress at which the material experiences a permanent residual strain that is not lost on unloading. The residual strain induced by a given stress can be determined by drawing an unloading line from the highest point reached on the  $\sigma - \epsilon$  curve at that stress back to the strain axis, drawn with a slope equal to that of the initial elastic loading line. This is done because the material unloads elastically, there being no force driving the molecular structure back to its original position.

A closely related term is the yield stress, denoted  $\sigma_Y$  in this section; this is the stress needed to induce plastic deformation in the specimen. Since it is often difficult to pinpoint the exact stress at which plastic deformation begins, the yield stress is often taken to be the stress needed to induce a specified amount of permanent strain, typically 0.2%. The construction used to find this “offset yield stress” is shown in Fig. 1.12, in which a line of slope  $E$  is drawn from the strain axis at  $\epsilon_e = 0.2\%$ ; this is the unloading line that would result in the specified permanent strain. The stress at the point of intersection with the  $\sigma_e - \epsilon_e$  curve is the offset yield stress.

Figure 1.13 shows the engineering stress-strain curve for copper with an enlarged scale, now showing strains from zero up to specimen fracture. Here it appears that the rate of strain hardening<sup>9</sup> diminishes up to a point labeled UTS, for Ultimate Tensile Strength (denoted  $\sigma_f$  in this text). Beyond that point, the material appears to strain soften, so that each increment of additional strain requires a smaller stress.

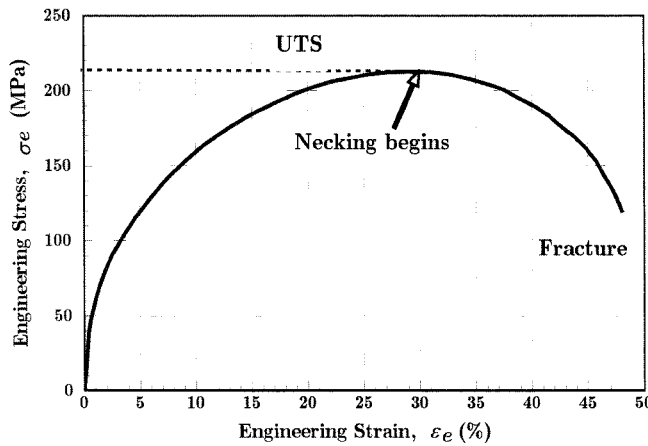


Figure 1.13: Full engineering stress-strain curve for annealed polycrystalline copper.

The apparent change from strain hardening to strain softening is an artifact of the plotting procedure, however, as is the maximum observed in the curve at the UTS. Beyond the yield point, molecular flow causes a substantial reduction in the specimen cross-sectional area  $A$ , so the true stress  $\sigma_t = P/A$  actually borne by the material is larger than the engineering stress computed from the original cross-sectional area ( $\sigma_e = P/A_0$ ). The load must equal the true stress times the actual area ( $P = \sigma_t A$ ), and as long as strain hardening can increase  $\sigma_t$  enough to compensate for the reduced area  $A$ , the load and therefore the engineering stress will continue to rise as the strain increases. Eventually, however, the decrease in area due to flow becomes larger than the increase in true stress due to strain hardening, and the load begins to fall. This is a geometrical effect, and if the true stress rather than the engineering stress were plotted no maximum would be observed in the curve.

At the UTS the differential of the load  $P$  is zero, giving an analytical relation between the true stress and the area at necking:

$$P = \sigma_t A \rightarrow dP = 0 = \sigma_t dA + Ad\sigma_t \rightarrow -\frac{dA}{A} = \frac{d\sigma_t}{\sigma_t} \quad (1.22)$$

The last expression states that the load and therefore the engineering stress will reach a maximum as a function of strain when the fractional decrease in area becomes equal to the fractional increase in true stress.

Even though the UTS is perhaps the materials property most commonly reported in tensile tests, it is not a direct measure of the material due to the influence of geometry as discussed above, and should be used with caution. The yield stress  $\sigma_Y$  is usually preferred to the UTS in designing with ductile metals, although the UTS is a valid design criterion for brittle materials that do not exhibit these flow-induced reductions in cross-sectional area.

---

<sup>9</sup>The strain hardening rate is the slope of the stress-strain curve, also called the *tangent modulus*.

The true stress is not quite uniform throughout the specimen, and there will always be some location - perhaps a nick or some other defect at the surface - where the local stress is maximum. Once the maximum in the engineering curve has been reached, the localized flow at this site cannot be compensated by further strain hardening, so the area there is reduced further. This increases the local stress even more, which accelerates the flow further. This localized and increasing flow soon leads to a “neck” in the gage length of the specimen such as that seen in Fig. 1.14.

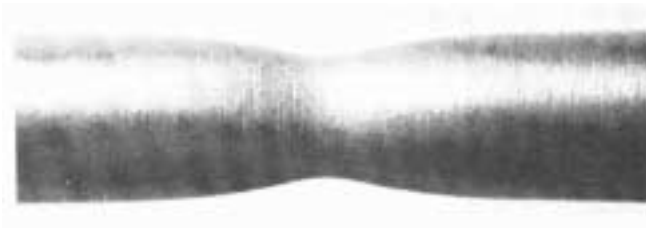


Figure 1.14: Necking in a tensile specimen.

Until the neck forms, the deformation is essentially uniform throughout the specimen, but after necking all subsequent deformation takes place in the neck. The neck becomes smaller and smaller, local true stress increasing all the time, until the specimen fails. This will be the failure mode for most ductile metals. As the neck shrinks, the nonuniform geometry there alters the uniaxial stress state to a complex one involving shear components as well as normal stresses. The specimen often fails finally with a “cup and cone” geometry as seen in Fig. 1.15, in which the outer regions fail in shear and the interior in tension. When the specimen fractures, the engineering strain at break — denoted  $\epsilon_f$  — will include the deformation in the necked region and the unnecked region together. Since the true strain in the neck is larger than that in the unnecked material, the value of  $\epsilon_f$  will depend on the fraction of the gage length that has necked. Therefore,  $\epsilon_f$  is a function of the specimen geometry as well as the material, and thus is only a crude measure of material ductility.

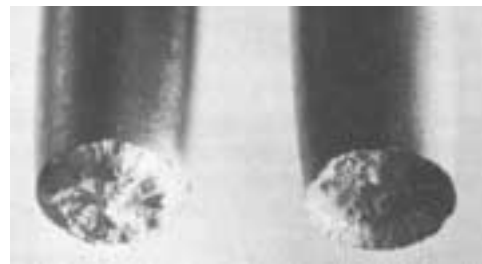


Figure 1.15: Cup-and-cone fracture in a ductile metal.

Figure 1.16 shows the engineering stress-strain curve for a semicrystalline thermoplastic. The response of this material is similar to that of copper seen in Fig. 1.13, in that it shows a proportional limit followed by a maximum in the curve at which necking takes place. (It is common to term this maximum as the yield stress in plastics, although plastic flow has actually begun at earlier strains.)

The polymer, however, differs dramatically from copper in that the neck does not continue

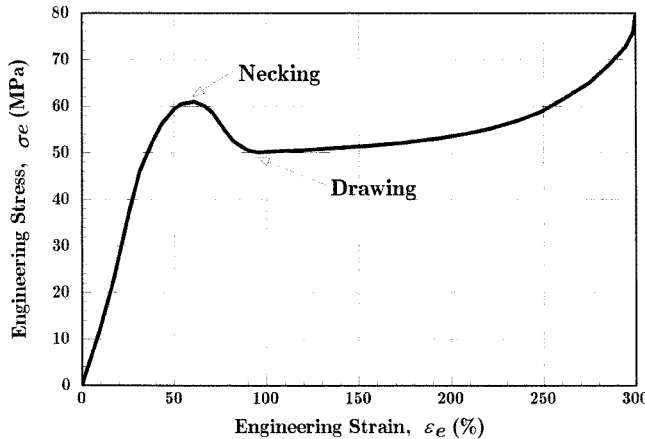


Figure 1.16: Stress-strain curve for polyamide (nylon) thermoplastic.

shrinking until the specimen fails. Rather, the material in the neck stretches only to a “natural draw ratio” which is a function of temperature and specimen processing, beyond which the material in the neck stops stretching and new material at the neck shoulders necks down. The neck then propagates until it spans the full gage length of the specimen, a process called *drawing*. This process can be observed without the need for a testing machine, by stretching a polyethylene “six-pack holder,” as seen in Fig. 1.17.



Figure 1.17: Necking and drawing in a 6-pack holder.

Not all polymers are able to sustain this drawing process. As will be discussed in the next section, it occurs when the necking process produces a strengthened microstructure whose breaking load is greater than that needed to induce necking in the untransformed material just outside the neck.

### 1.5.2 “True” Stress-Strain Curves

As discussed in the previous section, the engineering stress-strain curve must be interpreted with caution beyond the elastic limit, since the specimen dimensions experience substantial change from their original values. Using the true stress  $\sigma_t = P/A$  rather than the engineering stress  $\sigma_e = P/A_0$  can give a more direct measure of the material’s response in the plastic flow range. A measure of strain often used in conjunction with the true stress takes the increment of strain to be the incremental increase in displacement  $dL$  divided by the current length  $L$ :

$$d\epsilon_t = \frac{dL}{l} \rightarrow \epsilon_t = \int_{l_0}^L \frac{1}{L} dL = \ln \frac{L}{L_0} \quad (1.23)$$

This is called the “true” or “logarithmic” strain.

During yield and the plastic-flow regime following yield, the material flows with negligible change in volume; increases in length are offset by decreases in cross-sectional area. Prior to necking, when the strain is still uniform along the specimen length, this volume constraint can be written:

$$dV = 0 \rightarrow AL = A_0 L_0 \rightarrow \frac{L}{L_0} = \frac{A_0}{A} \quad (1.24)$$

The ratio  $L/L_0$  is the *extension ratio*, denoted as  $\lambda$ . Using these relations, it is easy to develop relations between true and engineering measures of tensile stress and strain:

$$\sigma_t = \sigma_e (1 + \epsilon_e) = \sigma_e \lambda, \quad \epsilon_t = \ln (1 + \epsilon_e) = \ln \lambda \quad (1.25)$$

These equations can be used to derive the true stress-strain curve from the engineering curve, up to the strain at which necking begins. Figure 1.18 is a replot of Fig. 1.13, with the true stress-strain curve computed by this procedure added for comparison.

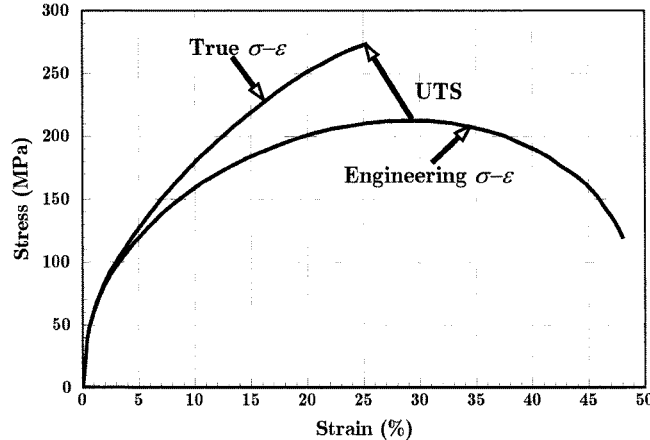


Figure 1.18: Comparison of engineering and true stress-strain curves for copper. An arrow indicates the position on the “true” curve of the UTS on the engineering curve.

Beyond necking, the strain is nonuniform in the gage length and to compute the true stress-strain curve for greater engineering strains would not be meaningful. However, a complete true stress-strain curve could be drawn if the neck area were monitored throughout the tensile test, since for logarithmic strain we have

$$\frac{L}{L_0} = \frac{A}{A_0} \rightarrow \epsilon_t = \ln \frac{L}{L_0} = \ln \frac{A}{A_0} \quad (1.26)$$

Ductile metals often have true stress-strain relations that can be described by a simple power-law relation of the form:

$$\sigma_t = A \epsilon_t^n \rightarrow \log \sigma_t = \log A + n \log \epsilon_t \quad (1.27)$$

Figure 1.19 is a log-log plot of the true stress-strain data<sup>10</sup> for copper from Fig. 1.18 that demonstrates this relation. Here the parameter  $n = 0.474$  is called the *strain hardening parameter*, useful as a measure of the resistance to necking. Ductile metals at room temperature usually exhibit values of  $n$  from 0.02 to 0.5.

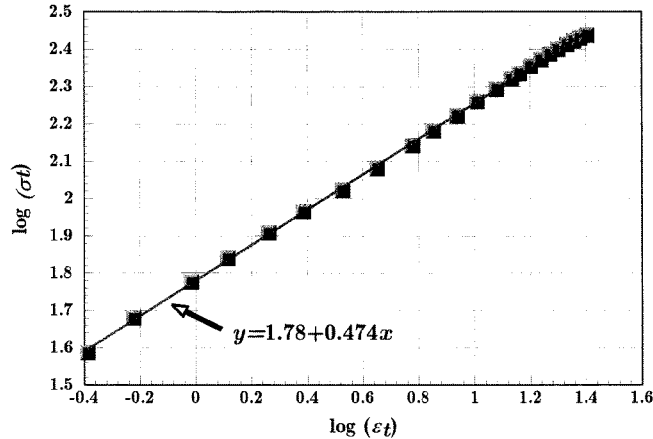


Figure 1.19: Power-law representation of the plastic stress-strain relation for copper.

The increase in strain hardening rate needed to sustain the drawing process in semicrystalline polymers arises from a dramatic transformation in the material's microstructure. These materials are initially "spherulitic," containing flat lamellar crystalline plates, perhaps 10 nm thick, arranged radially outward in a spherical domain. As the induced strain increases, these spherulites are first deformed in the straining direction. As the strain increases further, the spherulites are broken apart and the lamellar fragments rearranged with a dominantly axial molecular orientation to become what is known as the fibrillar microstructure. With the strong covalent bonds now dominantly lined up in the load-bearing direction, the material exhibits markedly greater strengths and stiffnesses — by perhaps an order of magnitude — than in the original material. This structure requires a much higher strain hardening rate for increased strain, causing an upturn in the true stress-strain curve.

### 1.5.3 Compression

The above discussion is concerned primarily with simple tension, i.e. uniaxial loading that increases the interatomic spacing. However, as long as the loads are sufficiently small (stresses less than the proportional limit), in many materials the relations outlined above apply equally well if loads are placed so as to put the specimen in compression rather than tension. The expression for deformation and a given load  $\delta = PL/AE$  applies just as in tension, with negative values for  $\delta$  and  $P$  indicating compression. Further, the modulus  $E$  is the same in tension and compression to a good approximation, and the stress-strain curve simply extends as a straight line into the third quadrant as shown in Fig. 1.20.

There are some practical difficulties in performing stress-strain tests in compression. If excessively large loads are mistakenly applied in a tensile test, perhaps by wrong settings on the testing machine, the specimen simply breaks and the test must be repeated with a new specimen. But in

<sup>10</sup>Here percent strain was used for  $\epsilon_t$ ; this produces the same value for  $n$  but a different  $A$  than if full rather than percentage values were used.

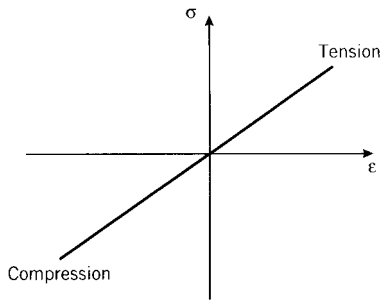


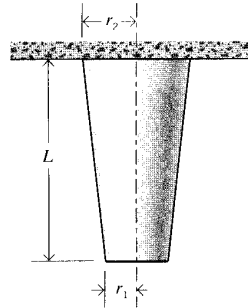
Figure 1.20: Stress-strain curve in tension and compression.

compression, a mistake can easily damage the load cell or other sensitive components, since even after specimen failure the loads are not necessarily relieved.

Specimen failure by cracking is inhibited in compression, since cracks will be closed up rather than opened by the stress state. A number of important materials are much stronger in compression than in tension for this reason. Concrete, for example, has good compressive strength and so finds extensive use in construction in which the dominant stresses are compressive. But it has essentially no strength in tension, as cracks in sidewalks and building foundations attest: tensile stresses appear as these structures settle, and cracks begin at very low tensile strain in unreinforced concrete.

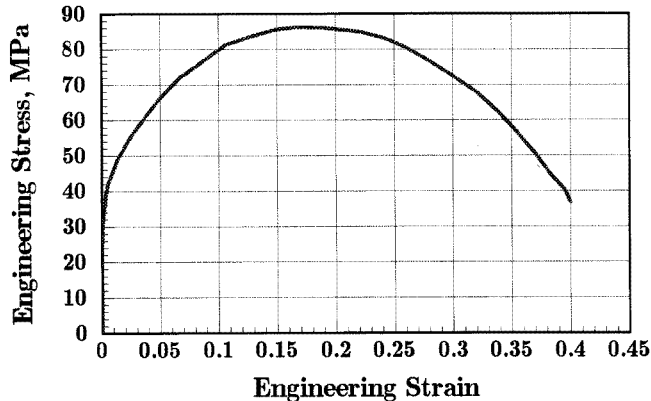
## 1.6 Problems

1. Determine the stress and total deformation of an aluminum wire, 30 m long and 5 mm in diameter, subjected to an axial load of 250 N.
2. A tapered column of modulus  $E$  and mass density  $\rho$  varies linearly from a radius of  $r_1$  to  $r_2$  in a length  $L$ , and is hanging from its broad end. Find the total deformation due to the weight of the bar.



*Prob. 2*

3. The figure below shows the engineering stress-strain curve for pure polycrystalline aluminum; the numerical data for this figure are in the file <http://web.mit.edu/course/3/3.225/alum.txt>, which can be imported into a spreadsheet or other analysis software. For this material, determine (a) Young's modulus, (b) the 0.2% offset yield strength, (c) the Ultimate Tensile Strength (UTS), (d) the modulus of resilience, and (e) the modulus of toughness.



Prob. 3

## References

1. Ashby, M., et al., *Materials: Engineering, Science, Processing and Design*, Elsevier, Amsterdam. 2007.
2. Boyer, H.F., *Atlas of Stress-Strain Curves*, ASM International, Metals Park, Ohio, 1987.
3. Courtney, T.H., *Mechanical Behavior of Materials*, McGraw-Hill, New York, 1990.
4. Hayden, H.W., W.G. Moffatt and J. Wulff, *The Structure and Properties of Materials: Vol. III Mechanical Behavior*, Wiley, New York, 1965.
5. Jenkins, C. and S. Khanna, *Mechanics of Materials*, Elsevier, Amsterdam, 2005.

# Chapter 2

# Thermodynamics of Mechanical Response

The first law of thermodynamics states that an input of heat  $dQ$  or mechanical work  $dW$  to a system leads to a change in internal energy  $dU$  according to  $dU = dW + dQ$ . For a reversible process the second law gives  $dQ = TdS$ , and we will be concerned with increments of mechanical work in the form  $dW = f dx$ . Combining these relations gives

$$f dx = dU - T dS \quad (2.1)$$

Hence an increment of mechanical work  $f dx$  done on the system can produce an increase in the internal energy  $dU$  or a decrease in the entropy  $dS$ . We will be concerned in this chapter first with materials of limited mobility that are unable to exhibit entropic configurational changes, so the response is solely enthalpic. We will then treat materials that are so mobile we can neglect the enthalpic component in comparison with the entropy change. Finally we will consider viscoelastic materials that exhibit appreciable amounts of both enthalpic and entropic effects in their response.

## 2.1 Enthalpic Response

For most materials, the amount of stretching experienced by a tensile specimen under a small fixed load is controlled in a relatively simple way by the tightness of the chemical bonds at the atomic level, and this makes it possible to relate stiffness to the chemical architecture of the material. This is in contrast to more complicated mechanical properties such as fracture, which are controlled by a diverse combination of microscopic as well as molecular aspects of the material's internal structure and surface. Further, the stiffness of some materials — notably rubber — arises not from bond stiffness but from disordering or entropic factors.

### 2.1.1 The Bond Energy Function

Chemical bonding between atoms can be viewed as arising from the electrostatic attraction between regions of positive and negative electronic charge. Materials can be classified based on the nature of these electrostatic forces, the three principal classes being

1. *Ionic materials*, such as NaCl, in which an electron is transferred from the less electronegative element (Na) to the more electronegative (Cl). The ions therefore differ by one electronic charge and are thus attracted to one another. Further, the two ions feel an attraction not only to each other but also to other oppositely charged ions in their vicinity; they also feel a repulsion from nearby ions of the same charge. Some ions may gain or lose more than one electron.
2. *Metallic materials*, such as iron and copper, in which one or more loosely bound outer electrons are released into a common pool which then acts to bind the positively charged atomic cores.

3. Covalent materials, such as diamond and polyethylene, in which atomic orbitals overlap to form a region of increased electronic charge to which both nuclei are attracted. This bond is directional, with each of the nuclear partners in the bond feeling an attraction to the negative region between them but not to any of the other atoms nearby.

In the case of ionic bonding, Coulomb's law of electrostatic attraction can be used to develop simple but effective relations for the bond stiffness. For ions of equal charge  $e$  the attractive force  $f_{attr}$  can be written:

$$f_{attr} = \frac{Ce^2}{r^2} \quad (2.2)$$

Here  $C$  is a conversion factor; For  $e$  in Coulombs,  $C = 8.988 \times 10^9 \text{ N}\cdot\text{m}^2/\text{Coul}^2$ . For singly ionized atoms,  $e = 1.602 \times 10^{-19}$  Coul is the charge on an electron. The *energy* associated with the Coulombic attraction is obtained by integrating the force, which shows that the bond energy varies inversely with the separation distance:

$$U_{attr} = \int f_{attr} dr = \frac{-Ce^2}{r} \quad (2.3)$$

where the energy of atoms at infinite separation is taken as zero.

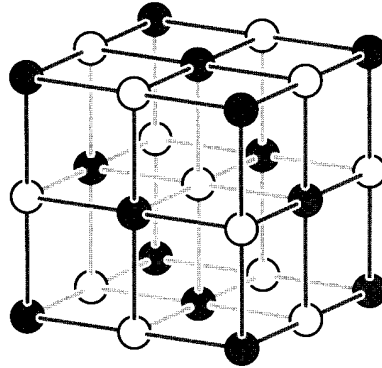


Figure 2.1: The interpenetrating cubic NaCl lattice.

If the material's atoms are arranged as a perfect crystal, it is possible to compute the electrostatic binding energy field in considerable detail. In the interpenetrating cubic lattice of the ionic NaCl structure shown in Fig. 2.1, for instance, each ion feels attraction to oppositely charged neighbors and repulsion from equally charged ones. A particular sodium atom is surrounded by 6 Cl<sup>-</sup> ions at a distance  $r$ , 12 Na<sup>+</sup> ions at a distance  $r\sqrt{2}$ , 8 Cl<sup>-</sup> ions at a distance  $r\sqrt{3}$ , etc. The total electronic field sensed by the first sodium ion is then:

$$\begin{aligned} U_{attr} &= -\frac{Ce^2}{r} \left( \frac{6}{\sqrt{1}} - \frac{12}{\sqrt{2}} + \frac{8}{\sqrt{3}} - \frac{6}{\sqrt{4}} + \frac{24}{\sqrt{5}} - \dots \right) \\ &= \frac{-ACe^2}{r} \end{aligned} \quad (2.4)$$

where  $A = 1.747558\dots$  is the result of the previous series, called the *Madelung constant*<sup>1</sup>. Note that it is not sufficient to consider only nearest-neighbor attractions in computing the bonding energy; in fact the second term in the series is larger in magnitude than the first. The specific value for the Madelung constant is determined by the crystal structure, being 1.763 for CsCl and 1.638 for cubic ZnS.

---

<sup>1</sup>C. Kittel, *Introduction to Solid State Physics*, John Wiley & Sons, New York, 1966. The Madelung series does not converge smoothly, and this text includes some approaches to computing the sum.

At close separation distances, the attractive electrostatic force is balanced by mutual repulsion forces that arise from interactions between overlapping electron shells of neighboring ions; this force varies much more strongly with the distance, and can be written:

$$U_{rep} = \frac{B}{r^n} \quad (2.5)$$

Compressibility experiments have determined the exponent  $n$  to be 7.8 for the NaCl lattice, so this is a much steeper function than  $U_{attr}$ .

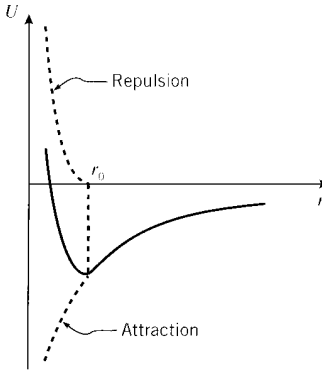


Figure 2.2: The bond energy function.

As shown in Fig. 2.2, the total binding energy of one ion due to the presence of all others is then the sum of the attractive and repulsive components:

$$U = -\frac{ACe^2}{r} + \frac{B}{r^n} \quad (2.6)$$

Note that the curve is *anharmonic* (not shaped like a sine curve), being more flattened out at larger separation distances. The system will adopt a configuration near the position of lowest energy, computed by locating the position of zero slope in the energy function:

$$(f)_{r=r_0} = \left( \frac{dU}{dr} \right)_{r=r_0} = \left( \frac{ACe^2}{r^2} - \frac{nB}{r^{n+1}} \right)_{r=r_0} = 0$$

$$r_o = \left( \frac{nB}{ACe^2} \right)^{\frac{1}{n-1}} \quad (2.7)$$

The range for  $n$  is generally 5–12, increasing as the number of outer-shell electrons that cause the repulsive force.

### Example 2.1

In practice the  $n$  and  $B$  parameters in Eqn. 2.6 are determined from experimental measurements, for instance by using a combination of X-ray diffraction to measure  $r_0$  and elastic modulus to infer the slope of the  $U(r)$  curve. As an illustration of this process, picture a tensile stress  $\sigma$  applied to a unit area of crystal ( $A = 1$ ) as shown in Fig. 2.3, in a direction perpendicular to the crystal cell face. The total force on this unit area is numerically equal to the stress:  $F = \sigma A = \sigma$ .

If the interionic separation is  $r_0$ , there will be  $1/r_0^2$  ions on the unit area, each being pulled by a force  $f$ . Since the total force  $F$  is just  $f$  times the number of ions, the stress can then be written

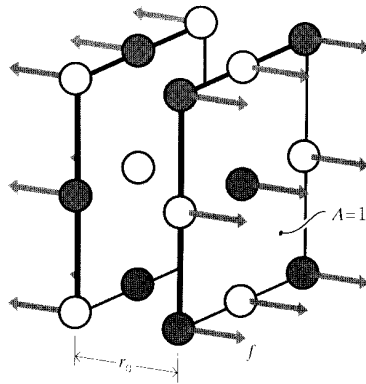


Figure 2.3: Simple tension applied to crystal face.

$$\sigma = F = f \frac{1}{r_0^2}$$

When the separation between two adjacent ions is increased by an amount  $\delta$ , the strain is  $\epsilon = \delta/r_0$ . The differential strain corresponding to a differential displacement is then

$$d\epsilon = \frac{dr}{r_0}$$

The elastic modulus  $E$  is now the ratio of stress to strain, in the limit as the strain approaches zero:

$$E = \left. \frac{d\sigma}{d\epsilon} \right|_{\epsilon \rightarrow 0} = \left. \frac{1}{r_0} \frac{df}{dr} \right|_{r \rightarrow r_0} = \left. \frac{1}{r_0} \frac{d}{dr} \left( \frac{ACe^2}{r^2} - \frac{nB}{r^{n+1}} \right) \right|_{r \rightarrow r_0}$$

Using  $B = ACe^2 r_0^{n-1}/n$  from Eqn. 2.7 and simplifying,

$$E = \frac{(n-1)ACe^2}{r_0^4}$$

Note the very strong dependence of  $E$  on  $r_0$ , which in turn reflects the tightness of the bond. If  $E$  and  $r_0$  are known experimentally,  $n$  can be determined. For NaCl,  $E = 3 \times 10^{10}$  N/m<sup>2</sup>; using this along with the X-ray diffraction value of  $r_0 = 2.82 \times 10^{-10}$  m, we find  $n = 1.47$ .

Using simple tension in this calculation is not really appropriate, because when a material is stretched in one direction, it will *contract* in the transverse directions. This is the *Poisson effect*, discussed in the previous chapter. Our tension-only example does not consider the transverse contraction, and the resulting value of  $n$  is too low. A better but slightly more complicated approach is to use hydrostatic compression, which moves all the ions closer to one another.

---

The stiffnesses of metallic and covalent systems will be calculated differently than the method used above for ionic crystals, but the concept of electrostatic attraction applies to these non-ionic systems as well. As a result, bond energy functions of a qualitatively similar nature result from all these materials. In general, the “tightness” of the bond, and hence the elastic modulus  $E$ , is related to the curvature of the bond energy function. Steeper bond functions will also be deeper as a rule, so that within similar classes of materials the modulus tends to correlate with the energy needed to rupture the bonds, for instance by melting. Materials such as tungsten that fill many bonding and few antibonding orbitals have very deep bonding functions<sup>2</sup>, with correspondingly high stiffnesses

<sup>2</sup>The cohesive energy of materials is an important topic in solid state physics; see for example J. Livingston, *Electronic Properties of Engineering Materials*, Wiley, 1999.

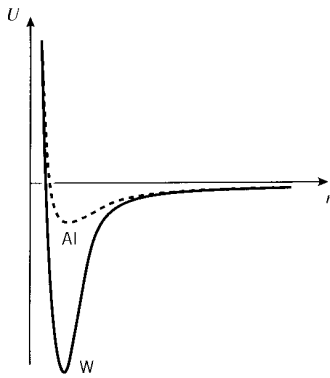


Figure 2.4: Bond energy functions for aluminum and tungsten.

and melting temperatures, as illustrated in Fig. 2.4. This correlation is obvious in Table 2.1, which lists the values of modulus for a number of metals, along with the values of melting temperature  $T_m$  and melting energy  $\Delta H$ .

Table 2.1: Modulus and bond strengths for transition metals.

Material	$E$ GPa (Mpsi)	$T_m$ °C	$\Delta H$ kJ/mol	$\alpha_L$ $\times 10^{-6}, ^\circ \text{C}^{-1}$
Pb	14 (2)	327	5.4	29
Al	69 (10)	660	10.5	22
Cu	117 (17)	1084	13.5	17
Fe	207 (30)	1538	15.3	12
W	407 (59)	3410	32	4.2

### 2.1.2 Thermal Expansion

The system will generally have sufficient thermal energy to reside at a level somewhat above the minimum in the bond energy function, and will oscillate between the two positions labeled  $A$  and  $B$  in Fig. 2.5, with an average position near  $r_0$ . This simple idealization provides a rationale for why materials expand when the temperature is raised. As the internal energy is increased by the addition of heat, the system oscillates between the positions labeled  $A'$  and  $B'$  with an average separation distance  $r'_0$ . Since the curve is anharmonic, the average separation distance is now greater than before, so the material has expanded or stretched. To a reasonable approximation, the relative thermal expansion  $\Delta L/L$  is often related linearly to the temperature rise  $\Delta T$ , and we can write:

$$\boxed{\frac{\Delta L}{L} = \epsilon_T = \alpha_L \Delta T} \quad (2.8)$$

where  $\epsilon_T$  is a *thermal strain* and the constant of proportionality  $\alpha_L$  is the *coefficient of linear thermal expansion*. The expansion coefficient  $\alpha_L$  will tend to correlate with the depth of the energy curve, as is seen in Table 2.1.

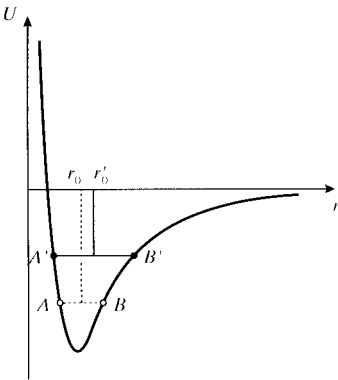


Figure 2.5: Anharmonicity of the bond energy function.

### Example 2.2

A steel bar of length  $L$  and cross-sectional area  $A$  is fitted snugly between rigid supports as shown in Fig. 2.6. We wish to find the compressive stress in the bar when the temperature is raised by an amount  $\Delta T$ .

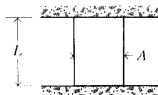


Figure 2.6: Bar between rigid supports.

If the bar were free to expand, it would increase in length by an amount given by Eqn. 2.8. Clearly, the rigid supports have to push on the bar – i.e. put it into compression – to suppress this expansion. The magnitude of this thermally induced compressive stress could be found by imagining the material free to expand, then solving  $\sigma = E\epsilon_T$  for the stress needed to “push the material back” to its unstrained state. Equivalently, we could simply set the sum of a thermally induced strain and a mechanical strain  $\epsilon_\sigma$  to zero:

$$\epsilon = \epsilon_\sigma + \epsilon_T = \frac{\sigma}{E} + \alpha_L \Delta T = 0$$

$$\sigma = -\alpha_L E \Delta T$$

The minus sign in this result reminds us that a negative (compressive) stress is induced by a positive temperature change (temperature rises.)

### Example 2.3

A glass container of stiffness  $E$  and thermal expansion coefficient  $\alpha_L$  is removed from a hot oven and plunged suddenly into cold water. We know from experience that this “thermal shock” could fracture the glass, and we’d like to see what materials parameters control this phenomenon. The analysis is very similar to that of the previous example.

In the time period just after the cold-water immersion, before significant heat transfer by conduction can take place, the outer surfaces of the glass will be at the temperature of the cold water while the interior

is still at the temperature of the oven. The outer surfaces will try to contract, but are kept from doing so by the still-hot interior; this causes a tensile stress to develop on the surface. As before, the stress can be found by setting the total strain to zero:

$$\epsilon = \epsilon_\sigma + \epsilon_T = \frac{\sigma}{E} + \alpha_L \Delta T = 0$$

$$\sigma = -\alpha_L E \Delta T$$

Here the temperature change  $\Delta T$  is negative if the glass is going from hot to cold, so the stress is positive (tensile). If the glass is not to fracture by thermal shock, this stress must be less than the ultimate tensile strength  $\sigma_f$ ; hence the maximum allowable temperature difference is

$$-\Delta T_{max} = \frac{\sigma_f}{\alpha_L E}$$

To maximize the resistance to thermal shock, the glass should have as low a value of  $\alpha_L E$  as possible. “Pyrex” glass was developed specifically for improved thermal shock resistance by using boron rather than soda and lime as process modifiers; this yields a much reduced value of  $\alpha_L$ .

Material properties for a number of important structural materials are listed in the *Module on Material Properties*. When the column holding Young’s Modulus is plotted against the column containing the Thermal Expansion Coefficients (using log-log coordinates), the graph shown in Fig. 2.7 is obtained. Here we see again the general inverse relationship between stiffness and thermal expansion, and the distinctive nature of polymers is apparent as well.

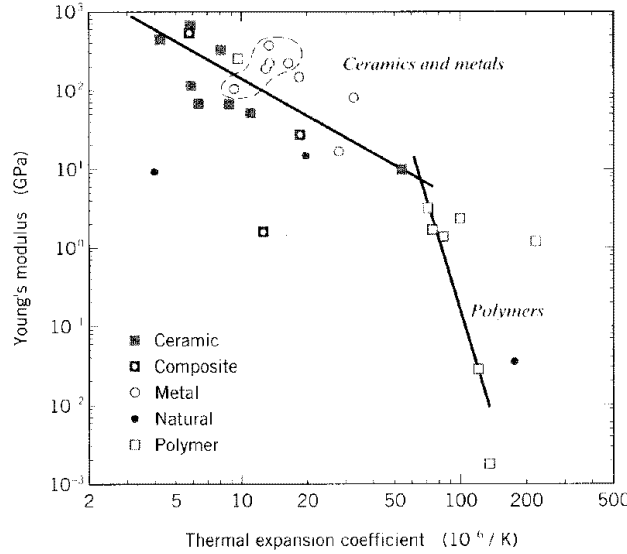


Figure 2.7: Correlation of stiffness and thermal expansion for materials of various types.

Not all types of materials can be described by these simple bond-energy concepts: *intramolecular* polymer covalent bonds have energies entirely comparable with ionic or metallic bonds, but most common polymers have substantially lower moduli than most metals or ceramics. This is due to the *intermolecular* bonding in polymers being due to secondary bonds which are much weaker than the strong intramolecular covalent bonds. Polymers can also have substantial entropic contributions to their stiffness, as will be described below, and these effects do not necessarily correlate with bond energy functions.

## 2.2 Entropic Response

The internal energy as given by the function  $U(r)$  is sufficient to determine the atomic positions in many engineering materials; the material “wants” to minimize its internal energy, and it does this by optimizing the balance of attractive and repulsive electrostatic bonding forces. But when the absolute temperature is greater than approximately two-thirds of the melting temperature, there can be sufficient molecular mobility that entropic or disordering effects must be considered as well. This is often the case for polymers even at room temperature, due to their weak intermolecular bonding.

When the temperature is high enough, polymer molecules can be viewed as an interpenetrating mass of (extremely long) wriggling worms, constantly changing their positions by rotation about carbon-carbon single bonds. This wriggling does not require straining the bond lengths or angles, and large changes in position are possible with no change in internal bonding energy.

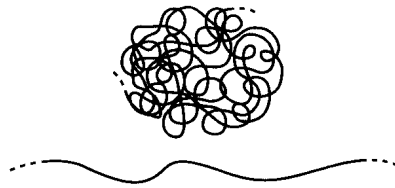


Figure 2.8: Conformational change in polymers.

The shape, or “conformation” of a polymer molecule can range from a fully extended chain to a randomly coiled sphere (see Fig. 2.8). Statistically, the coiled shape is much more likely than the extended one, simply because there are so many ways the chain can be coiled and only one way it can be fully extended. In thermodynamic terms, the entropy of the coiled conformation is very high (many possible “microstates”), and the entropy of the extended conformation is very low (only one possible microstate). If the chain is extended and then released, there will be more wriggling motions tending to the most probable state than to even more highly stretched states; the material would therefore shrink back to its unstretched and highest-entropy state. Equivalently, a person holding the material in the stretched state would feel a tensile force as the material tries to unstretch and is prevented from doing so. These effects are due to entropic factors, and not internal bond energy.

It is possible for materials to exhibit both internal energy and entropic elasticity. Energy effects dominate in most materials, but rubber is much more dependent on entropic effects. An *ideal rubber* is one in which the response is completely entropic, with the internal energy changes being negligible.

When we stretch a rubber band, the molecules in its interior become extended because they are *crosslinked* by chemical or physical junctions as shown in Fig. 2.9. Without these links, the molecules could simply slide past one another with little or no uncoiling. “Silly Putty” is an example of uncrosslinked polymer, and its lack of junction connections cause it to be a viscous fluid rather than a useful elastomer that can bear sustained loads without continuing flow. The crosslinks provide a means by which one molecule can pull on another, and thus establish load transfer within the materials. They also have the effect of limiting how far the rubber can be stretched before breaking, since the extent of the entropic uncoiling is limited by how far the material can extend before pulling up tight against the network of junction points. We will see below that the stiffness of a rubber can be controlled directly by adjusting the crosslink density, and this is an example of

process-structure-property control in materials.

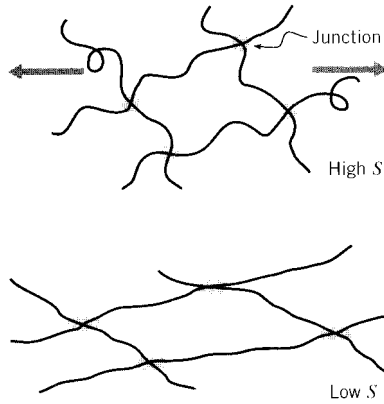


Figure 2.9: Stretching of crosslinked or entangled polymers.

As the temperature is raised, the Brownian-type wriggling of the polymer is intensified, so that the material seeks more vigorously to assume its random high-entropy state. This means that the force needed to hold a rubber band at fixed elongation *increases* with increasing temperature. Similarly, if the band is stretched by hanging a fixed weight on it, the band will *shrink* as the temperature is raised. In some thermodynamic formalisms it is convenient to model this behavior by letting the coefficient of thermal expansion be a variable parameter, with the ability to become negative for sufficiently large tensile strains. This is a little tricky, however; for instance, the stretched rubber band will contract only along its long axis when the temperature is raised, and will become thicker in the transverse directions. The coefficient of thermal expansion would have to be made not only stretch-dependent but also dependent on direction (“anisotropic”).

It is worthwhile to study the response of rubbery materials in some depth, partly because this provides a broader view of the elasticity of materials. But this isn’t a purely academic goal. Rubbery materials are being used in increasingly demanding mechanical applications (in addition to tires, which is a very demanding application itself). Elastomeric bearings, vibration-control supports, and biomedical prostheses are but a few examples. We will outline what is known as the “kinetic theory of rubber elasticity,” which treats the entropic effect using concepts of statistical thermodynamics. This theory stands as one of the very most successful atomistic theories of mechanical response. It leads to a result of satisfying accuracy without the need for adjustable parameters or other fudge factors.

From Eqn. 2.1 we have

$$f = \frac{dW}{dx} = \left( \frac{\partial U}{\partial x} \right)_T - T \left( \frac{\partial S}{\partial x} \right)_T \quad (2.9)$$

For an ideal rubber, the enthalpy change  $dU$  is negligible, so the force is related directly to the temperature and the change in entropy  $dS$  accompanying the extension  $dx$ .

To determine the force-deformation relationship, we obviously need to consider how  $S$  changes with deformation. We begin by writing an expression for the conformation, or shape, of the segment of polymer molecule between junction points as a statistical probability distribution. Here the length of the *segment* is the important molecular parameter, not the length of the entire molecule. In the simple form of this theory, which turns out to work quite well, each covalently bonded segment is idealized as a freely-jointed sequence of  $n$  rigid links each having length  $a$ .

A reasonable model for the end-to-end distance of a randomly wriggling segment is that of a

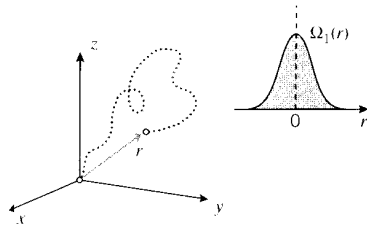


Figure 2.10: Random-walk model of polymer conformation

“random walk” Gaussian distribution treated in elementary statistics. One end of the chain is visualized at the origin of an  $xyz$  coordinate system as shown in Fig. 2.10, and each successive link in the chain is attached with a random orientation relative to the previous link. (An elaboration of the theory would constrain the orientation so as to maintain the  $109^\circ$  covalent bonding angle.) The probability  $\Omega_1(r)$  that the other end of the chain is at a position  $r = (x^2 + y^2 + z^2)^{1/2}$  can be shown to be

$$\Omega_1(r) = \left(\frac{\beta}{\sqrt{\pi}}\right)^3 \exp(-\beta^2 r^2) = \left(\frac{\beta}{\sqrt{\pi}}\right)^3 \exp[-\beta^2 (x^2 + y^2 + z^2)]$$

The parameter  $\beta$  is a scale factor related to the number of units  $n$  in the polymer segment and the bond length  $a$ ; specifically it turns out that  $\beta = \sqrt{3/2n}/a$ . This is the “bell-shaped curve” well known to seasoned test-takers. The most probable end-to-end distance is seen to be zero, which is expected because the chain will end up a given distance to the left (or up, or back) of the origin exactly as often as it ends up the same distance to the right.

When the molecule is now stretched or otherwise deformed, the relative positions of the two ends are changed. Deformation in elastomers is usually described in terms of *extension ratios*, which are the ratios of stretched to original dimensions,  $L/L_0$ . Stretches in the  $x$ ,  $y$ , and  $z$  directions are denoted by  $\lambda_x$ ,  $\lambda_y$ , and  $\lambda_z$  respectively. The deformation is assumed to be *affine*, i.e. the end-to-end distances of each molecular segment increase by these same ratios. Hence if we continue to view one end of the chain at the origin the other end will have moved to  $x_2 = \lambda_x x$ ,  $y_2 = \lambda_y y$ ,  $z_2 = \lambda_z z$ . The configurational probability of a segment being found in this stretched state is then

$$\Omega_2 = \left(\frac{\beta}{\sqrt{\pi}}\right)^3 \exp[-\beta^2 (\lambda_x^2 x^2 + \lambda_y^2 y^2 + \lambda_z^2 z^2)]$$

The relative change in probabilities between the perturbed and unperturbed states can now be written as

$$\ln \frac{\Omega_2}{\Omega_1} = -\beta^2 [(\lambda_x^2 - 1)x^2 + (\lambda_y^2 - 1)y^2 + (\lambda_z^2 - 1)z^2]$$

Several strategems have been used in the literature to simplify this expression. One simple approach is to let the initial position of the segment end  $x, y, z$  be such that  $x^2 = y^2 = z^2 = \bar{r}_0^2/3$ , where  $\bar{r}_0^2$  is the initial mean square end-to-end distance of the segment. (This is not zero, since when squares are taken the negative values no longer cancel the positive ones.) It can also be shown that the distance  $\bar{r}_0^2$  is related to the number of bonds  $n$  in the segment and the bond length  $a$  by  $\bar{r}_0^2 = na^2$ . Making these substitutions and simplifying, we have

$$\ln \frac{\Omega_2}{\Omega_1} = -\frac{1}{2} (\lambda_x^2 + \lambda_y^2 + \lambda_z^2 - 3) \quad (2.10)$$

As is taught in subjects in statistical thermodynamics, changes in configurational probability are related to corresponding changes in thermodynamic entropy by the “Boltzman relation” as

$$\Delta S = k \ln \frac{\Omega_2}{\Omega_1}$$

where  $k = 1.38 \times 10^{-23}$  J/K is Boltzman’s constant. Substituting Eqn. 2.10 in this relation:

$$\Delta S = -\frac{k}{2} (\lambda_x^2 + \lambda_y^2 + \lambda_z^2 - 3)$$

This is the entropy change for one segment. If there are  $N$  chain segments per unit volume, the total entropy change per unit volume  $\Delta S_V$  is just  $N$  times this quantity:

$$\Delta S_V = -\frac{Nk}{2} (\lambda_x^2 + \lambda_y^2 + \lambda_z^2 - 3) \quad (2.11)$$

The associated work (per unit volume) required to change the entropy by this amount is

$$\boxed{\Delta W_V = -T\Delta S_V = +\frac{NkT}{2} (\lambda_x^2 + \lambda_y^2 + \lambda_z^2 - 3)} \quad (2.12)$$

The quantity  $\Delta W_V$  is therefore the strain energy per unit volume contained in an ideal rubber stretched by  $\lambda_x, \lambda_y, \lambda_z$ .

To illustrate the use of Eqn. 2.12 for a simple but useful case, consider a rubber band, initially of length  $L_0$  which is stretched to a new length  $L$ . Hence  $\lambda = \lambda_x = L/L_0$ . To a very good approximation, rubbery materials maintain a constant volume during deformation, and this lets us compute the transverse contractions  $\lambda_y$  and  $\lambda_z$  which accompany the stretch  $\lambda_x$ . An expression for the change  $\Delta V$  in a cubical volume of initial dimensions  $a_0, b_0, c_0$  which is stretched to new dimensions  $a, b, c$  is

$$\Delta V = abc - a_0 b_0 c_0 = (a_0 \lambda_x)(b_0 \lambda_y)(c_0 \lambda_z) - a_0 b_0 c_0 = a_0 b_0 c_0 (\lambda_x \lambda_y \lambda_z - 1)$$

Setting this to zero gives

$$\lambda_x \lambda_y \lambda_z = 1 \quad (2.13)$$

Hence the contractions in the  $y$  and  $z$  directions are

$$\lambda_y^2 = \lambda_z^2 = \frac{1}{\lambda}$$

Using this in Eqn. 2.12, the force  $F$  needed to induce the deformation can be found by differentiating the total strain energy according to Eqn. 2.9:

$$F = \frac{dW}{dL} = \frac{d(V \Delta W_V)}{L_0 d\lambda} = A_0 \frac{NkT}{2} \left( 2\lambda - \frac{2}{\lambda^2} \right)$$

Here  $A_0 = V/L_0$  is the original area. Dividing by  $A_0$  to obtain the engineering stress:

$$\boxed{\sigma = NkT \left( \lambda - \frac{1}{\lambda^2} \right)} \quad (2.14)$$

Clearly, the parameter  $NkT$  is related to the stiffness of the rubber, as it gives the stress  $\sigma$  needed to induce a given extension  $\lambda$ . It can be shown that the initial modulus — the slope of the stress-strain curve at the origin — is controlled by the temperature and the crosslink density according to  $E = 3NkT$ .

Crosslinking in rubber is usually done in the “vulcanizing” process invented by Charles Goodyear in 1839. In this process sulfur abstracts reactive hydrogens adjacent to the double bonds in the rubber molecule, and forms permanent bridges between adjacent molecules. When crosslinking is done by using approximately 5% sulfur, a conventional rubber is obtained. When the sulfur is increased to  $\approx 30\text{--}50\%$ , a hard and brittle material named ebonite (or simply “hard rubber”) is produced instead.

The volume density of chain segments  $N$  is also the density of junction points. This quantity is related to the specimen density  $\rho$  and the molecular weight between crosslinks  $M_c$  as  $M_c = \rho N_A / N$ , where  $N$  is the number of crosslinks per unit volume and  $N_A = 6.023 \times 10^{23}$  is Avogadro’s Number. When  $N$  is expressed in terms of moles per unit volume, we have simply  $M_c = \rho / N$  and the quantity  $NkT$  in Eqn. 2.14 is replaced by  $NRT$ , where  $R = kN_A = 8.314 \text{ J/mol}\cdot\text{K}$  is the Gas Constant.

#### Example 2.4

The Young’s modulus of a rubber is measured at  $E = 3.5 \text{ MPa}$  for a temperature of  $T = 300 \text{ }^\circ\text{K}$ . The molar crosslink density is then

$$N = \frac{E}{3RT} = \frac{3.5 \times 10^6 \text{ N/m}^2}{3 \times 8.314 \frac{\text{N}\cdot\text{m}}{\text{mol}\cdot\text{K}} \times 300 \text{ K}} = 468 \text{ mol/m}^3$$

The molecular weight per segment is

$$M_c = \frac{\rho}{N} = \frac{1100 \text{ kg/m}^3}{468 \text{ mol/m}^3} = 2350 \text{ gm/mol}$$

Note that the stress-strain response for rubber elasticity is nonlinear, and that the stiffness as given by the stress needed to produce a given deformation is predicted to increase with increasing temperature. This is in accord with the concept of more vigorous wriggling with a statistical bias toward the more disordered state. The rubber elasticity equation works well at lower extensions, but tends to deviate from experimental values at high extensions where the segment configurations become nongaussian.

Deviations from Eqn. 2.14 can also occur due to crystallization at high elongations. (Rubbers are normally noncrystalline, and in fact polymers such as polyethylene that crystallize readily are not elastomeric due to the rigidity imparted by the crystallites.) However, the decreased entropy that accompanies stretching in rubber increases the crystalline melting temperature according to the well-known thermodynamic relation

$$T_m = \frac{\Delta U}{\Delta S} \tag{2.15}$$

where  $\Delta U$  and  $\Delta S$  are the change in internal energy and entropy on crystallization. The quantity  $\Delta S$  is reduced if stretching has already lowered the entropy, so the crystallization temperature rises. If it rises above room temperature, the rubber develops crystallites that stiffen it considerably and cause further deviation from the rubber elasticity equation. (Since the crystallization is exothermic, the material will also increase in temperature; this can often be sensed by stretching a rubber band and then touching it to the lips.) Strain-induced crystallization also helps inhibit crack growth, and the excellent abrasion resistance of natural rubber is related to the ease with which it crystallizes upon stretching.

## 2.3 Viscoelasticity

As mentioned at the outset of this chapter, some materials exhibit a combination of enthalpic and entropic mechanical response. “Viscoelastic” polymers are an example, in which an immediate and recoverable response due to bond distortion can take place, but also accompanied by an entropic response due to conformational change.

While not all polymers are viscoelastic to any important practical extent, and even fewer are *linearly* viscoelastic<sup>3</sup>, the linear theory provides a usable engineering approximation for many applications in polymer and composites engineering. Even in instances requiring more elaborate treatments, the linear viscoelastic theory is a useful starting point.

### 2.3.1 Rate of Conformational Change

When subjected to an applied stress, polymers may deform by either or both of two fundamentally different atomistic mechanisms. The lengths and angles of the chemical bonds connecting the atoms may distort, moving the atoms to new positions of greater internal energy. This is a small motion and occurs very quickly, requiring only  $\approx 10^{-12}$  seconds.

If the polymer has sufficient molecular mobility, larger-scale rearrangements of the atoms may also be possible. For instance, the relatively facile rotation around backbone carbon-carbon single bonds can produce large changes in the conformation of the molecule. Depending on the mobility, a polymer molecule can extend itself in the direction of the applied stress, which decreases its conformational entropy (the molecule is less “disordered”). Elastomers — rubber — respond almost wholly by this entropic mechanism, with little distortion of their covalent bonds or change in their internal energy.

In contrast to the instantaneous nature of the energetically controlled elasticity, the conformational or entropic changes are processes whose rates are sensitive to the local molecular mobility. This mobility is influenced by a variety of physical and chemical factors, such as molecular architecture, temperature, or the presence of absorbed fluids which may swell the polymer. Often, a simple mental picture of “free volume” — roughly, the space available for molecular segments to act cooperatively so as to carry out the motion or reaction in question — is useful in intuiting these rates.

These rates of conformational change can often be described with reasonable accuracy by Arrhenius-type expressions of the form

$$\text{rate} \propto \exp \frac{-E^\ddagger}{RT} \quad (2.16)$$

where  $E^\ddagger$  is an apparent activation energy of the process and  $R = 8.314\text{J/mol} - ^\circ\text{K}$  is the Gas Constant. At temperatures much above the “*glass transition temperature*,” labeled  $T_g$  in Fig. 2.11, the rates are so fast as to be essentially instantaneous, and the polymer acts in a rubbery manner in which it exhibits large, instantaneous, and fully reversible strains in response to an applied stress.

Conversely, at temperatures much less than  $T_g$ , the rates are so slow as to be negligible. Here the chain uncoiling process is essentially “frozen out,” so the polymer is able to respond only by bond stretching. It now responds in a “glassy” manner, responding instantaneously and reversibly but being incapable of being strained beyond a few percent before fracturing in a brittle manner.

In the range near  $T_g$ , the material is midway between the glassy and rubbery regimes. Its response is a combination of viscous fluidity and elastic solidity, and this region is termed “leathery,”

---

<sup>3</sup>For an overview of *nonlinear* viscoelastic theory, see for instance W.N. Findley et al., *Creep and Relaxation of Nonlinear Viscoelastic Materials*, Dover Publications, New York, 1989.

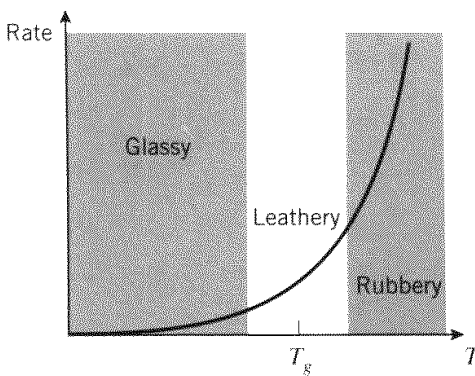


Figure 2.11: Temperature dependence of rate.

or, more technically, “viscoelastic”. The value of  $T_g$  is an important descriptor of polymer thermomechanical response, and is a fundamental measure of the material’s propensity for mobility. Factors that enhance mobility, such as absorbed diluents, expansive stress states, and lack of bulky molecular groups, all tend to produce lower values of  $T_g$ . The transparent polyvinyl butyral film used in automobile windshield laminates is an example of a material that is used in the viscoelastic regime, as viscoelastic response can be a source of substantial energy dissipation during impact.

At temperatures well below  $T_g$ , when entropic motions are frozen and only elastic bond deformations are possible, polymers exhibit a relatively high modulus, called the “glassy modulus”  $E_g$ , which is on the order of 3 GPa (400 kpsi). As the temperature is increased through  $T_g$ , the stiffness drops dramatically, by perhaps two orders of magnitude, to a value called the “rubbery modulus”  $E_r$ . In elastomers that have been permanently crosslinked by sulphur vulcanization or other means, the value of  $E_r$  is determined primarily by the crosslink density; the kinetic theory of rubber elasticity described in the previous section gave this value as  $E_r = 3NRT$ .

If the material is not crosslinked, the stiffness exhibits a short plateau due to the ability of molecular entanglements to act as network junctions; at still higher temperatures the entanglements slip and the material becomes a viscous liquid. Neither the glassy nor the rubbery modulus depends strongly on time, but in the vicinity of the transition near  $T_g$  time effects can be very important. Clearly, a plot of modulus versus temperature, such as is shown in Fig. 2.12, is a vital tool in polymer materials science and engineering. It provides a map of a vital engineering property, and is also a fingerprint of the molecular motions available to the material.

### 2.3.2 Creep Compliance

In the viscoelastic range where the entropic configurational change is neither so slow as to be negligible or so rapid as to be essentially immediate, the material exhibits a “delayed” mechanical response; this is the “viscous” part of viscoelasticity. A number of experimental procedures are available to probe and quantify the time dependence of this delayed response; this chapter will consider just one of these: the creep test.

The creep test consists of measuring the time dependent strain  $\epsilon(t) = \delta(t)/L_0$  resulting from the application of a steady uniaxial stress  $\sigma_0$  as illustrated in Fig. 2.13. These three curves are the strains measured at three different stress levels, each one twice the magnitude of the previous one.

Note in Fig. 2.13 that when the stress is doubled, the resulting strain is doubled over its full range of time. This occurs if the material is *linear* in its response. If the strain-stress relation is

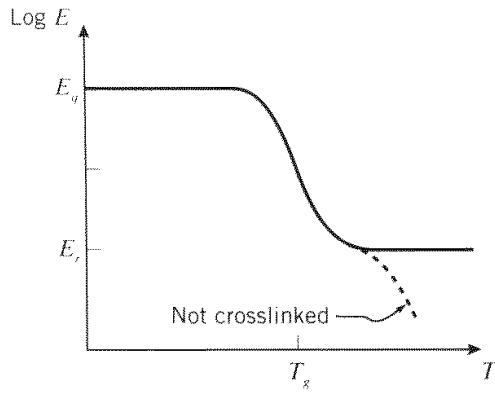


Figure 2.12: A generic modulus-temperature map for polymers.

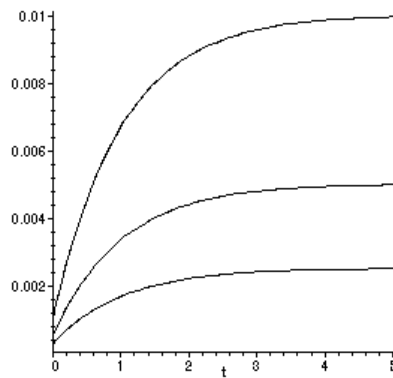


Figure 2.13: Creep strain at various constant stresses.

linear, the strain resulting from a stress  $a\sigma$ , where  $a$  is a constant, is just the constant  $a$  times the strain resulting from  $\sigma$  alone. Mathematically,

$$\epsilon(a\sigma) = a\epsilon(\sigma)$$

This is just a case of “double the stress, double the strain.”

If the creep strains produced at a given time are plotted as the abscissa against the applied stress as the ordinate, an “isochronous” stress-strain curve would be produced. If the material is linear, this “curve” will be a straight line, with a slope that increases as the chosen time is decreased.

For linear materials, the family of strain histories  $\epsilon(t)$  obtained at various constant stresses may be superimposed by normalizing them based on the applied stress. The ratio of strain to stress is called the “compliance”  $C$ , and in the case of time-varying strain arising from a constant stress the ratio is the “creep compliance”:

$$C_{crp}(t) = \frac{\epsilon(t)}{\sigma_0}$$

A typical form of this function is shown in Fig. 2.14, plotted against the logarithm of time. Note that the logarithmic form of the plot changes the shape of the curve drastically, stretching out the short-time portion of the response and compressing the long-time region. Upon loading, the

material strains initially to the “glassy” compliance  $C_g$ ; this is the elastic deformation corresponding to bond distortion. In time, the compliance rises exponentially to an equilibrium or “rubbery” value  $C_r$ , corresponding to the rubbery extension of the material. The value along the abscissa labeled “ $\log \tau$ ” marks the inflection from rising to falling slope, and  $\tau$  is called the “relaxation time” of the creep process.

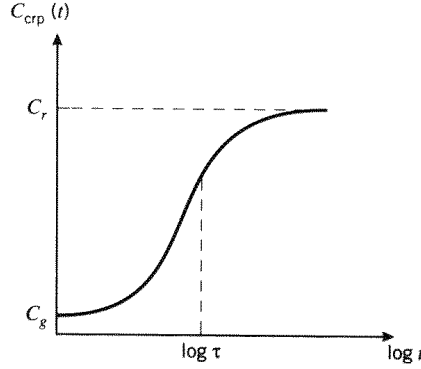


Figure 2.14: The creep compliance function  $C_{crp}(t)$ .

By inspection, we can model the compliance function of Fig. 2.14 with a first-order relation of the form

$$C_{crp}(t) = C_g + (C_r - C_g) \left(1 - e^{-\frac{t}{\tau}}\right) \quad (2.17)$$

### 2.3.3 The Boltzman Superposition Integral

The stress-strain relations for viscoelastic materials can be written as either differential or integral equations, and this section will explore the integral formulation.

Integrals are summing operations, and this view of viscoelasticity takes the response of the material at time  $t$  to be the sum of the responses to excitations imposed at all previous times. The ability to sum these individual responses requires the material to obey a more general statement of linearity than we have invoked previously, specifically that the response to a number of individual excitations be the sum of the responses that would have been generated by each excitation acting alone. Mathematically, if the strain due to a stress  $\sigma_1(t)$  is  $\epsilon(\sigma_1)$  and that due to a different stress  $\sigma_2(t)$  is  $\epsilon(\sigma_2)$ , then the strain due to both stresses is  $\epsilon(\sigma_1 + \sigma_2) = \epsilon(\sigma_1) + \epsilon(\sigma_2)$ . Combining this with the condition for multiplicative scaling used earlier, we have as a general statement of linear viscoelasticity:

$$\epsilon(a\sigma_1 + b\sigma_2) = a\epsilon(\sigma_1) + b\epsilon(\sigma_2) \quad (2.18)$$

The “Boltzman Superposition Integral” statement of linear viscoelastic response follows from this definition. Consider the strain  $\epsilon_1(t)$  at time  $t$  due to the application of a small stress  $\Delta\sigma_1$  applied at a time  $\xi_1$  previous to  $t$ ; this is given directly from the definition of the creep compliance as

$$\epsilon_1(t) = C_{crp}(t - \xi_1)\Delta\sigma_1$$

Similarly, the strain  $\epsilon_2(t)$  due to a stress increment  $\Delta\sigma_2$  applied at a different time  $\xi_2$  is

$$\epsilon_2(t) = C_{crp}(t - \xi_2)\Delta\sigma_2$$

If the material is linear, the total strain at time  $t$  due to both strain increments together can be obtained by superposition of these two individual effects:

$$\epsilon(t) = \epsilon_1(t) + \epsilon_2(t) = C_{crp}(t - \xi_1)\Delta\sigma_1 + C_{crp}(t - \xi_2)\Delta\sigma_2$$

As the number of applied strain increments increases so as to approach a continuous distribution, this becomes:

$$\begin{aligned} \epsilon(t) &= \sum_j \epsilon_j(t) = \sum_j C_{crp}(t - \xi_j)\Delta\sigma_j \\ \longrightarrow \epsilon(t) &= \int_{-\infty}^t C_{crp}(t - \xi) d\sigma = \int_{-\infty}^t C_{crp}(t - \xi) \frac{d\sigma(\xi)}{d\xi} d\xi \end{aligned} \quad (2.19)$$

## References

1. Aklonis, J.J., MacKnight, W.J., and Shen, M., *Introduction to Polymer Viscoelasticity*, Wiley-Interscience, New York, 1972.
2. Callister, W.D., *Materials Science and Engineering: An Introduction*, J. Wiley, New York, 1994.
3. Williams, M.L., "Structural Analysis of Viscoelastic Materials," *AIAA Journal*, p. 785, May 1964.

## 2.4 Problems

1. The *Thermal Shock Resistance*, or  $TSR$ , of an item relates to its resistance to fracture when suddenly quenched from a high temperature to a lower one. Justify the expression for the  $TSR$ :

$$TSR = \frac{\sigma_f k}{E\alpha}$$

where  $k$  is the coefficient of thermal conductivity. Look up reasonable values for these parameters, and compare the  $TSR$  of quartz, soda-lime and borosilicate (Pyrex) glass. Explain the differences between these values on an atomistic basis.

2. A thin microelectronic "chip" is bonded to a much thicker substrate. Show that the biaxial stress induced in the chip when the temperature is raised by  $\Delta T$  is

$$\sigma_x = \sigma_y = \frac{(\alpha_{\text{substrate}} - \alpha_{\text{chip}}) E \Delta T}{1 - \nu}$$

3. Show the stress-extension relationship for equi-biaxial extension ( $\lambda_x = \lambda_y \equiv \lambda$ ) to be

$$\sigma_{\text{true}} = 2NkT \left( \lambda^2 - \frac{1}{\lambda^4} \right)$$

4. Show the pressure-extension relationship for a spherical balloon to be

$$\frac{pr_0}{2Gt_0} = \frac{1}{\lambda_r} - \frac{1}{\lambda_r^7}$$

Plot the function on the right-hand-side, and explain why it shows a maximum (which is readily felt when blowing up a party balloon).

5. Determine the apparent activation energy in ( $E^\dagger$  in Eqn. 2.16) for a viscoelastic relaxation in which the initial rate is observed to double when the temperature is increased from 20°C to 30°C. (Answer:  $E^\dagger = 51$  kJ/mol.)
6. Plot the strain response  $\epsilon(t)$  to a load-unload stress input defined as

$$\sigma(t) = \begin{cases} 0, & t < 1 \\ 1, & 1 < t < 4.5 \\ -1, & 4.5 < t < 5 \\ 0, & t > 5 \end{cases}$$

The material obeys the first-order compliance law (Eqn. 2.17) with  $C_g = 5$ ,  $C_r = 10$ , and  $\tau = 2$ .

# Chapter 3

# Composites

This chapter introduces basic concepts of stiffness and strength underlying the mechanics of fiber-reinforced advanced composite materials. This aspect of composite materials technology is sometimes terms “micromechanics,” because it deals with the relations between macroscopic engineering properties and the microscopic distribution of the material’s constituents, namely the volume fraction of fiber. This chapter will deal primarily with unidirectionally-reinforced continuous-fiber composites, and with properties measured along and transverse to the fiber direction.

## 3.1 Materials

The term *composite* could mean almost anything if taken at face value, since all materials are composed of dissimilar subunits if examined at close enough detail. But in modern materials engineering, the term *usually* refers to a “matrix” material that is reinforced with fibers. For instance, the term “FRP” (for Fiber Reinforced Plastic) usually indicates a thermosetting polyester matrix containing glass fibers, and this particular composite has the lion’s share of today’s commercial market. Figure 3.1 shows a laminate fabricated by “crossplying” unidirectionally-reinforced layers in a  $0^\circ$ - $90^\circ$  stacking sequence.

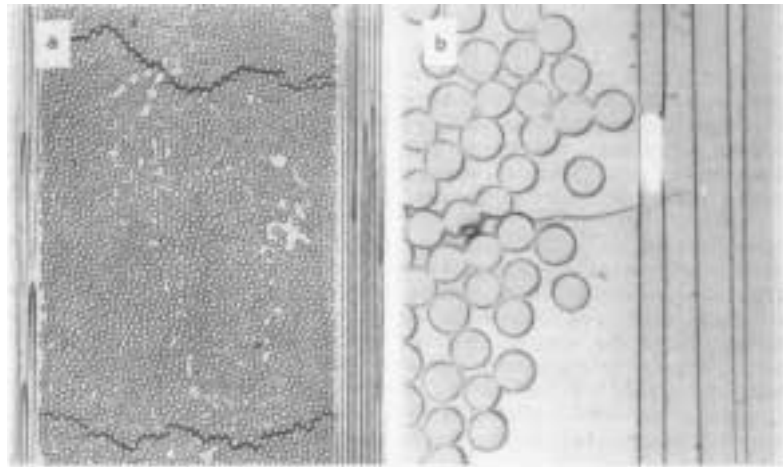


Figure 3.1: A crossplied FRP laminate, showing nonuniform fiber packing and microcracking (from Harris, 1986).

Many composites used today are at the leading edge of materials technology, with performance and costs appropriate to ultrademanding applications such as spacecraft. But heterogeneous materials combining the best aspects of dissimilar constituents have been used by nature for millions of years. Ancient society, imitating nature, used this approach as well: the Book of Exodus speaks of using straw to reinforce mud in brickmaking, without which the bricks would have almost no strength.

As seen in Table 3.1<sup>1</sup>, the fibers used in modern composites have strengths and stiffnesses far above those of traditional bulk materials. The high strengths of the glass fibers are due to processing that avoids the internal or surface flaws which normally weaken glass, and the strength and stiffness of the polymeric aramid fiber is a consequence of the nearly perfect alignment of the molecular chains with the fiber axis.

Table 3.1: Properties of Composite Reinforcing Fibers.

Material	$E$ (GPa)	$\sigma_b$ (GPa)	$\epsilon_b$ (%)	$\rho$ (Mg/m <sup>3</sup> )	$E/\rho$ (MJ/kg)	$\sigma_b/\rho$ (MJ/kg)	cost (\$/kg)
E-glass	72.4	2.4	2.6	2.54	28.5	0.95	1.1
S-glass	85.5	4.5	2.0	2.49	34.3	1.8	22–33
aramid	124	3.6	2.3	1.45	86	2.5	22–33
boron	400	3.5	1.0	2.45	163	1.43	330–440
HS graphite	253	4.5	1.1	1.80	140	2.5	66–110
HM graphite	520	2.4	0.6	1.85	281	1.3	220–660

Of course, these materials are not generally usable as fibers alone, and typically they are impregnated by a matrix material that acts to transfer loads to the fibers, and also to protect the fibers from abrasion and environmental attack. The matrix dilutes the properties to some degree, but even so very high specific (weight-adjusted) properties are available from these materials. Metal and glass are available as matrix materials, but these are currently very expensive and largely restricted to R&D laboratories. Polymers are much more commonly used, with unsaturated styrene-hardened polyesters having the majority of low-to-medium performance applications and epoxy or more sophisticated thermosets having the higher end of the market. Thermoplastic matrix composites are increasingly attractive materials, with processing difficulties being perhaps their principal limitation.

## 3.2 Stiffness

The fibers may be oriented randomly within the material, but it is also possible to arrange for them to be oriented preferentially in the direction expected to have the highest stresses. Such a material is said to be *anisotropic* (different properties in different directions), and control of the anisotropy is an important means of optimizing the material for specific applications. At a microscopic level, the properties of these composites are determined by the orientation and distribution of the fibers, as well as by the properties of the fiber and matrix materials. The topic known as composite *micromechanics* is concerned with developing estimates of the overall material properties from these parameters.

---

<sup>1</sup>F.P. Gerstle, “Composites,” *Encyclopedia of Polymer Science and Engineering*, Wiley, New York, 1991. Here  $E$  is Young’s modulus,  $\sigma_b$  is breaking stress,  $\epsilon_b$  is breaking strain, and  $\rho$  is density.

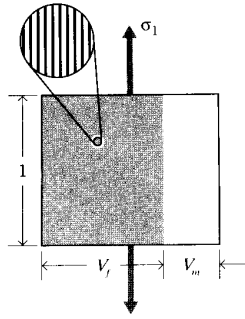


Figure 3.2: Loading parallel to the fibers.

Consider a typical region of material of unit dimensions, containing a volume fraction  $V_f$  of fibers all oriented in a single direction. The matrix volume fraction is then  $V_m = 1 - V_f$ . This region can be idealized as shown in Fig. 3.2 by gathering all the fibers together, leaving the matrix to occupy the remaining volume — this is sometimes called the “slab model.” If a stress  $\sigma_1$  is applied along the fiber direction, the fiber and matrix phases act in *parallel* to support the load. In these parallel connections the strains in each phase must be the same, so the strain  $\epsilon_1$  in the fiber direction can be written as:

$$\epsilon_f = \epsilon_m = \epsilon_1$$

The forces in each phase must add to balance the total load on the material. Since the forces in each phase are the phase stresses times the area (here numerically equal to the volume fraction), we have

$$\sigma_1 = \sigma_f V_f + \sigma_m V_m = E_f \epsilon_1 V_f + E_m \epsilon_1 V_m$$

The stiffness in the fiber direction is found by dividing by the strain:

$$E_1 = \frac{\sigma_1}{\epsilon_1} = V_f E_f + V_m E_m \quad (3.1)$$

This relation is known as a *rule of mixtures* prediction of the overall modulus in terms of the moduli of the constituent phases and their volume fractions.

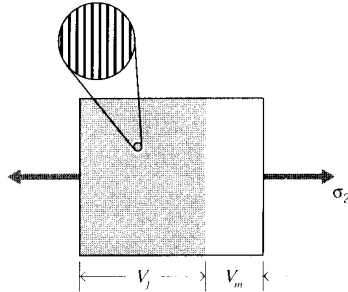


Figure 3.3: Loading perpendicular to the fibers.

If the stress is applied in the direction transverse to the fibers as depicted in Fig. 3.3, the slab model can be applied with the fiber and matrix materials acting *in series*. In this case the stress in the fiber and matrix are equal (an idealization), but the deflections add to give the overall transverse deflection. In this case it can be shown (see Prob. 1)

$$\frac{1}{E_2} = \frac{V_f}{E_f} + \frac{V_m}{E_m} \quad (3.2)$$

Figure 3.4 shows the functional form of the parallel (Eqn. 3.1) and series (Eqn. 3.2) predictions for the fiber- and transverse-direction moduli.

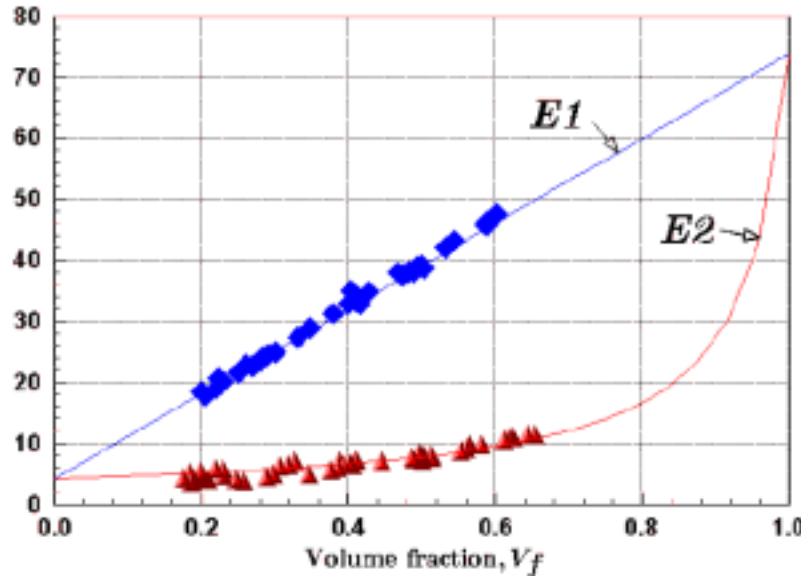


Figure 3.4: Rule-of-mixtures predictions for longitudinal ( $E_1$ ) and transverse ( $E_2$ ) modulus, for glass-polyester composite ( $E_f = 73.7$  MPa,  $E_m = 4$  GPa). Experimental data taken from Hull (1996).

The prediction of transverse modulus given by the series slab model (Eqn. 3.2) is considered unreliable, in spite of its occasional agreement with experiment. Among other deficiencies the assumption of uniform matrix strain being untenable; both analytical and experimental studies have shown substantial nonuniformity in the matrix strain. Figure 3.5 shows the photoelastic fringes in the matrix caused by the perturbing effect of the stiffer fibers.

In more complicated composites, for instance those with fibers in more than one direction or those having particulate or other nonfibrous reinforcements, Eqn. 3.1 provides an *upper bound* to the composite modulus, while Eqn. 3.2 is a *lower bound* (see Fig. 3.4). Most practical cases will be somewhere between these two values, and the search for reasonable models for these intermediate cases has occupied considerable attention in the composites research community. Perhaps the most popular model is an empirical one known as the *Halpin-Tsai* equation<sup>2</sup>, which can be written in the form:

$$E = \frac{E_m[E_f + \xi(V_f E_f + V_m E_m)]}{V_f E_m + V_m E_f + \xi E_m} \quad (3.3)$$

---

<sup>2</sup>c.f. J.C.. Halpin and J.L. Kardos, *Polymer Engineering and Science*, Vol. 16, May 1976, pp. 344–352.

Here  $\xi$  is an adjustable parameter that results in series coupling for  $\xi = 0$  and parallel averaging for very large  $\xi$ .

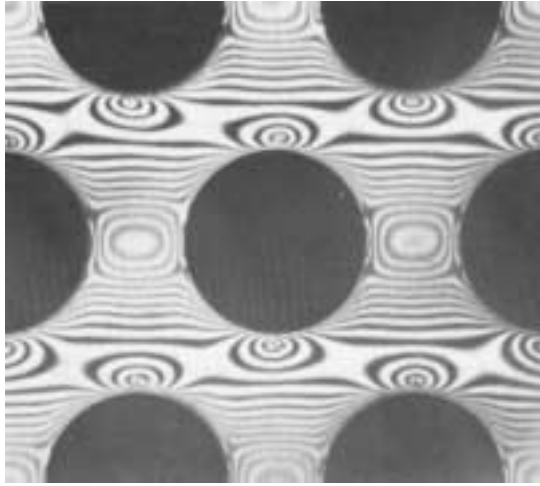


Figure 3.5: Photoelastic (isochromatic) fringes in a composite model subjected to transverse tension (from Hull, 1996).

### 3.3 Strength

Rule of mixtures estimates for strength proceed along lines similar to those for stiffness. For instance, consider a unidirectionally reinforced composite that is strained up to the value at which the fibers begin to break. Denoting this value  $\epsilon_{fb}$ , the stress transmitted by the composite is given by multiplying the stiffness (Eqn. 3.1):

$$\sigma_b = \epsilon_{fb} E_1 = V_f \sigma_{fb} + (1 - V_f) \sigma^*$$

The stress  $\sigma^*$  is the stress in the matrix, which is given by  $\epsilon_{fb} E_m$ . This relation is linear in  $V_f$ , rising from  $\sigma^*$  to the fiber breaking strength  $\sigma_{fb} = E_f \epsilon_{fb}$ . However, this relation is not realistic at low fiber concentration, since the breaking strain of the matrix  $\epsilon_{mb}$  is usually substantially greater than  $\epsilon_{fb}$ . If the matrix had *no* fibers in it, it would fail at a stress  $\sigma_{mb} = E_m \epsilon_{mb}$ . If the fibers were considered to carry no load at all, having broken at  $\epsilon = \epsilon_{fb}$  and leaving the matrix to carry the remaining load, the strength of the composite would fall off with fiber fraction according to

$$\sigma_b = (1 - V_f) \sigma_{mb}$$

Since the breaking strength actually observed in the composite is the greater of these two expressions, there will be a range of fiber fraction in which the composite is *weakened* by the addition of fibers. These relations are depicted in Fig. 3.6.

## References

1. Ashton, J.E., J.C. Halpin and P.H. Petit, *Primer on Composite Materials: Analysis*, Technomic Press, Westport, CT, 1969.

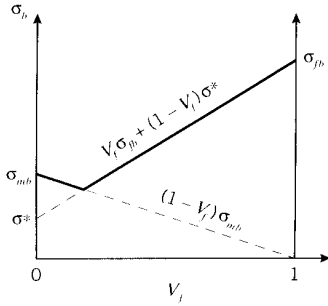


Figure 3.6: Strength of unidirectional composite in fiber direction.

2. , Harris, B., *Engineering Composite Materials*, The Institute of Metals, London, 1986.
3. Hull, D. and T.W. Clyne, *An Introduction to Composites Materials*, Cambridge University Press, 1996.
4. Jones, R.M., *Mechanics of Composite Materials*, McGraw-Hill, New York, 1975.
5. Powell, P.C, *Engineering with Polymers*, Chapman and Hall, London, 1983.
6. Roylance, D., *Mechanics of Materials*, Wiley & Sons, New York, 1996.

### 3.4 Problems

1. Using the slab model and assuming uniform strain in the matrix, show the transverse modulus of a unidirectionally-reinforced composite to be

$$\frac{1}{E_2} = \frac{V_f}{E_f} + \frac{V_m}{E_m}$$

or in terms of compliances

$$C_2 = C_f V_f + C_m V_m$$

2. Plot the longitudinal tensile strength of a E-glass/epoxy unidirectionally-reinforced composite, as a function of the volume fraction  $V_f$ .

### Mechanical Properties of Composite Materials

The following table lists physical and mechanical property values for representative ply and core materials widely used in fiber-reinforced composite laminates. Ply properties are taken from F.P.Gerstle, “Composites,” *Encyclopedia of Polymer Science and Engineering*, Wiley, New York, 1991, which should be consulted for data from a wider range of materials. See also G. Lubin, *Handbook of Composites*, Van Nostrand, New York, 1982.

	S-glass/ epoxy	Kevlar/ epoxy	HM Graphite/ epoxy	Pine	Rohacell 51 rigid foam
Elastic Properties:					
$E_1$ , GPa	55	80	230	13.4	0.07
$E_2$ , GPa	16	5.5	6.6	0.55	0.07
$G_{12}$ , GPa	7.6	2.1	4.8	0.83	0.021
$\nu_{12}$	0.26	0.31	0.25	0.30	
Tensile Strengths:					
$\sigma_1$ , MPa	1800	2000	1100	78	1.9
$\sigma_2$ , MPa	40	20	21	2.1	1.9
$\sigma_{12}$ , MPa	80	40	65	6.2	0.8
Compressive Strengths:					
$\sigma_1$ , MPa	690	280	620	33	0.9
$\sigma_2$ , MPa	140	140	170	3.0	0.9
Physical Properties:					
$\alpha_1$ , $10^{-6}/^{\circ}\text{C}$	2.1	-4.0	-0.7		33
$\alpha_2$ , $10^{-6}/^{\circ}\text{C}$	6.3	60	28		33
Volume fraction	0.7	0.54	0.7		
Thickness, mm	0.15	0.13	0.13		
Density, $\text{Mg/m}^3$	2.0	1.38	1.63	0.55	0.05



## Chapter 4

# General Concepts of Stress and Strain

For much work in mechanical properties of materials, it is necessary to have a deeper exposure to concepts of stress and strain than we needed in the previous chapters. Without attempting a truly thorough treatment of solid mechanics, this chapter will give enough of the formal theory to cope with the more advanced literature of the field.

### 4.1 Kinematics: the Strain–Displacement Relations

The *kinematic* or *strain-displacement* equations describe how the strains – the stretching and distortion – within a loaded body relate to the body’s displacements. The displacement components in the  $x$ ,  $y$ , and  $z$  directions are denoted by the vector  $\mathbf{u} \equiv u_i \equiv (u, v, w)$ , and are functions of position within the body:  $\mathbf{u} = \mathbf{u}(x, y, z)$ . If all points within the material experience the same displacement ( $\mathbf{u} = \text{constant}$ ), the structure moves as a rigid body, but does not stretch or deform internally. For stretching to occur, points within the body must experience *different* displacements.

#### 4.1.1 Infinitesimal strain

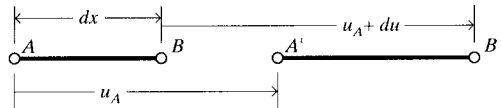


Figure 4.1: Incremental deformation.

Consider two points  $A$  and  $B$  separated initially by a small distance  $dx$  as shown in Fig. 4.1, and experiencing motion in the  $x$  direction. If the displacement at point  $A$  is  $u_A$ , the displacement at  $B$  can be expressed by a Taylor’s series expansion of  $u(x)$  around the point  $x = A$ :

$$u_B = u_A + du = u_A + \frac{\partial u}{\partial x} dx$$

where here the expansion has been truncated after the second term. The *differential* motion  $\delta$  between the two points is then

$$\delta = u_B - u_A = \left( u_A + \frac{\partial u}{\partial x} dx \right) - u_A = \frac{\partial u}{\partial x} dx$$

In our concept of stretching as being the differential displacement per unit length, the  $x$  component of strain is then

$$\epsilon_x = \frac{\delta}{dx} = \frac{\partial u}{\partial x} \quad (4.1)$$

Hence the strain is a *displacement gradient*. Applying similar reasoning to differential motion in the  $y$  direction, the  $y$ -component of strain is the gradient of the vertical displacement  $v$  with respect to  $y$ :

$$\epsilon_y = \frac{\partial v}{\partial y} \quad (4.2)$$

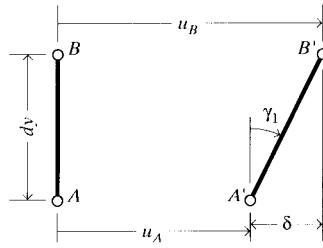


Figure 4.2: Shearing distortion.

The distortion of the material, which can be described as the change in originally right angles, is the sum of the tilts imparted to vertical and horizontal lines. As shown in Fig. 4.2, the tilt of an originally vertical line is the relative horizontal displacement of two nearby points along the line:

$$\delta = u_B - u_A = \left( u_A + \frac{\partial u}{\partial y} dy \right) - u_A = \frac{\partial u}{\partial y} dy$$

The change in angle is then

$$\gamma_1 \approx \tan \gamma_1 = \frac{\delta}{dy} = \frac{\partial u}{\partial y}$$

Similarly (see Fig. 4.3), the tilt  $\gamma_2$  of an originally horizontal line is the gradient of  $v$  with respect to  $x$ . The shear strain in the  $xy$  plane is then

$$\gamma_{xy} = \gamma_1 + \gamma_2 = \frac{\partial v}{\partial x} + \frac{\partial u}{\partial y} \quad (4.3)$$

This notation, using  $\epsilon$  for normal strain and  $\gamma$  for shearing strain, is sometimes known as the “classical” description of strain.

#### 4.1.2 Matrix Formulation

The “indicial notation” described in the Module on Matrix and Index Notation<sup>1</sup> provides a concise method of writing out all the components of three-dimensional states of strain:

<sup>1</sup><http://web.mit.edu/course/3/3.11/www/modules/index.pdf>

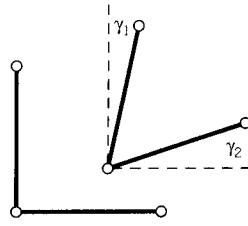


Figure 4.3: Shearing strain.

$$\epsilon_{ij} = \frac{1}{2} \left( \frac{\partial u_i}{\partial x_j} + \frac{\partial u_j}{\partial x_i} \right) \equiv \frac{1}{2} (u_{i,j} + u_{j,i}) \quad (4.4)$$

where the comma denotes differentiation with respect to the following spatial variable. This double-subscript index notation leads naturally to a matrix arrangement of the strain components, in which the  $i$ - $j$  component of the strain becomes the matrix element in the  $i^{\text{th}}$  row and the  $j^{\text{th}}$  column:

$$\epsilon_{ij} = \begin{bmatrix} \frac{\partial u}{\partial x} & \frac{1}{2} \left( \frac{\partial u}{\partial y} + \frac{\partial v}{\partial x} \right) & \frac{1}{2} \left( \frac{\partial u}{\partial z} + \frac{\partial w}{\partial x} \right) \\ \frac{1}{2} \left( \frac{\partial u}{\partial y} + \frac{\partial v}{\partial x} \right) & \frac{\partial v}{\partial y} & \frac{1}{2} \left( \frac{\partial v}{\partial z} + \frac{\partial w}{\partial y} \right) \\ \frac{1}{2} \left( \frac{\partial w}{\partial x} + \frac{\partial u}{\partial z} \right) & \frac{1}{2} \left( \frac{\partial v}{\partial z} + \frac{\partial w}{\partial y} \right) & \frac{\partial w}{\partial z} \end{bmatrix} \quad (4.5)$$

Note that the strain matrix is symmetric, i.e.  $\epsilon_{ij} = \epsilon_{ji}$ . This symmetry means that there are six rather than nine independent strains, as might be expected in a  $3 \times 3$  matrix. Also note that the indicial description of strain yields the same result for the normal components as in the classical description:  $\epsilon_{11} = \epsilon_x$ . However, the indicial components of shear strain are half their classical counterparts:  $\epsilon_{12} = \gamma_{xy}/2$ .

In still another useful notational scheme, the classical strain-displacement equations can be written out in a vertical list, similar to a vector:

$$\begin{Bmatrix} \epsilon_x \\ \epsilon_y \\ \epsilon_z \\ \gamma_{yz} \\ \gamma_{xz} \\ \gamma_{xy} \end{Bmatrix} = \begin{Bmatrix} \partial u / \partial x \\ \partial v / \partial y \\ \partial w / \partial z \\ \partial v / \partial z + \partial w / \partial y \\ \partial u / \partial z + \partial w / \partial x \\ \partial u / \partial y + \partial v / \partial x \end{Bmatrix}$$

This vector-like arrangement of the strain components is for convenience only, and is sometimes called a *pseudovector*. Strain is actually a *second-rank tensor*, like stress or moment of inertia, and has mathematical properties very different than those of vectors. The ordering of the elements in the pseudovector form is arbitrary, but it is conventional to list them as we have here by moving down the diagonal of the strain matrix of Eqn. 4.5 from upper left to lower right, then move up the third column, and finally move one column to the left on the first row; this gives the ordering 1,1; 2,2; 3,3; 2,3; 1,3; 1,2.

Following the rules of matrix multiplication, the strain pseudovector can also be written in

terms of the displacement vector as

$$\left\{ \begin{array}{l} \epsilon_x \\ \epsilon_y \\ \epsilon_z \\ \gamma_{yz} \\ \gamma_{xz} \\ \gamma_{xy} \end{array} \right\} = \left[ \begin{array}{ccc} \partial/\partial x & 0 & 0 \\ 0 & \partial/\partial y & 0 \\ 0 & 0 & \partial/\partial z \\ 0 & \partial/\partial z & \partial/\partial y \\ \partial/\partial z & 0 & \partial/\partial x \\ \partial/\partial y & \partial/\partial x & 0 \end{array} \right] \left\{ \begin{array}{l} u \\ v \\ w \end{array} \right\} \quad (4.6)$$

The matrix in brackets above, whose elements are differential operators, can be abbreviated as  $\mathbf{L}$ :

$$\mathbf{L} = \left[ \begin{array}{ccc} \partial/\partial x & 0 & 0 \\ 0 & \partial/\partial y & 0 \\ 0 & 0 & \partial/\partial z \\ 0 & \partial/\partial z & \partial/\partial y \\ \partial/\partial z & 0 & \partial/\partial x \\ \partial/\partial y & \partial/\partial x & 0 \end{array} \right] \quad (4.7)$$

The strain-displacement equations can then be written in the concise “pseudovector-matrix” form:

$$\boldsymbol{\epsilon} = \mathbf{Lu} \quad (4.8)$$

Equations such as this must be used in a well-defined context, as they apply only when the somewhat arbitrary pseudovector listing of the strain components is used.

#### 4.1.3 Volumetric strain

Since the normal strain is just the change in length per unit of original length, the new length  $L'$  after straining is found as

$$\epsilon = \frac{L' - L_0}{L_0} \Rightarrow L' = (1 + \epsilon)L_0 \quad (4.9)$$

If a cubical volume element, originally of dimension  $abc$ , is subjected to normal strains in all three directions, the change in the element's volume is

$$\begin{aligned} \frac{\Delta V}{V} &= \frac{a'b'c' - abc}{abc} = \frac{a(1 + \epsilon_x) b(1 + \epsilon_y) c(1 + \epsilon_z) - abc}{abc} \\ &= (1 + \epsilon_x)(1 + \epsilon_y)(1 + \epsilon_z) - 1 \approx \epsilon_x + \epsilon_y + \epsilon_z \end{aligned} \quad (4.10)$$

where products of strains are neglected in comparison with individual values. The volumetric strain is therefore the sum of the normal strains, i.e. the sum of the diagonal elements in the strain matrix (this is also called the *trace* of the matrix, or  $\text{Tr}[\boldsymbol{\epsilon}]$ ). In index notation, this can be written simply

$$\frac{\Delta V}{V} = \epsilon_{kk}$$

This is known as the volumetric, or “dilatational” component of the strain.

#### Example 4.1

To illustrate how volumetric strain is calculated, consider a thin sheet of steel subjected to strains in its plane given by  $\epsilon_x = 3$ ,  $\epsilon_y = -4$ , and  $\gamma_{xy} = 6$  (all in  $\mu\text{in/in}$ ). The sheet is not in plane strain, since it can

undergo a Poisson strain in the  $z$  direction given by  $\epsilon_z = -\nu(\epsilon_x + \epsilon_y) = -0.3(3 - 4) = 0.3$ . The total state of strain can therefore be written as the matrix

$$[\boldsymbol{\epsilon}] = \begin{bmatrix} 3 & 6 & 0 \\ 6 & -4 & 0 \\ 0 & 0 & 0.3 \end{bmatrix} \times 10^{-6}$$

where the brackets on the  $[\boldsymbol{\epsilon}]$  symbol emphasize that the matrix rather than pseudovector form of the strain is being used. The volumetric strain is:

$$\frac{\Delta V}{V} = (3 - 4 + 0.3) \times 10^{-6} = -0.7 \times 10^{-6}$$

Engineers often refer to “microinches” of strain; they really mean microinches per inch. In the case of volumetric strain, the corresponding (but awkward) unit would be micro-cubic-inches per cubic inch.

---

## 4.2 Equilibrium: the Stress Relations

The kinematic relations described in the previous section are purely geometric, and do not involve considerations of material behavior. The equilibrium relations to be discussed in this section have this same independence from the material. They are simply Newton’s law of motion, stating that in the absence of acceleration all of the forces acting on a body (or a piece of it) must balance. This allows us to state how the stress within a body, but evaluated just below the surface, is related to the external force applied to the surface. It also governs how the stress varies from position to position within the body.

### 4.2.1 Cauchy stress

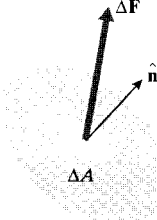


Figure 4.4: Traction vector.

In earlier chapters, we expressed the normal stress as force per unit area acting perpendicularly to a selected area, and a shear stress was a force per unit area acting transversely to the area. To generalize this concept, consider the situation depicted in Fig. 4.4, in which a *traction vector*  $\mathbf{T}$  acts on an arbitrary plane within or on the external boundary of the body, and at an arbitrary direction with respect to the orientation of the plane. The traction is a simple force vector having magnitude and direction, but its magnitude is expressed in terms of force per unit of area:

$$\mathbf{T} = \lim_{\Delta A \rightarrow 0} \left( \frac{\Delta \mathbf{F}}{\Delta A} \right)$$

(4.11)

where  $\Delta A$  is the magnitude of the area on which  $\Delta \mathbf{F}$  acts. The *Cauchy*<sup>2</sup> stresses, which are a generalization of our earlier definitions of stress, are the forces per unit area acting on the Cartesian  $x$ ,  $y$ , and  $z$  planes to balance the traction. In two dimensions this balance can be written by drawing a simple free body diagram with the traction vector acting on an area of arbitrary size  $A$  (Fig. 4.5), remembering to obtain the forces by multiplying by the appropriate area.

$$\sigma_x(A \cos \theta) + \tau_{xy}(A \sin \theta) = T_x A$$

$$\tau_{xy}(A \cos \theta) + \sigma_y(A \sin \theta) = T_y A$$

Cancelling the factor  $A$ , this can be written in matrix form as

$$\begin{bmatrix} \sigma_x & \tau_{xy} \\ \tau_{xy} & \sigma_y \end{bmatrix} \begin{Bmatrix} \cos \theta \\ \sin \theta \end{Bmatrix} = \begin{Bmatrix} T_x \\ T_y \end{Bmatrix} \quad (4.12)$$

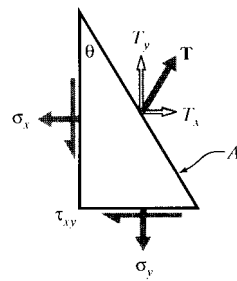


Figure 4.5: Cauchy stress.

### Example 4.2

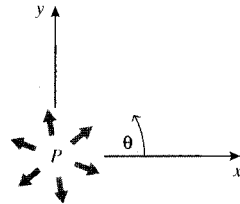


Figure 4.6: Constant pressure on internal circular boundary.

Consider a circular cavity containing an internal pressure  $p$ . The components of the traction vector are then  $T_x = -p \cos \theta$ ,  $T_y = -p \sin \theta$ . The Cartesian Cauchy stresses in the material at the boundary must then satisfy the relations

$$\sigma_x \cos \theta + \tau_{xy} \sin \theta = -p \cos \theta$$

<sup>2</sup>Baron Augustin-Louis Cauchy (1789–1857) was a prolific French engineer and mathematician.

$$\tau_{xy} \cos \theta + \sigma_y \sin \theta = -p \sin \theta$$

At  $\theta = 0$ ,  $\sigma_x = -p$ ,  $\sigma_y = \tau_{xy} = 0$ ; at  $\theta = \pi/2$ ,  $\sigma_y = -p$ ,  $\sigma_x = \tau_{xy} = 0$ . The shear stress  $\tau_{xy}$  vanishes for  $\theta = 0$  or  $\pi/2$ ; in a later section it will be seen that the normal stresses  $\sigma_x$  and  $\sigma_y$  are therefore *principal* stresses at those points.

The vector  $(\cos \theta, \sin \theta)$  on the left hand side of Eqn. 4.12 is also the vector  $\hat{\mathbf{n}}$  of direction cosines of the normal to the plane on which the traction acts, and serves to define the orientation of this plane. This matrix equation, which is sometimes called *Cauchy's relation*, can be abbreviated as

$$[\boldsymbol{\sigma}] \hat{\mathbf{n}} = \mathbf{T} \quad (4.13)$$

The brackets here serve as a reminder that the stress is being written as the square matrix of Eqn. 4.12 rather than in pseudovector form. This relation serves to define the stress concept as an entity that relates the traction (a vector) acting on an arbitrary surface to the orientation of the surface (another vector). The stress is therefore of a higher degree of abstraction than a vector, and is technically a *second-rank tensor*. The difference between vectors (first-rank tensors) and second-rank tensors shows up in how they *transform* with respect to coordinate rotations, which is treated in a later section. As illustrated by the previous example, Cauchy's relation serves both to define the stress and to compute its magnitude at boundaries where the tractions are known.

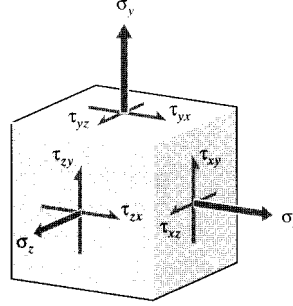


Figure 4.7: Cartesian Cauchy stress components in three dimensions.

In three dimensions, the matrix form of the stress state shown in Fig. 4.7 is the symmetric  $3 \times 3$  array obtained by an obvious extension of the one in Eqn. 4.12:

$$[\boldsymbol{\sigma}] = \sigma_{ij} = \begin{bmatrix} \sigma_x & \tau_{xy} & \tau_{xz} \\ \tau_{xy} & \sigma_y & \tau_{yz} \\ \tau_{xz} & \tau_{yz} & \sigma_z \end{bmatrix} \quad (4.14)$$

The element in the  $i^{th}$  row and the  $j^{th}$  column of this matrix is the stress on the  $i^{th}$  face in the  $j^{th}$  direction. Moment equilibrium requires that the stress matrix be symmetric, so the order of subscripts of the off-diagonal shearing stresses is immaterial.

#### 4.2.2 Differential governing equations

Determining the variation of the stress components as functions of position within the interior of a body is obviously a principal goal in stress analysis. This is a type of *boundary value problem*

often encountered in the theory of differential equations, in which the *gradients* of the variables, rather than the explicit variables themselves, are specified. In the case of stress, the gradients are governed by conditions of static equilibrium: the stresses cannot change arbitrarily between two points  $A$  and  $B$ , or the material between those two points may not be in equilibrium.

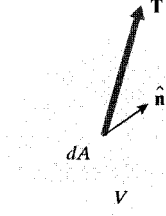


Figure 4.8: Traction vector  $\mathbf{T}$  acting on differential area  $dA$  with direction cosines  $\hat{\mathbf{n}}$ .

To develop this idea formally, we require that the integrated value of the surface traction  $\mathbf{T}$  over the surface  $A$  of an arbitrary volume element  $dV$  within the material (see Fig. 4.8) must sum to zero in order to maintain static equilibrium :

$$0 = \int_A \mathbf{T} dA = \int_A [\boldsymbol{\sigma}] \hat{\mathbf{n}} dA$$

Here we assume the lack of gravitational, centripetal, or other “body” forces acting on material within the volume. The surface integral in this relation can be converted to a volume integral by Gauss’ divergence theorem<sup>3</sup>:

$$\int_V \nabla [\boldsymbol{\sigma}] dV = 0$$

Since the volume  $V$  is arbitrary, this requires that the integrand be zero:

$$\nabla [\boldsymbol{\sigma}] = 0 \quad (4.15)$$

For Cartesian problems in three dimensions, this expands to:

$$\boxed{\begin{aligned} \frac{\partial \sigma_x}{\partial x} + \frac{\partial \tau_{xy}}{\partial y} + \frac{\partial \tau_{xz}}{\partial z} &= 0 \\ \frac{\partial \tau_{xy}}{\partial x} + \frac{\partial \sigma_y}{\partial y} + \frac{\partial \tau_{yz}}{\partial z} &= 0 \\ \frac{\partial \tau_{xz}}{\partial x} + \frac{\partial \tau_{yz}}{\partial y} + \frac{\partial \sigma_z}{\partial z} &= 0 \end{aligned}} \quad (4.16)$$

Using index notation, these can be written:

$$\sigma_{ij,j} = 0 \quad (4.17)$$

Or in pseudovector-matrix form, we can write

$$\left[ \begin{array}{cccccc} \frac{\partial}{\partial x} & 0 & 0 & 0 & \frac{\partial}{\partial z} & \frac{\partial}{\partial y} \\ 0 & \frac{\partial}{\partial y} & 0 & \frac{\partial}{\partial z} & 0 & \frac{\partial}{\partial x} \\ 0 & 0 & \frac{\partial}{\partial z} & \frac{\partial}{\partial y} & \frac{\partial}{\partial x} & 0 \end{array} \right] \left\{ \begin{array}{c} \sigma_x \\ \sigma_y \\ \sigma_z \\ \tau_{yz} \\ \tau_{xz} \\ \tau_{xy} \end{array} \right\} = \left\{ \begin{array}{c} 0 \\ 0 \\ 0 \end{array} \right\} \quad (4.18)$$

<sup>3</sup>Gauss’ Theorem states that  $\int_A X \hat{\mathbf{n}} dA = \int_S \nabla X dV$  where  $X$  is a scalar, vector, or tensor quantity.

Noting that the differential operator matrix in the brackets is just the transpose of the one that appeared in Eqn. 4.7, we can write this as:

$$\mathbf{L}^T \boldsymbol{\sigma} = \mathbf{0} \quad (4.19)$$

### Example 4.3

It isn't hard to come up with functions of stress that satisfy the equilibrium equations; any constant will do, since the stress gradients will then be identically zero. The catch is that they must satisfy the boundary conditions as well, and this complicates things considerably. Methods are available for solving the equations directly, but in some simple cases a solution can be seen by inspection.

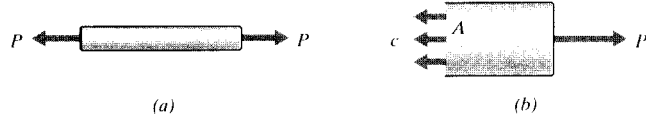


Figure 4.9: A tensile specimen.

Consider a tensile specimen subjected to a load  $P$  as shown in Fig. 4.9. A trial solution that certainly satisfies the equilibrium equations is

$$[\boldsymbol{\sigma}] = \begin{bmatrix} c & 0 & 0 \\ 0 & 0 & 0 \\ 0 & 0 & 0 \end{bmatrix}$$

where  $c$  is a constant we must choose so as to satisfy the boundary conditions. To maintain horizontal equilibrium in the free-body diagram of Fig. 4.9(b), it is immediately obvious that  $cA = P$ , or  $\sigma_x = c = P/A$ . This familiar relation was used in Chapter 1 to define the stress, but we see here that it can be viewed as a consequence of equilibrium considerations rather than a basic definition.

## 4.3 Transformation of Stresses and Strains

One of the most common problems in mechanics of materials involves *transformation of axes*. For instance, we may know the stresses acting on  $xy$  planes, but are really more interested in the stresses acting on planes oriented at, say,  $30^\circ$  to the  $x$  axis as seen in Fig. 4.10, perhaps because these are close-packed atomic planes on which sliding is prone to occur, or is the angle at which two pieces of lumber are glued together in a “scarf” joint. We seek a means to transform the stresses to these new  $x'y'$  planes.

These transformations are vital in analyses of stress and strain, both because they are needed to compute critical values of these entities and also because the tensorial nature of stress and strain is most clearly seen in their transformation properties. Other entities, such as moment of inertia and curvature, also transform in a manner similar to stress and strain. All of these are *second-rank tensors*, an important concept that will be outlined later in this chapter.

### 4.3.1 Direct approach

The rules for stress transformations can be developed directly from considerations of static equilibrium. For illustration, consider the case of uniaxial tension shown in Fig. 4.11 in which all stresses

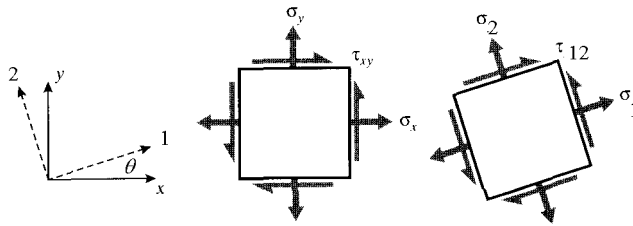


Figure 4.10: Rotation of axes in two dimensions.

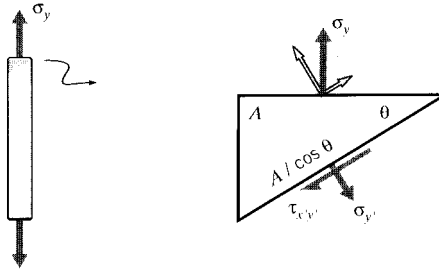


Figure 4.11: An inclined plane in a tensile specimen.

other than  $\sigma_y$  are zero. A free body diagram is then constructed in which the specimen is “cut” along the inclined plane on which the stresses, labeled  $\sigma_{y'}$  and  $\tau_{x'y'}$ , are desired. The key here is to note that the area on which these transformed stresses act is different than the area normal to the  $y$  axis, so that both the areas and the forces acting on them need to be “transformed.” Balancing forces in the  $y'$  direction (the direction normal to the inclined plane):

$$(\sigma_y A) \cos \theta = \sigma_{y'} \left( \frac{A}{\cos \theta} \right)$$

$$\sigma_{y'} = \sigma_y \cos^2 \theta \quad (4.20)$$

Similarly, a force balance in the tangential direction gives

$$\tau_{x'y'} = \sigma_y \sin \theta \cos \theta \quad (4.21)$$

#### Example 4.4

Consider a unidirectionally reinforced composite ply with strengths  $\hat{\sigma}_1$  in the fiber direction,  $\hat{\sigma}_2$  in the transverse direction, and  $\hat{\tau}_{12}$  in shear. As the angle  $\theta$  between the fiber direction and an applied tensile stress  $\sigma_y$  is increased, the stress in the fiber direction will decrease according to Eqn. 4.20. If the ply were to fail by fiber fracture alone, the stress  $\sigma_{y,b}$  needed to cause failure would *increase* with misalignment according to  $\sigma_{y,b} = \hat{\sigma}_1 / \cos^2 \theta$ .

However, the shear stresses as given by Eqn. 4.21 *increase* with  $\theta$ , so the  $\sigma_y$  stress needed for shear failure drops. The strength  $\sigma_{y,b}$  is the smaller of the stresses needed to cause fiber-direction or shear failure, so the strength becomes limited by shear after only a few degrees of misalignment. In fact, a 15° off-axis tensile specimen has been proposed as a means of measuring intralaminar shear strength. When the orientation

angle approaches  $90^\circ$ , failure is dominated by the transverse strength. The experimental data shown in Fig. 4.12 are for glass-epoxy composites<sup>4</sup>, which show good but not exact agreement with these simple expressions.

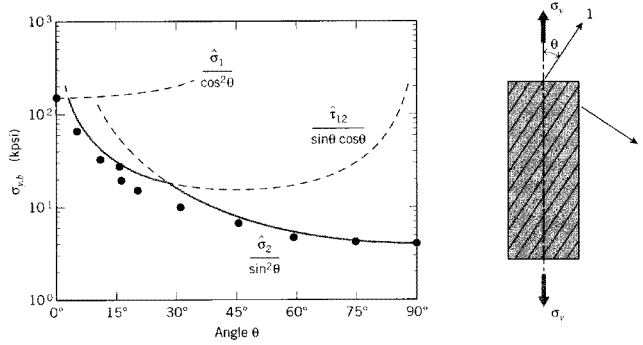


Figure 4.12: Stress applied at an angle to the fibers in a one-dimensional ply.

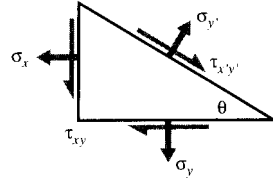


Figure 4.13: Stresses on inclined plane.

A similar approach, but generalized to include stresses  $\sigma_x$  and  $\tau_{xy}$  on the original  $xy$  planes as shown in Fig. 4.13 gives:

$$\boxed{\begin{aligned}\sigma_{x'} &= \sigma_x \cos^2 \theta + \sigma_y \sin^2 \theta + 2\tau_{xy} \sin \theta \cos \theta \\ \sigma_{y'} &= \sigma_x \sin^2 \theta + \sigma_y \cos^2 \theta - 2\tau_{xy} \sin \theta \cos \theta \\ \tau_{x'y'} &= (\sigma_y - \sigma_x) \sin \theta \cos \theta + \tau_{xy} (\cos^2 \theta - \sin^2 \theta)\end{aligned}} \quad (4.22)$$

These relations can be written in pseudovector-matrix form as

$$\left\{ \begin{array}{c} \sigma_{x'} \\ \sigma_{y'} \\ \tau_{x'y'} \end{array} \right\} = \left[ \begin{array}{ccc} c^2 & s^2 & 2sc \\ s^2 & c^2 & -2sc \\ -sc & sc & c^2 - s^2 \end{array} \right] \left\{ \begin{array}{c} \sigma_x \\ \sigma_y \\ \tau_{xy} \end{array} \right\} \quad (4.23)$$

where  $c = \cos \theta$  and  $s = \sin \theta$ . This can be abbreviated as

$$\boldsymbol{\sigma}' = \mathbf{A} \boldsymbol{\sigma} \quad (4.24)$$

where  $\mathbf{A}$  is the transformation matrix in brackets above. This expression would be valid for three dimensional as well as two dimensional stress states, although the particular form of  $\mathbf{A}$  given in Eqn. 4.23 is valid in two dimensions only (plane stress), and for Cartesian coordinates.

<sup>4</sup>R.M. Jones, *Mechanics of Composite Materials*, McGraw-Hill, 1975.

Using either mathematical or geometric arguments, it can be shown that the components of infinitesimal strain transform by *almost* the same relations:

$$\begin{Bmatrix} \epsilon_{x'} \\ \epsilon_{y'} \\ \frac{1}{2}\gamma_{x'y'} \end{Bmatrix} = \mathbf{A} \begin{Bmatrix} \epsilon_x \\ \epsilon_y \\ \frac{1}{2}\gamma_{xy} \end{Bmatrix} \quad (4.25)$$

The factor of 1/2 on the shear components arises from the classical definition of shear strain, which is twice the tensorial shear strain. This introduces some awkwardness into the transformation relations, some of which can be reduced by defining the *Reuter's matrix* as

$$[\mathbf{R}] = \begin{bmatrix} 1 & 0 & 0 \\ 0 & 1 & 0 \\ 0 & 0 & 2 \end{bmatrix} \quad \text{or} \quad [\mathbf{R}]^{-1} = \begin{bmatrix} 1 & 0 & 0 \\ 0 & 1 & 0 \\ 0 & 0 & \frac{1}{2} \end{bmatrix} \quad (4.26)$$

We can now write:

$$\begin{Bmatrix} \epsilon_{x'} \\ \epsilon_{y'} \\ \gamma_{x'y'} \end{Bmatrix} = \mathbf{R} \begin{Bmatrix} \epsilon_x \\ \epsilon_y \\ \frac{1}{2}\gamma_{xy} \end{Bmatrix} = \mathbf{R}\mathbf{A} \begin{Bmatrix} \epsilon_x \\ \epsilon_y \\ \frac{1}{2}\gamma_{xy} \end{Bmatrix} = \mathbf{R}\mathbf{A}\mathbf{R}^{-1} \begin{Bmatrix} \epsilon_x \\ \epsilon_y \\ \gamma_{xy} \end{Bmatrix}$$

Or

$$\boldsymbol{\epsilon}' = \mathbf{R}\mathbf{A}\mathbf{R}^{-1}\boldsymbol{\epsilon} \quad (4.27)$$

As can be verified by expanding this relation, the transformation equations for strain can also be obtained from the stress transformation equations (e.g. Eqn. 4.22) by replacing  $\sigma$  with  $\epsilon$  and  $\tau$  with  $\gamma/2$ :

$\epsilon_{x'} = \epsilon_x \cos^2 \theta + \epsilon_y \sin^2 \theta + \gamma_{xy} \sin \theta \cos \theta$ $\epsilon_{y'} = \epsilon_x \sin^2 \theta + \epsilon_y \cos^2 \theta - \gamma_{xy} \sin \theta \cos \theta$ $\gamma_{x'y'} = 2(\epsilon_y - \epsilon_x) \sin \theta \cos \theta + \gamma_{xy} (\cos^2 \theta - \sin^2 \theta)$	(4.28)
--	--------

### Example 4.5

Consider the biaxial strain state

$$\boldsymbol{\epsilon} = \begin{Bmatrix} \epsilon_{x'} \\ \epsilon_{y'} \\ \gamma_{x'y'} \end{Bmatrix} = \begin{Bmatrix} 0.01 \\ -0.01 \\ 0 \end{Bmatrix}$$

The state of strain  $\boldsymbol{\epsilon}'$  referred to axes rotated by  $\theta = 45^\circ$  from the  $x$ - $y$  axes can be computed by matrix multiplication as:

$$\mathbf{A} = \begin{bmatrix} c^2 & s^2 & 2sc \\ s^2 & c^2 & -2sc \\ -sc & sc & c^2 - s^2 \end{bmatrix} = \begin{bmatrix} 0.5 & 0.5 & 1.0 \\ 0.5 & 0.5 & -1.0 \\ -0.5 & 0.5 & 0.0 \end{bmatrix}$$

Then

$$\begin{aligned} \boldsymbol{\epsilon}' &= \mathbf{R}\mathbf{A}\mathbf{R}^{-1}\boldsymbol{\epsilon} \\ &= \begin{bmatrix} 1.0 & 0.0 & 0.0 \\ 0.0 & 1.0 & 0.0 \\ 0.0 & 0.0 & 2.0 \end{bmatrix} \begin{bmatrix} 0.5 & 0.5 & 1.0 \\ 0.5 & 0.5 & -1.0 \\ -0.5 & 0.5 & 0.0 \end{bmatrix} \begin{bmatrix} 1.0 & 0.0 & 0.0 \\ 0.0 & 1.0 & 0.0 \\ 0.0 & 0.0 & 0.5 \end{bmatrix} = \begin{Bmatrix} 0.00 \\ 0.00 \\ -0.02 \end{Bmatrix} \end{aligned}$$

Obviously, the matrix multiplication method is tedious unless matrix-handling software is available, in which case it becomes very convenient.

### 4.3.2 Mohr's circle

Everyday experience with such commonplace occurrences as pushing objects at an angle gives us all a certain intuitive sense of how vector transformations work. Second-rank tensor transformations seem more abstract at first, and a device to help visualize them is of great value. As it happens, the transformation equations have a famous (among engineers) graphical interpretation known as *Mohr's circle*<sup>5</sup>. The Mohr procedure is justified mathematically by using the trigonometric double-angle relations to show that Eqns. 4.22 have a circular representation, but it can probably best be learned simply by memorizing the following recipe<sup>6</sup>:

1. Draw the stress square, noting the values on the  $x$  and  $y$  faces; Fig. 4.14(a) shows a hypothetical case for illustration. *For the purpose of Mohr's circle only*, regard a shear stress acting in a clockwise-rotation sense as being positive, and counter-clockwise as negative. The shear stresses on the  $x$  and  $y$  faces must then have opposite signs. The normal stresses are positive in tension and negative in compression, as usual.

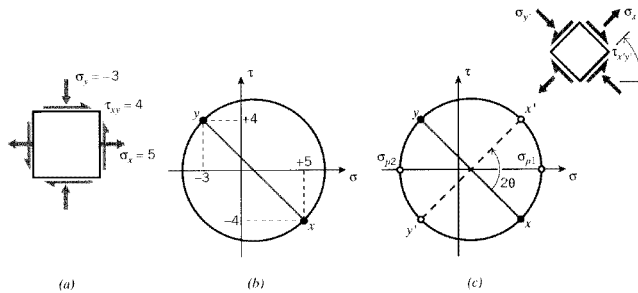


Figure 4.14: Stress square (a) and Mohr's circle (b) for  $\sigma_x = +5$ ,  $\sigma_y = -3$ ,  $\tau_{xy} = +4$ . (c) Stress state on inclined plane.

2. Construct a graph with  $\tau$  as the ordinate ( $y$  axis) and  $\sigma$  as abscissa, and plot the stresses on the  $x$  and  $y$  faces of the stress square as two points on this graph. Since the shear stresses on these two faces are the negative of one another, one of these points will be above the  $\sigma$ -axis exactly as far as the other is below. It is helpful to label the two points as  $x$  and  $y$ .
3. Connect these two points with a straight line. It will cross the  $\sigma$  axis at the line's midpoint. This point will be at  $(\sigma_x + \sigma_y)/2$ , which in our illustration is  $[5 + (-3)]/2 = 1$ .
4. Place the point of a compass at the line's midpoint, and set the pencil at the end of the line. Draw a circle with the line as a diameter. The completed circle for our illustrative stress state is shown in Fig. 4.14(b).

<sup>5</sup>Presented in 1900 by the German engineer Otto Mohr (1835–1918).

<sup>6</sup>An interactive web demonstration of Mohr's circle construction is available at <http://web.mit.edu/course/3/3.11/www/java/mohr.html>.

5. To determine the stresses on a stress square that has been rotated through an angle  $\theta$  with respect to the original square, rotate the diametral line *in the same direction* through twice this angle; i.e.  $2\theta$ . The new end points of the line can now be labeled  $x'$  and  $y'$ , and their  $\sigma$ - $\tau$  values are the stresses on the rotated  $x'$ - $y'$  axes as shown in Fig. 4.14(c).

There is nothing mysterious or magical about the Mohr's circle; it is simply a device to help visualize how stresses and other second-rank tensors change when the axes are rotated.

It is clear in looking at the Mohr's circle in Fig. 4.14(c) that there is something special about axis rotations that cause the diametral line to become either horizontal or vertical. In the first case, the normal stresses assume maximal values and the shear stresses are zero. These normal stresses are known as the *principal* stresses,  $\sigma_{p1}$  and  $\sigma_{p2}$ , and the planes on which they act are the *principal* planes. If the material is prone to fail by tensile cracking, it will do so by cracking along the principal planes when the value of  $\sigma_{p1}$  exceeds the tensile strength.

#### Example 4.6

It is instructive to use a Mohr's circle construction to predict how a piece of blackboard chalk will break in torsion, and then verify it in practice. The torsion produces a state of pure shear as shown in Fig. 4.15, which causes the principal planes to appear at  $\pm 45^\circ$  to the chalk's long axis. The crack will appear transverse to the principal tensile stress, producing a spiral-like failure surface. (As the crack progresses into the chalk, the state of pure shear is replaced by a more complicated stress distribution, so the last part of the failure surface deviates from this ideal path to one running along the axial direction.) This is the same type of fracture that occurred all too often in skiers' femurs, before the advent of modern safety bindings.

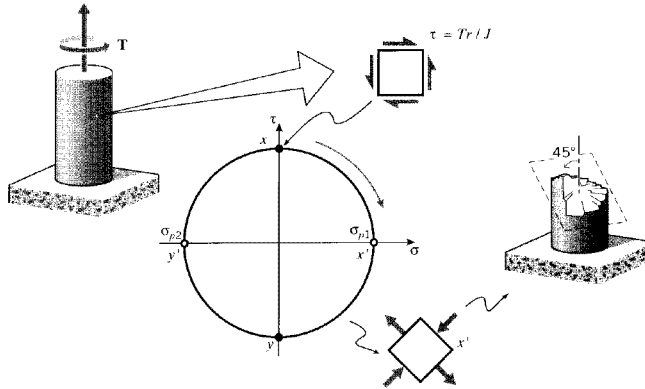


Figure 4.15: Mohr's circle for simple torsion.

By direct Pythagorean construction as shown in Fig. 4.16, the Mohr's circle shows that the angle from the  $x$ - $y$  axes to the principal planes is

$$\tan 2\theta_p = \frac{\tau_{xy}}{(\sigma_x - \sigma_y)/2} \quad (4.29)$$

and the values of the principal stresses are

$$\sigma_{p1,p2} = \frac{\sigma_x + \sigma_y}{2} \pm \sqrt{\left(\frac{\sigma_x - \sigma_y}{2}\right)^2 + \tau_{xy}^2} \quad (4.30)$$

where the first term above is the  $\sigma$ -coordinate of the circle's center, and the second is its radius.

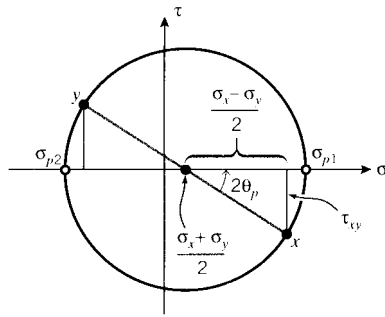


Figure 4.16: Principal stresses on Mohr's circle.

When the Mohr's circle diametral line is vertical, the shear stresses become maximum, equal in magnitude to the radius of the circle:

$$\tau_{\max} = \sqrt{\left(\frac{\sigma_x - \sigma_y}{2}\right)^2 + \tau_{xy}^2} = \frac{\sigma_{p1} - \sigma_{p2}}{2} \quad (4.31)$$

The points of maximum shear are  $90^\circ$  away from the principal stress points on the Mohr's circle, so on the actual specimen the planes of maximum shear are  $45^\circ$  from the principal planes. The molecular sliding associated with yield is driven by shear, and usually takes place on the planes of maximum shear. A tensile specimen has principal planes along and transverse to its loading direction, so shear slippage will occur on planes  $\pm 45^\circ$  from the loading direction. These slip planes can often be observed as "shear bands" on the specimen.

Note that normal stresses may appear on the planes of maximum shear, so the situation is not quite the converse of the principal planes, on which the shear stresses vanish while the normal stresses are maximum. If the normal stresses happen to vanish on the planes of maximum shear, the stress state is said to be one of "pure shear," such as is induced by simple torsion. A state of pure shear is therefore one for which a rotation of axes exists such that the normal stresses vanish, which is possible only if the center of the Mohr's circle is at the origin, i.e.  $(\sigma_x + \sigma_y)/2 = 0$ . More generally, a state of pure shear is one in which the trace of the stress (and strain) matrix vanishes.

---

### Example 4.7

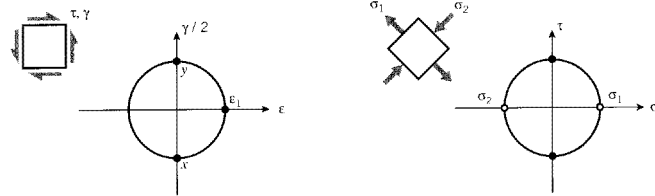


Figure 4.17: Strain and stress Mohr's circles for simple shear.

Mohr's circles can be drawn for strains as well as stresses, with shear strain plotted on the ordinate and normal strain on the abscissa. However, the ordinate must be  $\gamma/2$  rather than just  $\gamma$ , due to the way classical infinitesimal strains are defined. Consider a state of pure shear with strain  $\gamma$  and stress  $\tau$  as shown

in Fig. 4.17, such as might be produced by placing a circular shaft in torsion. A Mohr's circle for strain quickly shows the principal strain, on a plane  $45^\circ$  away, is given by  $\epsilon_1 = \gamma/2$ . Hooke's law for shear gives  $\tau = G\gamma$ , so  $\epsilon_1 = \tau/2G$ . The principal strain is also related to the principal stresses by

$$\epsilon_1 = \frac{1}{E}(\sigma_1 - \nu\sigma_2)$$

The Mohr's circle for stress gives  $\sigma_1 = -\sigma_2 = \tau$ , so this can be written

$$\frac{\tau}{2G} = \frac{1}{E}[\tau - \nu(-\tau)]$$

Cancelling  $\tau$  and rearranging, we have the relation among elastic constants stated earlier without proof:

$$G = \frac{E}{2(1 + \nu)}$$


---

### 4.3.3 General Approach

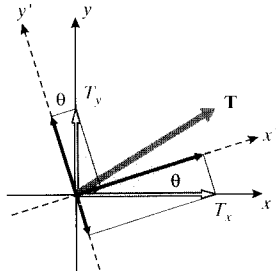


Figure 4.18: Transformation of vectors.

Another approach to the stress transformation equations, capable of easy extension to three dimensions, starts with the familiar relations by which *vectors* are transformed in two dimensions (see Fig. 4.18):

$$T_{x'} = T_x \cos \theta + T_y \sin \theta$$

$$T_{y'} = -T_x \sin \theta + T_y \cos \theta$$

In matrix form, this is

$$\begin{Bmatrix} T_{x'} \\ T_{y'} \end{Bmatrix} = \begin{bmatrix} \cos \theta & \sin \theta \\ -\sin \theta & \cos \theta \end{bmatrix} \begin{Bmatrix} T_x \\ T_y \end{Bmatrix}$$

or

$$\mathbf{T}' = \mathbf{a}\mathbf{T} \quad (4.32)$$

where  $\mathbf{a}$  is another transformation matrix that serves to transform the vector components in the original coordinate system to those in the primed system. In index-notation terms, this could also be denoted  $a_{ij}$ , so that

$$T'_i = a_{ij}T_j$$

The individual elements of  $a_{ij}$  are the cosines of the angles between the  $i^{th}$  primed axis and the  $j^{th}$  unprimed axis.

It can be shown by direct examination that the  $\mathbf{a}$  matrix has the useful property that its inverse equals its transpose; i.e.,  $\mathbf{a}^{-1} = \mathbf{a}^T$ . We can multiply Eqn. 4.32 by  $\mathbf{a}^T$  to give

$$\mathbf{a}^T \mathbf{T}' = (\mathbf{a}^T \mathbf{a}) \mathbf{T} = \mathbf{T} \quad (4.33)$$

so the transformation can go from primed to unprimed, or the reverse.

These relations can be extended to yield an expression for transformation of stresses (or strains, or moments of inertia, or other similar quantities). Recall Cauchy's relation in matrix form:

$$[\boldsymbol{\sigma}] \hat{\mathbf{n}} = \mathbf{T}$$

Using Eqn. 4.33 to transform the  $\hat{\mathbf{n}}$  and  $\mathbf{T}$  vectors into their primed counterparts, we have

$$[\boldsymbol{\sigma}] \mathbf{a}^T \hat{\mathbf{n}}' = \mathbf{a}^T \mathbf{T}'$$

Multiplying through by  $\mathbf{a}$ :

$$(\mathbf{a}[\boldsymbol{\sigma}] \mathbf{a}^T) \hat{\mathbf{n}}' = (\mathbf{a} \mathbf{a}^T) \mathbf{T}' = \mathbf{T}'$$

This is just Cauchy's relation again, but in the primed coordinate frame. The quantity in parentheses must therefore be  $[\boldsymbol{\sigma}']$ :

$$[\boldsymbol{\sigma}'] = \mathbf{a}[\boldsymbol{\sigma}] \mathbf{a}^T \quad (4.34)$$

Therefore, transformation of stresses and can be done by pre- and postmultiplying by the same transformation matrix applicable to vector transformation. This can also be written out using index notation, which provides another illustration of the transformation differences between scalars (zero-rank tensors), vectors (first-rank tensors), and second-rank tensors:

$$\begin{aligned} \text{rank 0: } & b' = b \\ \text{rank 1: } & T'_i = a_{ij} T_j \\ \text{rank 2: } & \sigma'_{ij} = a_{ij} a_{kl} \sigma_{kl} \end{aligned} \quad (4.35)$$

In practical work, it is not always a simple matter to write down the nine elements of the  $\mathbf{a}$  matrix needed in Eqn. 4.34. The squares of the components of  $\hat{\mathbf{n}}$  for any given plane must sum to unity, and in order for the three planes of the transformed stress cube to be mutually perpendicular the dot product between any two plane normals must vanish. So not just any nine numbers will make sense. Obtaining  $\mathbf{a}$  is made much easier by using "Euler angles" to describe axis transformations in three dimensions.

As shown in Fig. 4.19, the final transformed axes are visualized as being achieved in three steps: first, rotate the original  $x$ - $y$ - $z$  axes by an angle  $\psi$  (psi) around the  $z$ -axis to obtain a new frame we may call  $x'$ - $y'$ - $z$ . Next, rotate this new frame by an angle  $\theta$  about the  $x'$  axis to obtain another frame we can call  $x''$ - $y''$ - $z'$ . Finally, rotate this frame by an angle  $\phi$  (phi) around the  $z'$  axis to obtain the final frame  $x'''$ - $y'''$ - $z'$ . These three transformations correspond to the transformation matrix

$$\mathbf{a} = \begin{bmatrix} \cos \psi & \sin \psi & 0 \\ -\sin \psi & \cos \psi & 0 \\ 0 & 0 & 1 \end{bmatrix} \begin{bmatrix} 1 & 0 & 0 \\ 0 & \cos \theta & \sin \theta \\ 0 & -\sin \theta & \cos \theta \end{bmatrix} \begin{bmatrix} \cos \phi & \sin \phi & 0 \\ -\sin \phi & \cos \phi & 0 \\ 0 & 0 & 1 \end{bmatrix}$$

This multiplication would certainly be a pain if done manually, but is a natural for a computational approach.

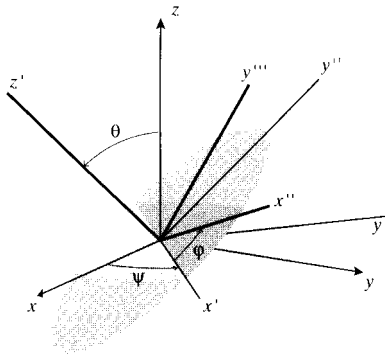


Figure 4.19: Transformation in terms of Euler angles.

---

**Example 4.8**

The output below shows a computer evaluation of a three-dimensional stress transformation, in this case using Maple<sup>TM</sup> symbolic mathematics software.

```
# read linear algebra library
> with(linalg):
# Define Euler-angle transformation matrices:
> a1:=array(1..3,1..3,[[cos(psi),sin(psi),0],[-sin(psi),cos(psi),0],[0,0
> ,1]]);
      [cos(psi)      sin(psi)      0]
      a1 := [-sin(psi)    cos(psi)      0]
              [ 0           0           1]
> a2:=array(1..3,1..3,[[1,0,0],[0,cos(theta),sin(theta)],[0,-sin(theta),
> cos(theta)]]);
      [1           0           0       ]
      a2 := [0           cos(theta)   sin(theta)]
              [0           -sin(theta)  cos(theta)]
> a3:=array(1..3,1..3,[[cos(phi),sin(phi),0],[-sin(phi),cos(phi),0],[0,0
> ,1]]);
      [cos(phi)      sin(phi)      0]
      a3 := [-sin(phi)    cos(phi)      0]
              [ 0           0           1]
# Overall transformation matrix (multiply individual Euler matrices):
> a:=a1&*a2&*a3;
      a := (a1 &* a2) &* a3
# Set precision and read in Euler angles (converted to radians); here
# we are rotating 30 degrees around the z axis only.
> Digits:=4;psi:=0;theta:=30*(Pi/180);phi:=0;
      Digits := 4
      psi := 0
      theta := 1/6 Pi
      phi := 0
# Display transformation matrix for these angles: "evalf" evaluates the
# matrix element, and "map" applies the evaluation to each element of
# the matrix.
```

```

> aa:=map(evalf,evalm(a));
      [1.          0.          0.  ]
      aa := [0.          .8660       .5000]
              [0.          -.5000       .8660]
# Define the stress matrix in the unprimed frame:
> sigma:=array(1..3,1..3,[[1,2,3],[2,4,5],[3,5,6]]);
      [1    2    3]
      sigma := [2    4    5]
              [3    5    6]
# The stress matrix in the primed frame is then given by Eqn. 15:
> 'sigma_prime'=map(evalf,evalm(aa&&*sigma&&*transpose(aa)));
      [ 1.          3.232       1.598]
      sigma_prime = [3.232       8.830       3.366]
                  [1.598       3.366       1.170]

```

---

#### 4.3.4 Principal Stresses and Planes in Three Dimensions

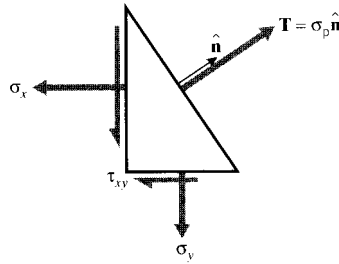


Figure 4.20: Traction vector normal to principal plane.

The Mohr's circle procedure is not capable of finding principal stresses for three-dimensional stress states, and a more general method is needed. In three dimensions, we seek orientations of axes such that no shear stresses appear, leaving only normal stresses in three orthogonal directions. The vanishing of shear stresses on a plane means that the stress vector  $\mathbf{T}$  is normal to the plane, illustrated in two dimensions in Fig. 4.20. The traction vector can therefore be written as

$$\mathbf{T} = \sigma_p \hat{\mathbf{n}}$$

where  $\sigma_p$  is a simple scalar quantity, the *magnitude* of the stress vector. Using this in Cauchy's relation:

$$\boldsymbol{\sigma} \hat{\mathbf{n}} = \mathbf{T} = \sigma_p \hat{\mathbf{n}}$$

$$(\boldsymbol{\sigma} - \sigma_p \mathbf{I}) \hat{\mathbf{n}} = \mathbf{0} \quad (4.36)$$

Here  $\mathbf{I}$  is the unit matrix. This system will have a nontrivial solution ( $\hat{\mathbf{n}} \neq \mathbf{0}$ ) only if its determinant is zero:

$$|\boldsymbol{\sigma} - \sigma_p \mathbf{I}| = \begin{vmatrix} \sigma_x - \sigma_p & \tau_{xy} & \tau_{xz} \\ \tau_{xy} & \sigma_y - \sigma_p & \tau_{yz} \\ \tau_{xz} & \tau_{yz} & \sigma_z - \sigma_p \end{vmatrix} = \mathbf{0}$$

Expanding the determinant yields a cubic polynomial equation in  $\sigma_p$ :

$$f(\sigma_p) = \sigma_p^3 - I_1\sigma_p^2 + I_2\sigma_p - I_3 = 0 \quad (4.37)$$

This is the *characteristic equation* for stress, where the coefficients are

$$I_1 = \sigma_x + \sigma_y + \sigma_z = \sigma_{kk} \quad (4.38)$$

$$I_2 = \sigma_x\sigma_y + \sigma_x\sigma_z + \sigma_y\sigma_z - \tau_{xy}^2 - \tau_{yz}^2 - \tau_{xz}^2 = \frac{1}{2} (\sigma_{ii}\sigma_{jj} - \sigma_{ij}\sigma_{ij}) \quad (4.39)$$

$$I_3 = \det |\boldsymbol{\sigma}| = \frac{1}{3} \sigma_{ij} \sigma_{jk} \sigma_{ki} \quad (4.40)$$

These  $I$  parameters are known as the *invariants* of the stress state; they do not change with transformation of the coordinates and can be used to characterize the overall nature of the stress. For instance  $I_1$ , which has been identified earlier as the trace of the stress matrix, will be seen in a later section to be a measure of the tendency of the stress state to induce hydrostatic dilation or compression. We have already noted that the stress state is one of pure shear if its trace vanishes.

Since the characteristic equation is cubic in  $\sigma_p$ , it will have three roots, and it can be shown that all three roots must be real. These roots are just the principal stresses  $\sigma_{p1}$ ,  $\sigma_{p2}$ , and  $\sigma_{p3}$ .

### Example 4.9

Consider a state of simple shear with  $\tau_{xy} = 1$  and all other stresses zero:

$$[\boldsymbol{\sigma}] = \begin{bmatrix} 0 & 1 & 0 \\ 1 & 0 & 0 \\ 0 & 0 & 0 \end{bmatrix}$$

The invariants are

$$I_1 = 0, \quad I_2 = -1, \quad I_3 = 0$$

and the characteristic equation is

$$\sigma_p^3 - \sigma_p = 0$$

This equation has roots of (-1,0,1) corresponding to principal stresses  $\sigma_{p1} = 1$ ,  $\sigma_{p2} = 0$ ,  $\sigma_{p3} = -1$ , and is plotted in Fig. 4.21. This is the same stress state considered in Example 4.6, and the roots of the characteristic equation agree with the principal values shown by the Mohr's circle.

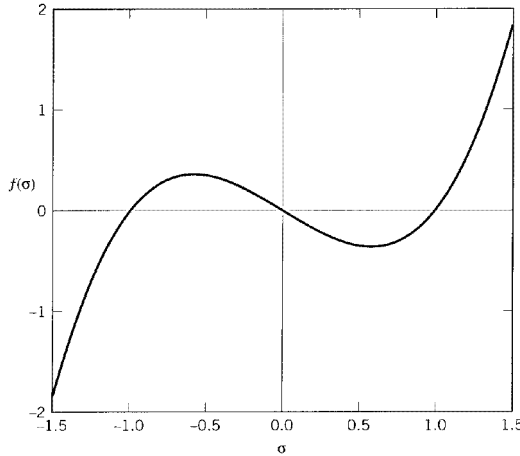


Figure 4.21: The characteristic equation for  $\tau_{xy} = 1$ , all other stresses zero.

## 4.4 Constitutive Relations

The previous sections in this chapter contain concepts vital to Mechanics of Materials, but they do not provide insight on the role of the material itself. The kinematic equations relate strains to displacement gradients, and the equilibrium equations relate stress to the applied tractions on loaded boundaries and also govern the relations among stress gradients within the material. In three dimensions there are six kinematic equations and three equilibrium equations, for a total of nine. However, there are fifteen variables: three displacements, six strains, and six stresses. We need six more equations, and these are provided by the material's *constitutive* relations: six expressions relating the stresses to the strains. These are a sort of mechanical equation of state, and describe how the material is *constituted mechanically*.

With these constitutive relations, the vital role of the material is reasserted: The elastic constants that appear in this chapter are material properties, subject to control by processing and microstructural modification. This is an important tool for the engineer, and points up the necessity of considering design *of* the material as well as *with* the material.

### 4.4.1 Isotropic Elastic Materials

In the general case of a linear relation between components of the strain and stress tensors, we might propose a statement of the form

$$\epsilon_{ij} = S_{ijkl} \sigma_{kl}$$

where the  $S_{ijkl}$  is a *fourth-rank* tensor. This constitutes a sequence of nine equations, since each component of  $\epsilon_{ij}$  is a linear combination of all the components of  $\sigma_{ij}$ . For instance:

$$\epsilon_{23} = S_{2311} \sigma_{11} + S_{2312} \sigma_{12} + \cdots + S_{2333} \epsilon_{33}$$

Based on each of the indices of  $S_{ijkl}$  taking on values from 1 to 3, we might expect a total of 81 independent components in  $S$ . However, both  $\epsilon_{ij}$  and  $\sigma_{ij}$  are symmetric, with six rather than nine independent components each. This reduces the number of  $S$  components to 36, as can be seen from a linear relation between the pseudovector forms of the strain and stress:

$$\begin{Bmatrix} \epsilon_x \\ \epsilon_y \\ \epsilon_z \\ \gamma_{yz} \\ \gamma_{xz} \\ \gamma_{xy} \end{Bmatrix} = \begin{bmatrix} S_{11} & S_{12} & \cdots & S_{16} \\ S_{21} & S_{22} & \cdots & S_{26} \\ \vdots & \vdots & \ddots & \vdots \\ S_{61} & S_{26} & \cdots & S_{66} \end{bmatrix} \begin{Bmatrix} \sigma_x \\ \sigma_y \\ \sigma_z \\ \tau_{yz} \\ \tau_{xz} \\ \tau_{xy} \end{Bmatrix} \quad (4.41)$$

It can be shown<sup>7</sup> that the  $\mathbf{S}$  matrix in this form is also symmetric. It therefore it contains only 21 independent elements, as can be seen by counting the elements in the upper right triangle of the matrix, including the diagonal elements ( $1 + 2 + 3 + 4 + 5 + 6 = 21$ ).

If the material exhibits symmetry in its elastic response, the number of independent elements in the  $\mathbf{S}$  matrix can be reduced still further. In the simplest case of an *isotropic* material, whose stiffnesses are the same in all directions, only *two* elements are independent. We have earlier shown that in two dimensions the relations between strains and stresses in isotropic materials can be written as

$$\begin{aligned} \epsilon_x &= \frac{1}{E}(\sigma_x - \nu\sigma_y) \\ \epsilon_y &= \frac{1}{E}(\sigma_y - \nu\sigma_x) \\ \gamma_{xy} &= \frac{1}{G}\tau_{xy} \end{aligned} \quad (4.42)$$

along with the relation

$$G = \frac{E}{2(1+\nu)}$$

Extending this to three dimensions, the pseudovector-matrix form of Eqn. 4.41 for isotropic materials is

$$\begin{Bmatrix} \epsilon_x \\ \epsilon_y \\ \epsilon_z \\ \gamma_{yz} \\ \gamma_{xz} \\ \gamma_{xy} \end{Bmatrix} = \begin{bmatrix} \frac{1}{E} & \frac{-\nu}{E} & \frac{-\nu}{E} & 0 & 0 & 0 \\ \frac{-\nu}{E} & \frac{1}{E} & \frac{-\nu}{E} & 0 & 0 & 0 \\ \frac{-\nu}{E} & \frac{-\nu}{E} & \frac{1}{E} & 0 & 0 & 0 \\ 0 & 0 & 0 & \frac{1}{G} & 0 & 0 \\ 0 & 0 & 0 & 0 & \frac{1}{G} & 0 \\ 0 & 0 & 0 & 0 & 0 & \frac{1}{G} \end{bmatrix} \begin{Bmatrix} \sigma_x \\ \sigma_y \\ \sigma_z \\ \tau_{yz} \\ \tau_{xz} \\ \tau_{xy} \end{Bmatrix} \quad (4.43)$$

The quantity in brackets is called the *compliance matrix* of the material, denoted  $\mathbf{S}$  or  $S_{ij}$ . It is important to grasp the physical significance of its various terms. Directly from the rules of matrix multiplication, the element in the  $i^{\text{th}}$  row and  $j^{\text{th}}$  column of  $S_{ij}$  is the contribution of the  $j^{\text{th}}$  stress to the  $i^{\text{th}}$  strain. For instance the component in the 1,2 position is the contribution of the  $y$ -direction stress to the  $x$ -direction strain: multiplying  $\sigma_y$  by  $1/E$  gives the  $y$ -direction strain generated by  $\sigma_y$ , and then multiplying this by  $-\nu$  gives the Poisson strain induced in the  $x$  direction. The zero elements show the lack of coupling between the normal and shearing components.

The isotropic constitutive law can also be written using index notation as

$$\epsilon_{ij} = \frac{1+\nu}{E}\sigma_{ij} - \frac{\nu}{E}\delta_{ij}\sigma_{kk} \quad (4.44)$$

where here the indicial form of strain is used and  $G$  has been eliminated using  $G = E/2(1+\nu)$ . The symbol  $\delta_{ij}$  is the *Kronecker delta*, described in the Module on Matrix and Index Notation.

---

<sup>7</sup>G.M. Mase, *Schaum's Outline of Theory and Problems of Continuum Mechanics*, McGraw-Hill, 1970.

If we wish to write the stresses in terms of the strains, Eqns. 4.43 can be inverted. In cases of plane stress ( $\sigma_z = \tau_{xz} = \tau_{yz} = 0$ ), this yields

$$\begin{Bmatrix} \sigma_x \\ \sigma_y \\ \tau_{xy} \end{Bmatrix} = \frac{E}{1-\nu^2} \begin{bmatrix} 1 & \nu & 0 \\ \nu & 1 & 0 \\ 0 & 0 & (1-\nu)/2 \end{bmatrix} \begin{Bmatrix} \epsilon_x \\ \epsilon_y \\ \gamma_{xy} \end{Bmatrix} \quad (4.45)$$

where again  $G$  has been replaced by  $E/2(1+\nu)$ . Or, in abbreviated notation:

$$\boldsymbol{\sigma} = \mathbf{D}\boldsymbol{\epsilon} \quad (4.46)$$

where  $\mathbf{D} = \mathbf{S}^{-1}$  is the *stiffness matrix*.

#### 4.4.2 Hydrostatic and Distortional Components

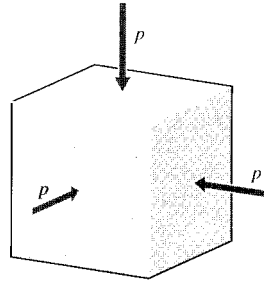


Figure 4.22: Hydrostatic compression.

A state of hydrostatic compression, depicted in Fig. 4.22, is one in which no shear stresses exist and where all the normal stresses are equal to the hydrostatic pressure:

$$\sigma_x = \sigma_y = \sigma_z = -p$$

where the minus sign indicates that compression is conventionally positive for pressure but negative for stress. For this stress state it is obviously true that

$$\frac{1}{3}(\sigma_x + \sigma_y + \sigma_z) = \frac{1}{3}\sigma_{kk} = -p$$

so that the hydrostatic pressure is the negative *mean normal stress*. This quantity is just one third of the stress invariant  $I_1$ , which is a reflection of hydrostatic pressure being the same in all directions, not varying with axis rotations.

In many cases other than direct hydrostatic compression, it is still convenient to “dissociate” the hydrostatic (or “dilatational”) component from the stress tensor:

$$\sigma_{ij} = \frac{1}{3}\sigma_{kk}\delta_{ij} + \Sigma_{ij} \quad (4.47)$$

Here  $\Sigma_{ij}$  is what is left over from  $\sigma_{ij}$  after the hydrostatic component is subtracted. The  $\Sigma_{ij}$  tensor can be shown to represent a state of pure shear, i.e. there exists an axis transformation such that all normal stresses vanish. The  $\Sigma_{ij}$  is called the distortional, or deviatoric, component of the stress. Hence all stress states can be thought of as having two components as shown in Fig. 4.23, one

purely extensional and one purely distortional. This concept is convenient because the material responds to these stress components in very different ways. For instance, plastic and viscous flow is driven dominantly by distortional components, with the hydrostatic component causing only elastic deformation.

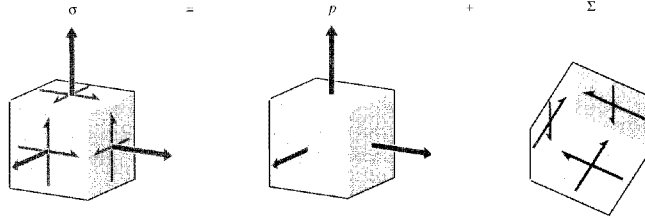


Figure 4.23: Dilatational and deviatoric components of the stress tensor.

---

### Example 4.10

Consider the stress state

$$\sigma = \begin{bmatrix} 5 & 6 & 7 \\ 6 & 8 & 9 \\ 7 & 9 & 2 \end{bmatrix}, \text{ GPa}$$

The mean normal stress is  $\sigma_{kk}/3 = (5 + 8 + 2)/3 = 5$ , so the stress decomposition is

$$\sigma = \frac{1}{3} \sigma_{kk} \delta_{ij} + \Sigma_{ij} = \begin{bmatrix} 5 & 0 & 0 \\ 0 & 5 & 0 \\ 0 & 0 & 5 \end{bmatrix} + \begin{bmatrix} 0 & 6 & 7 \\ 6 & 3 & 9 \\ 7 & 9 & -3 \end{bmatrix}$$

It is not obvious that the deviatoric component given in the second matrix represents pure shear, since there are nonzero components on its diagonal. However, a stress transformation using Euler angles  $\psi = \phi = 0, \theta = -9.22^\circ$  gives the stress state

$$\Sigma' = \begin{bmatrix} 0.00 & 4.80 & 7.87 \\ 4.80 & 0.00 & 9.49 \\ 7.87 & 9.49 & 0.00 \end{bmatrix}$$


---

The hydrostatic component of stress is related to the volumetric strain through the modulus of compressibility ( $-p = K \Delta V/V$ ), so

$$\frac{1}{3} \sigma_{kk} = K \epsilon_{kk} \quad (4.48)$$

Similarly to the stress, the strain can also be dissociated as

$$\epsilon_{ij} = \frac{1}{3} \epsilon_{kk} \delta_{ij} + e_{ij}$$

where  $e_{ij}$  is the deviatoric component of strain. The deviatoric components of stress and strain are related by the material's shear modulus:

$$\Sigma_{ij} = 2G e_{ij} \quad (4.49)$$

where the factor 2 is needed because tensor descriptions of strain are half the classical strains for which values of  $G$  have been tabulated. Writing the constitutive equations in the form of Eqns. 4.48 and 4.49 produces a simple form without the coupling terms in the conventional  $E$ - $\nu$  form.

---

### Example 4.11

Using the stress state of the previous example along with the elastic constants for steel ( $E = 207$  GPa,  $\nu = 0.3$ ,  $K = E/3(1 - 2\nu) = 173$  GPa,  $G = E/2(1 + \nu) = 79.6$  GPa), the dilatational and distortional components of strain are

$$\delta_{ij}\epsilon_{kk} = \frac{\delta_{ij}\sigma_{kk}}{3K} = \begin{bmatrix} 0.0289 & 0 & 0 \\ 0 & 0.0289 & 0 \\ 0 & 0 & 0.0289 \end{bmatrix}$$

$$e_{ij} = \frac{\Sigma_{ij}}{2G} = \begin{bmatrix} 0 & 0.0378 & 0.0441 \\ 0.0378 & 0.0189 & 0.0567 \\ 0.0441 & 0.0567 & -0.0189 \end{bmatrix}$$

The total strain is then

$$\epsilon_{ij} = \frac{1}{3}\epsilon_{kk}\delta_{ij} + e_{ij} = \begin{bmatrix} 0.00960 & 0.0378 & 0.0441 \\ 0.0378 & 0.0285 & 0.0567 \\ 0.0441 & 0.0567 & -0.00930 \end{bmatrix}$$

If we evaluate the total strain using Eqn. 4.44, we have

$$\epsilon_{ij} = \frac{1+\nu}{E}\sigma_{ij} - \frac{\nu}{E}\delta_{ij}\sigma_{kk} = \begin{bmatrix} 0.00965 & 0.0377 & 0.0440 \\ 0.0377 & 0.0285 & 0.0565 \\ 0.0440 & 0.0565 & -0.00915 \end{bmatrix}$$

These results are the same, differing only by roundoff error.

---

#### 4.4.3 Anisotropic materials

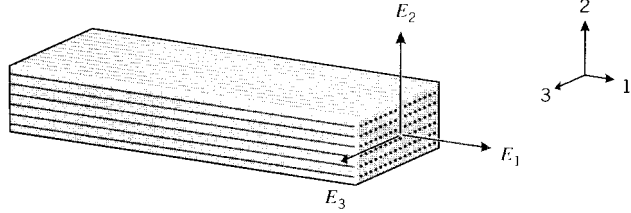


Figure 4.24: An orthotropic material.

If the material has a texture like wood or unidirectionally-reinforced fiber composites as shown in Fig. 4.24, the modulus  $E_1$  in the fiber direction will typically be larger than those in the transverse directions ( $E_2$  and  $E_3$ ). When  $E_1 \neq E_2 \neq E_3$ , the material is said to be *orthotropic*. It is common, however, for the properties in the plane transverse to the fiber direction to be isotropic to a good approximation ( $E_2 = E_3$ ); such a material is called *transversely isotropic*. The elastic constitutive laws must be modified to account for this anisotropy, and the following form is an extension of Eqn. 4.43 for transversely isotropic materials:

$$\begin{Bmatrix} \epsilon_1 \\ \epsilon_2 \\ \gamma_{12} \end{Bmatrix} = \begin{bmatrix} 1/E_1 & -\nu_{21}/E_2 & 0 \\ -\nu_{12}/E_1 & 1/E_2 & 0 \\ 0 & 0 & 1/G_{12} \end{bmatrix} \begin{Bmatrix} \sigma_1 \\ \sigma_2 \\ \tau_{12} \end{Bmatrix} \quad (4.50)$$

The parameter  $\nu_{12}$  is the *principal Poisson's ratio*; it is the ratio of the strain induced in the 2-direction by a strain applied in the 1-direction. This parameter is not limited to values less than 0.5 as in isotropic materials. Conversely,  $\nu_{21}$  gives the strain induced in the 1-direction by a strain applied in the 2-direction. Since the 2-direction (transverse to the fibers) usually has much less stiffness than the 1-direction, it should be clear that a given strain in the 1-direction will usually develop a much larger strain in the 2-direction than will the same strain in the 2-direction induce a strain in the 1-direction. Hence we will usually have  $\nu_{12} > \nu_{21}$ . There are five constants in the above equation ( $E_1$ ,  $E_2$ ,  $\nu_{12}$ ,  $\nu_{21}$  and  $G_{12}$ ). However, only four of them are independent; since the  $S$  matrix is symmetric,  $\nu_{21}/E_2 = \nu_{12}/E_1$ .

A table of elastic constants and other properties for widely used anisotropic materials can be found at the end of this chapter.

The simple form of Eqn. 4.50, with zeroes in the terms representing coupling between normal and shearing components, is obtained only when the axes are aligned along the *principal material directions*; i.e. along and transverse to the fiber axes. If the axes are oriented along some other direction, all terms of the compliance matrix will be populated, and the symmetry of the material will not be evident. If for instance the fiber direction is off-axis from the loading direction, the material will develop shear strain as the fibers try to orient along the loading direction as shown in Fig. 4.25. There will therefore be a coupling between a normal stress and a shearing strain, which never occurs in an isotropic material.

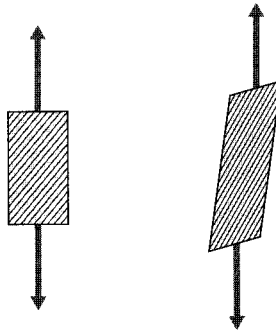


Figure 4.25: Shear-normal coupling.

The transformation law for compliance can be developed from the transformation laws for strains and stresses, using the procedures described earlier. By successive transformations, the pseudovector form for strain in an arbitrary  $x$ - $y$  direction shown in Fig. 4.26 is related to strain in the 1-2 (principal material) directions, then to the stresses in the 1-2 directions, and finally to the stresses in the  $x$ - $y$  directions. The final grouping of transformation matrices relating the  $x$ - $y$  strains to the  $x$ - $y$  stresses is then the transformed compliance matrix in the  $x$ - $y$  direction:

$$\begin{Bmatrix} \epsilon_x \\ \epsilon_y \\ \gamma_{xy} \end{Bmatrix} = \mathbf{R} \begin{Bmatrix} \epsilon_x \\ \epsilon_y \\ \frac{1}{2}\gamma_{xy} \end{Bmatrix} = \mathbf{R}\mathbf{A}^{-1} \begin{Bmatrix} \epsilon_1 \\ \epsilon_2 \\ \frac{1}{2}\gamma_{12} \end{Bmatrix} = \mathbf{R}\mathbf{A}^{-1}\mathbf{R}^{-1} \begin{Bmatrix} \epsilon_1 \\ \epsilon_2 \\ \gamma_{12} \end{Bmatrix}$$

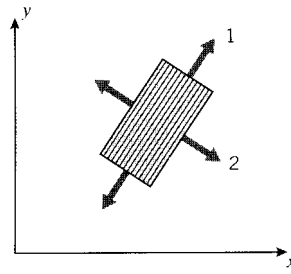


Figure 4.26: Axis transformation for constitutive equations.

$$= \mathbf{R} \mathbf{A}^{-1} \mathbf{R}^{-1} \mathbf{S} \begin{Bmatrix} \sigma_1 \\ \sigma_2 \\ \tau_{12} \end{Bmatrix} = \mathbf{R} \mathbf{A}^{-1} \mathbf{R}^{-1} \mathbf{S} \mathbf{A} \begin{Bmatrix} \sigma_x \\ \sigma_y \\ \tau_{xy} \end{Bmatrix} \equiv \bar{\mathbf{S}} \begin{Bmatrix} \sigma_x \\ \sigma_y \\ \tau_{xy} \end{Bmatrix}$$

where  $\bar{\mathbf{S}}$  is the *transformed compliance matrix* relative to  $x$ - $y$  axes. Here  $\mathbf{A}$  is the transformation matrix, and  $\mathbf{R}$  is the Reuter's matrix defined in Eqn. 4.26. The inverse of  $\bar{\mathbf{S}}$  is  $\bar{\mathbf{D}}$ , the stiffness matrix relative to  $x$ - $y$  axes:

$$\boxed{\bar{\mathbf{S}} = \mathbf{R} \mathbf{A}^{-1} \mathbf{R}^{-1} \mathbf{S} \mathbf{A}, \quad \bar{\mathbf{D}} = \bar{\mathbf{S}}^{-1}} \quad (4.51)$$

### Example 4.12

Consider a ply of Kevlar-epoxy composite with a stiffnesses  $E_1 = 82$ ,  $E_2 = 4$ ,  $G_{12} = 2.8$  (all GPa) and  $\nu_{12} = 0.25$ . The compliance matrix  $\mathbf{S}$  in the 1-2 (material) direction is:

$$\mathbf{S} = \begin{bmatrix} 1/E_1 & -\nu_{21}/E_2 & 0 \\ -\nu_{12}/E_1 & 1/E_2 & 0 \\ 0 & 0 & 1/G_{12} \end{bmatrix} = \begin{bmatrix} .1220 \times 10^{-10} & -.3050 \times 10^{-11} & 0 \\ -.3050 \times 10^{-11} & .2500 \times 10^{-9} & 0 \\ 0 & 0 & .3571 \times 10^{-9} \end{bmatrix}$$

If the ply is oriented with the fiber direction (the “1” direction) at  $\theta = 30^\circ$  from the  $x$ - $y$  axes, the appropriate transformation matrix is

$$\mathbf{A} = \begin{bmatrix} c^2 & s^2 & 2sc \\ s^2 & c^2 & -2sc \\ -sc & sc & c^2 - s^2 \end{bmatrix} = \begin{bmatrix} .7500 & .2500 & .8660 \\ .2500 & .7500 & -.8660 \\ -.4330 & .4330 & .5000 \end{bmatrix}$$

The compliance matrix relative to the  $x$ - $y$  axes is then

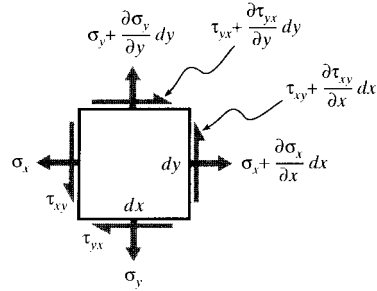
$$\bar{\mathbf{S}} = \mathbf{R} \mathbf{A}^{-1} \mathbf{R}^{-1} \mathbf{S} \mathbf{A} = \begin{bmatrix} .8830 \times 10^{-10} & -.1970 \times 10^{-10} & -.1222 \times 10^{-9} \\ -.1971 \times 10^{-10} & .2072 \times 10^{-9} & -.8371 \times 10^{-10} \\ -.1222 \times 10^{-9} & -.8369 \times 10^{-10} & -.2905 \times 10^{-9} \end{bmatrix}$$

Note that this matrix is symmetric (to within numerical roundoff error), but that nonzero coupling values exist. A user not aware of the internal composition of the material would consider it completely anisotropic.

The apparent engineering constants that would be observed if the ply were tested in the  $x$ - $y$  rather than 1-2 directions can be found directly from the transformed  $\bar{\mathbf{S}}$  matrix. For instance, the apparent elastic modulus in the  $x$  direction is  $E_x = 1/\bar{\mathbf{S}}_{1,1} = 1/(.8830 \times 10^{-10}) = 11.33$  GPa.

## 4.5 Problems

1. Write out the abbreviated strain-displacement equation  $\boldsymbol{\epsilon} = \mathbf{L}\mathbf{u}$  (Eqn. 4.8) for two dimensions.
2. Develop the two-dimensional form of the Cartesian equilibrium equations by drawing a free-body diagram of an infinitesimal section:



*Prob. 2*

3. Draw the Mohr's circles and determine the magnitudes of the principal stresses for the following stress states. Denote the principal stress state on a suitably rotated stress square.
  - (a)  $\sigma_x = 30$  MPa,  $\sigma_y = -10$  MPa,  $\tau_{xy} = 25$  MPa.
  - (b)  $\sigma_x = -30$  MPa,  $\sigma_y = -90$  MPa,  $\tau_{xy} = -40$  MPa.
  - (c)  $\sigma_x = -10$  MPa,  $\sigma_y = 20$  MPa,  $\tau_{xy} = -15$  MPa.
4. (a) Write out the compliance matrix  $\mathbf{S}$  of Eqn. 4.43 for polycarbonate using data in the Module on Material Properties.
- (b) Use matrix inversion to obtain the stiffness matrix  $\mathbf{D}$ .
- (c) Use matrix multiplication to obtain the stresses needed to induce the strains

$$\boldsymbol{\epsilon} = \begin{Bmatrix} \epsilon_x \\ \epsilon_y \\ \epsilon_z \\ \gamma_{yz} \\ \gamma_{xz} \\ \gamma_{xy} \end{Bmatrix} = \begin{Bmatrix} 0.02 \\ 0.0 \\ 0.03 \\ 0.01 \\ 0.025 \\ 0.0 \end{Bmatrix}$$

# Chapter 5

## Yield and Plastic Flow

In our overview of the tensile stress-strain curve in Chapter 1, we described yield as a permanent molecular rearrangement that begins at a sufficiently high stress, denoted  $\sigma_Y$  in Fig. 5.1. The yielding process is very material-dependent, being related directly to molecular mobility. It is often possible to control the yielding process by optimizing the materials processing in a way that influences mobility. General purpose polystyrene, for instance, is a weak and brittle plastic often credited with giving plastics a reputation for shoddiness that plagued the industry for years. This occurs because polystyrene at room temperature has so little molecular mobility that it experiences brittle fracture at stresses less than those needed to induce yield with its associated ductile flow. But when that same material is blended with rubber particles of suitable size and composition, it becomes so tough that it is used for batting helmets and ultra-durable children's toys. This magic is done by control of the yielding process. Yield control to balance strength against toughness is one of the most important aspects of materials engineering for structural applications, and all engineers should be aware of the possibilities.

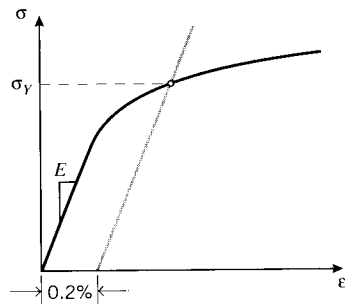


Figure 5.1: Yield stress  $\sigma_Y$  as determined by the 0.2% offset method.

Another important reason for understanding yield is more prosaic: if the material is not allowed to yield, it is not likely to fail. This is not true of brittle materials such as ceramics that fracture before they yield, but in most of the tougher structural materials no damage occurs before yield. It is common design practice to size the structure so as to keep the stresses in the elastic range, short of yield by a suitable safety factor. We therefore need to be able to predict when yielding will occur in general multidimensional stress states, given an experimental value of  $\sigma_Y$ .

Fracture is driven by *normal* stresses, acting to separate one atomic plane from another. Yield, conversely, is driven by *shearing* stresses, sliding one plane along another. These two distinct

mechanisms are illustrated in Fig. 5.2. Of course, bonds must be broken during the sliding associated with yield, but unlike in fracture are allowed to reform in new positions. This process can generate substantial change in the material, even leading eventually to fracture (as in bending a metal rod back and forth repeatedly to break it). The “plastic” deformation that underlies yielding is essentially a viscous flow process, and follows kinetic laws quite similar to liquids. Like flow in liquids, plastic flow usually takes place without change in volume, corresponding to Poisson’s ratio  $\nu = 1/2$ .

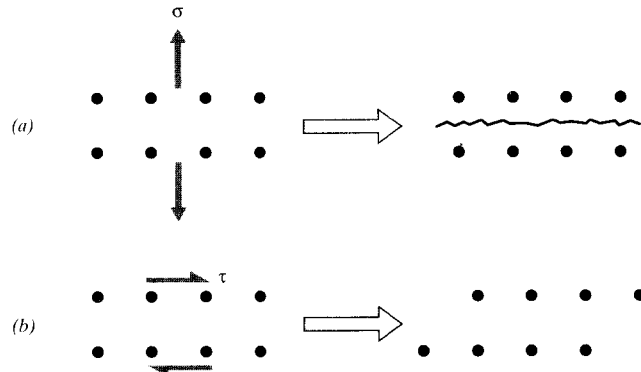


Figure 5.2: Cracking is caused by normal stresses (a), sliding is caused by shear stresses (b).

## 5.1 Multiaxial Stress States

The yield stress  $\sigma_Y$  is usually determined in a tensile test, where a single uniaxial stress acts. However, the engineer must be able to predict when yield will occur in more complicated real-life situations involving multiaxial stresses. This is done by use of a *yield criterion*, an observation derived from experimental evidence as to just what it is about the stress state that causes yield. One of the simplest of these criteria, known as the maximum shear stress or *Tresca* criterion, states that yield occurs when the maximum shear stress reaches a critical value  $\tau_{max} = k$ . The numerical value of  $k$  for a given material could be determined directly in a pure-shear test, such as torsion of a circular shaft, but it can also be found indirectly from the tension test as well. As shown in Fig. 5.3, Mohr’s circle shows that the maximum shear stress acts on a plane  $45^\circ$  away from the tensile axis, and is half the tensile stress in magnitude; then  $k = \sigma_Y/2$ .

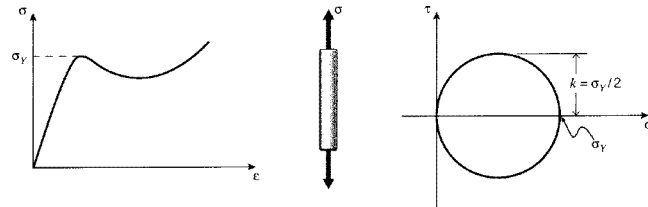


Figure 5.3: Mohr’s circle construction for yield in uniaxial tension.

In cases of plane stress, Mohr’s circle gives the maximum shear stress *in that plane* as half the difference of the principal stresses:

$$\boxed{\tau_{max} = \frac{\sigma_{p1} - \sigma_{p2}}{2}} \quad (5.1)$$

---

**Example 5.1**

Using  $\sigma_{p1} = \sigma_\theta = pr/b$  and  $\sigma_{p2} = \sigma_z = pr/2b$  in Eqn. 5.1, the shear stress in a cylindrical pressure vessel with closed ends is

$$\tau_{max,\theta z} = \frac{1}{2} \left( \frac{pr}{b} - \frac{pr}{2b} \right) = \frac{pr}{4b}$$

where the  $\theta z$  subscript indicates a shear stress in a plane tangential to the vessel wall. Based on this, we might expect the pressure vessel to yield when

$$\tau_{max,\theta z} = k = \frac{\sigma_Y}{2}$$

which would occur at a pressure of

$$p_Y = \frac{4b\tau_{max,\theta z}}{r} = \frac{2b\sigma_Y}{r}$$

However, this analysis is in error, as can be seen by drawing Mohr's circles not only for the  $\theta z$  plane but for the  $\theta r$  and  $r z$  planes as well as shown in Fig. 5.4.

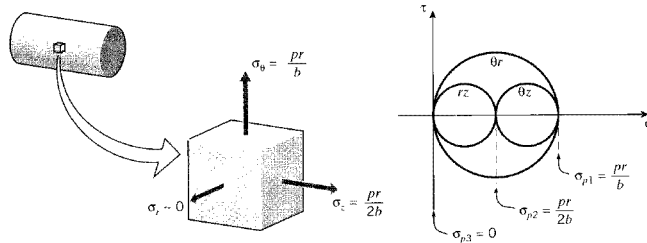


Figure 5.4: Principal stresses and Mohr's circle for closed-end pressure vessel

The shear stresses in the  $\theta r$  plane are seen to be twice those in the  $\theta z$  plane, since in the  $\theta r$  plane the second principal stress is zero:

$$\tau_{max,\theta r} = \frac{1}{2} \left( \frac{pr}{b} - 0 \right) = \frac{pr}{2b}$$

Yield will therefore occur in the  $\theta r$  plane at a pressure of  $b\sigma_Y/r$ , half the value needed to cause yield in the  $\theta z$  plane. Failing to consider the shear stresses acting in this third direction would lead to a seriously underdesigned vessel.

---

Situations similar to this example occur in plane stress whenever the principal stresses in the  $xy$  plane are of the same sign (both tensile or both compressive). The maximum shear stress, which controls yield, is half the *difference* between the principal stresses; if they are both of the same sign, an even larger shear stress will occur on the perpendicular plane containing the larger of the principal stresses in the  $xy$  plane.

This concept can be used to draw a “yield locus” as shown in Fig. 5.5, an envelope in  $\sigma_1$ - $\sigma_2$  coordinates outside of which yield is predicted. This locus obviously crosses the coordinate axes at values corresponding to the tensile yield stress  $\sigma_Y$ . In the I and III quadrants the principal stresses

are of the same sign, so according to the maximum shear stress criterion yield is determined by the difference between the larger principal stress and zero. In the II and IV quadrants the locus is given by  $\tau_{max} = |\sigma_1 - \sigma_2|/2 = \sigma_Y/2$ , so  $\sigma_1 - \sigma_2 = \text{const}$ ; this gives straight diagonal lines running from  $\sigma_Y$  on one axis to  $-\sigma_Y$  on the other.

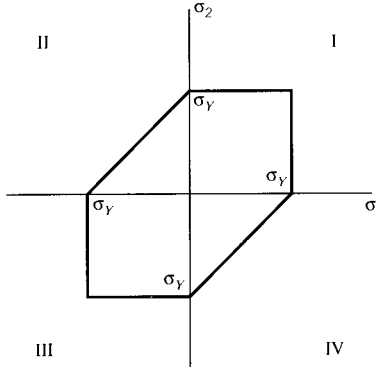


Figure 5.5: Yield locus for the maximum-shear stress criterion.

---

### Example 5.2

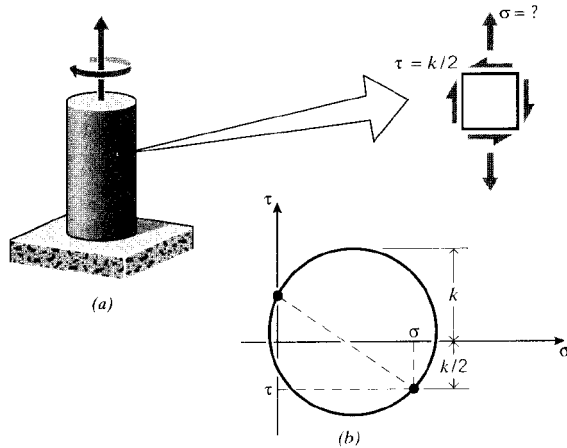


Figure 5.6: (a) Circular shaft subjected to simultaneous twisting and tension. (b) Mohr's circle construction.

A circular shaft is subjected to a torque of half that needed to cause yielding as shown in Fig. 5.6; we now ask what tensile stress could be applied simultaneously without causing yield.

A Mohr's circle is drawn with shear stress  $\tau = k/2$  and unknown tensile stress  $\sigma$ . Using the Tresca maximum-shear yield criterion, yield will occur when  $\sigma$  is such that

$$\begin{aligned}\tau_{max} &= k = \sqrt{\left(\frac{\sigma}{2}\right)^2 + \left(\frac{k}{2}\right)^2} \\ \sigma &= \sqrt{3}k\end{aligned}$$

---

The Tresca criterion is convenient to use in practice, but a somewhat better fit to experimental data can often be obtained from the “von Mises” criterion, in which the driving force for yield is the strain energy associated with the deviatoric components of stress. The *von Mises stress* (also called the *equivalent* or *effective* stress) is defined as

$$\sigma_M = \sqrt{\frac{1}{2} [(\sigma_x - \sigma_y)^2 + (\sigma_x - \sigma_z)^2 + (\sigma_y - \sigma_z)^2 + 6(\tau_{xy} + \tau_{yz} + \tau_{xz})]}$$

In terms of the principal stresses this is

$$\sigma_M = \sqrt{\frac{1}{2} [(\sigma_1 - \sigma_2)^2 + (\sigma_1 - \sigma_3)^2 + (\sigma_2 - \sigma_3)^2]}$$

where the stress differences in parentheses are proportional to the maximum shear stresses on the three principal planes<sup>1</sup>. (Since the quantities are squared, the order of stresses inside the parentheses is unimportant.) The Mises stress can also be written in compact form in terms of the second invariant of the deviatoric stress tensor  $\Sigma_{ij}$ :

$$\sigma_M = \sqrt{3\Sigma_{ij}\Sigma_{ij}/2} \quad (5.2)$$

It can be shown that this is proportional to the total distortional strain energy in the material, and also to the shear stress  $\tau_{oct}$  on the “octahedral” plane oriented equally to the 1-2-3 axes. The von Mises stress is the driving force for damage in many ductile engineering materials, and is routinely computed by most commercial finite element stress analysis codes.

The value of von Mises stress  $\sigma_{M,Y}$  needed to cause yield can be determined from the tensile yield stress  $\sigma_Y$ , since in tension at the yield point we have  $\sigma_1 = \sigma_Y$ ,  $\sigma_2 = \sigma_3 = 0$ . Then

$$\sigma_{M,Y} = \sqrt{\frac{1}{2} [(\sigma_Y - 0)^2 + (\sigma_Y - 0)^2 + (0 - 0)^2]} = \sigma_Y$$

Hence the value of von Mises stress needed to cause yield is the same as the simple tensile yield stress.

The shear yield stress  $k$  can similarly be found by inserting the principal stresses corresponding to a state of pure shear in the Mises equation. Using  $k = \sigma_1 = -\sigma_3$  and  $\sigma_2 = 0$ , we have

$$\sqrt{\frac{1}{2} [(k - 0)^2 + (k + k)^2 + (0 - k)^2]} = \sqrt{\frac{6k^2}{2}} = \sigma_Y$$

$$k = \frac{\sigma_Y}{\sqrt{3}}$$

Note that this result is different than the Tresca case, in which we had  $k = \sigma_Y/2$ .

The von Mises criterion can be plotted as a yield locus as well. Just as the Tresca criterion, it must pass through  $\sigma_Y$  on each axis. However, it plots as an ellipse rather than the prismatic shape of the Tresca criterion (see Fig. 5.7).

---

<sup>1</sup>Some authors use a factor other than 1/2 within the radical. This is immaterial, since it will be absorbed by the calculation of the critical value of  $\sigma_M$ .

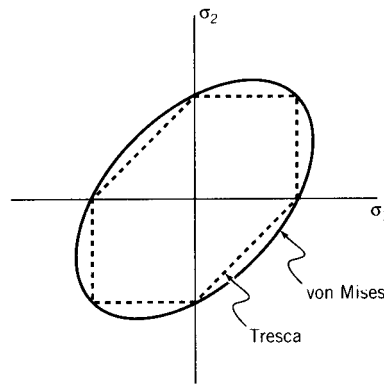


Figure 5.7: Yield locus for the von Mises criterion.

## 5.2 Effect of Hydrostatic Pressure

Since in the discussion up to now yield has been governed only by shear stress, it has not mattered whether a uniaxial stress is compressive or tensile; yield occurs when  $\sigma = \pm\sigma_Y$ . This corresponds to the hydrostatic component of the stress  $-p = (\sigma_x + \sigma_y + \sigma_z)/3$  having no influence on yield, which is observed experimentally to be valid for slip in metallic systems. Polymers, however, are much more resistant to yielding in compressive stress states than in tension. The atomistic motions underlying slip in polymers can be viewed as requiring “free volume” as the molecular segments move, and this free volume is diminished by compressive stresses. It is thus difficult to form solid polymers by deformation processing such as stamping and forging in the same way steel can be shaped; this is one reason the vast majority of automobile body panels continue to be made of steel rather than plastic.

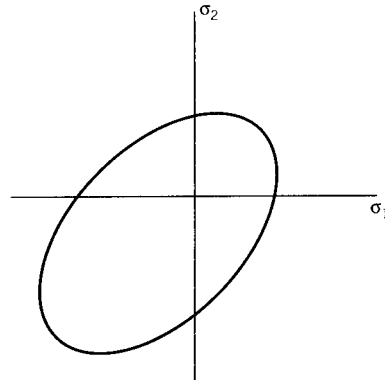


Figure 5.8: Effect of pressure on the von Mises yield envelope.

This dependency on hydrostatic stress can be modeled by modifying the yield criterion to state that yield occurs when

$$\tau_{max} \text{ or } \sigma_M \geq \tau_0 + Ap \quad (5.3)$$

where  $\tau_0$  and  $A$  are constants. As  $p$  increases (the hydrostatic component of stress becomes more

positive) the shear stress needed for yield becomes greater as well, since there is less free volume and more hindrance to molecular motion. The effect of this modification is to slide the von Mises ellipse to extend less into the I quadrant and more into the III quadrant as shown in Fig. 5.8. This shows graphically that greater stresses are needed for yield in compression, and lesser stresses in tension.

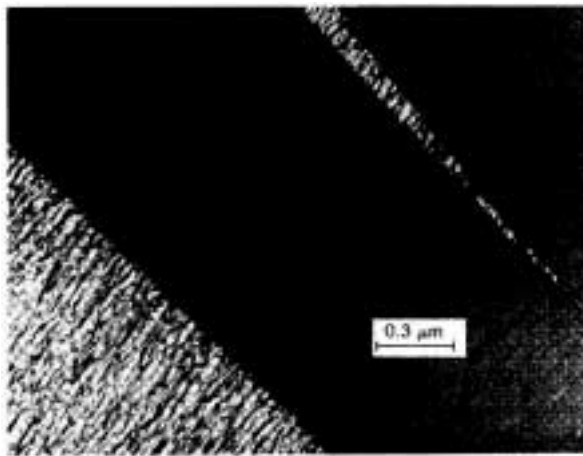


Figure 5.9: A craze in polystyrene (from R. Kambour, “Crazing,” *Encyclopedia of Polymer Science and Engineering*, Wiley-Interscience, 1991).

Several amorphous glassy polymers — notably polystyrene, polymethylmethacrylate, and polycarbonate — are subject to a yield mechanism termed “crazing” in which long elongated voids are created within the material by a tensile cavitation process. Figure 5.9 shows a craze in polystyrene, grown in plasticizing fluid near  $T_g$ . The voids, or crazes, are approximately 1000 Å thick and microns or more in length, and appear visually to be much like conventional cracks. They differ from cracks, however, in that the broad faces of the crazes are spanned by a great many elongated fibrils that have been drawn from the polymer as the craze opens. The fibril formation requires shear flow, but the process is also very dependent on free volume. A successful multiaxial stress criterion for crazing that incorporates both these features has been proposed<sup>2</sup> of the form

$$\sigma_1 - \sigma_2 = A(T) + \frac{B(T)}{\sigma_1 + \sigma_2}$$

The left hand side of this relation is proportional to the shear stress, and the denominator in the second term on the right hand side is related to the hydrostatic component of the stress. As the hydrostatic tension increases, the shear needed to cause crazing decreases. The parameters  $A$  and  $B$  are adjustable, and both depend on temperature. This relation plots as a batwing on the yield locus diagram as seen in Fig. 5.10, approaching a 45° diagonal drawn through the II and IV quadrants. Crazing occurs to the right of the curve; note that crazing never occurs in compressive stress fields.

Crazing is a yield mechanism, but it also precipitates brittle fracture as the craze height increases and the fibrils are brought to rupture. The point where the craze locus crosses the shear yielding locus is therefore a type of mechanically induced ductile-brittle transition, as the failure mode switches from shear yielding to craze embrittlement. Environmental agents such as acetone that

<sup>2</sup>S. Sternstein and L. Ongchin, *Polymer Preprints*, **10**, 1117, 1969.

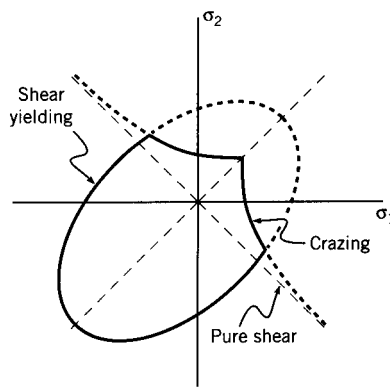


Figure 5.10: The Sternstein envelopes for crazing and pressure-inhibited shear yielding.

expand the free volume in these polymers greatly exacerbate the tendency for craze brittleness. Conversely, modifications such as rubber particle inclusions that stabilize the crazes and prevent them from becoming true cracks can provide remarkable toughness. Rubber particles not only stabilize crazes, they also cause a great increase in the number of crazes, so the energy absorption of craze formation can add to the toughness as well. This is the basis of the “high impact polystyrene,” or HIPS, mentioned at the outset of this chapter.

### 5.3 Effect of Rate and Temperature

The yield process can be viewed as competing with fracture, and whichever process has the lowest stress requirements will dominate. As the material is made less and less mobile, for instance by lowering the temperature or increasing the number and tightness of chemical bonds, yielding becomes more and more difficult. The fracture process is usually much less dependent on mobility. Both yield and fracture stresses usually increase with decreasing temperature, but yield is more temperature-dependent (see Fig. 5.11). This implies that below a critical temperature (called the ductile-brittle transition temperature  $T_{DB}$ ) the material will fracture before it yields. Several notable failures in ships and pipelines have occurred during winter temperatures when the steels used in their manufacture were stressed below their  $T_{DB}$  and were thus unable to resist catastrophic crack growth. In polymers, the ductile-brittle transition temperature is often coincident with the glass transition temperature. Clearly, we need an engineering model capable of showing how yield depends on temperature, and one popular approach is outlined below.

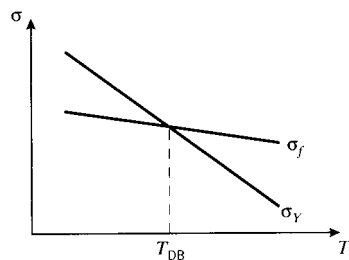


Figure 5.11: Schematic illustration of the temperature dependence of yield and fracture stress.

Yield processes are thermally activated, stress driven motions, much like the flow of viscous liquids. Even without going into much detail as to the specifics of the motions, it is possible to write down quite effective expressions for the dependency of these motions on strain rate and temperature. In the Eyring view of thermally activated processes, an energy barrier  $E_Y^*$  must be overcome for the motion to proceed. (We shall use the asterisk superscript to indicate activation parameters, and the  $Y$  subscript here indicates the yield process.) A stress acts to lower the barrier when it acts in the direction of flow, and to raise it when it opposes the flow.

Consider now a constant strain rate test ( $\dot{\epsilon} = \text{const}$ ), in which the stress rises until yield occurs at  $\sigma = \sigma_Y$ . At the yield point we have  $d\sigma/d\epsilon = 0$ , so a fluidlike state is achieved in which an increment of strain can occur without a corresponding incremental increase in stress. Analogously with rate theories for viscous flow, an Eyring rate equation can be written for the yielding process as

$$\boxed{\dot{\epsilon} = \dot{\epsilon}_0 \exp \frac{-(E_Y^* - \sigma_Y V^*)}{kT}} \quad (5.4)$$

Here  $k$  is Boltzman's constant and  $V^*$  is a factor governing the effectiveness of the stress in reducing the activation barrier. It must have units of volume for the product  $\sigma_Y V^*$  to have units of energy, and is called the "activation volume" of the process. Taking logs and rearranging,

$$\frac{\sigma_Y}{T} = \frac{E_Y^*}{V^* T} + \left( \frac{k}{V^*} \right) \ln \left( \frac{\dot{\epsilon}}{\dot{\epsilon}_0} \right)$$

Hence plots of  $\sigma_Y/T$  versus  $\ln \dot{\epsilon}$  should be linear with a slope  $k/V^*$  as seen in Fig. 5.12, from which the activation volume may be computed. The horizontal spacing between two lines at differing temperatures  $T_1$  and  $T_2$  gives the activation energy:

$$E_Y^* = \frac{k (\ln \dot{\epsilon}^{T_2} - \ln \dot{\epsilon}^{T_1})}{\left( \frac{1}{T_1} - \frac{1}{T_2} \right)}$$

Apparent activation volumes in polymers are on the order of  $5000\text{\AA}^3$ , much larger than a single repeat unit. This is taken to indicate that yield in polymers involves the cooperative motion of several hundred repeat units.

### Example 5.3

The yield stress for polycarbonate is reported at 60 MPa at room-temperature ( $23^\circ\text{C} = 296^\circ\text{K}$ ), and we wish to know its value at  $0^\circ\text{C}$  ( $273^\circ\text{K}$ ), keeping the strain rate the same.

This can be accomplished by writing Eqn. 5.4 out twice, once for each temperature, and then dividing one by the other. The parameters  $\dot{\epsilon}$  and  $\dot{\epsilon}_0$  cancel, leaving

$$1 = \exp \left( \frac{E_Y^* - \sigma_Y^{273} V^*}{R(273)} - \frac{E_Y^* - \sigma_Y^{296} V^*}{R(296)} \right)$$

From the data in Fig. 5.12, the yield activation parameters are  $E_Y^* = 309 \text{ kJ/mol}$ ,  $V^* = 3.9 \times 10^{-3} \text{ m}^3/\text{mol}$ . Using these along with  $R = 8.314 \text{ J/mol}$  and  $\sigma_Y^{296} = 60 \times 10^6 \text{ N/m}^2$ , we have

$$\sigma_Y^{273} = 61.5 \text{ MPa}$$

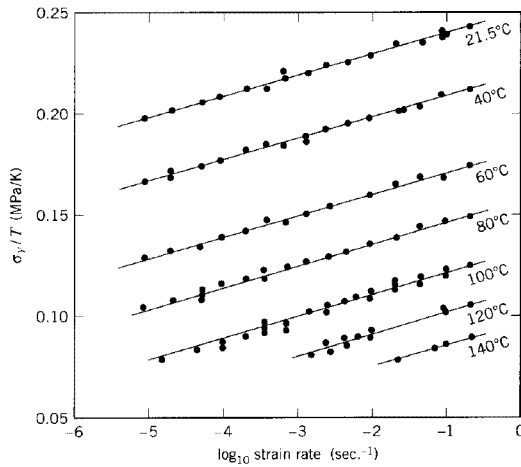


Figure 5.12: Eyring plot showing dependence of yield strength on temperature and strain rate in polycarbonate (from N.G. McCrum, C.P Buckley and C.B. Bucknall, *Principles of Polymer Engineering*, Oxford University Press, 1988).

## 5.4 Continuum Plasticity

Plasticity theory, which seeks to determine stresses and displacements in structures all or part of which have been stressed beyond the yield point, is an important aspect of solid mechanics. The situation is both materially and geometrically nonlinear, so it is not a trivial undertaking. However, in such areas as metal forming, plasticity theory has provided valuable insight. We will outline only a few aspects of this field in the following paragraphs, to introduce some of the fundamental concepts that the reader can extend in future study.

### 5.4.1 Plastic deformation

A useful idealization in modeling plastic behavior takes the material to be linearly elastic up to the yield point as shown in Fig. 5.13, and then “perfectly plastic” at strains beyond yield. Strains up to yield (the line between points  $a$  and  $b$ ) are recoverable, and the material unloads along the same elastic line it followed during loading; this is conventional elastic response. But if the material is strained beyond yield (point  $b$ ), the “plastic” straining beyond  $b$  takes place at constant stress and is unrecoverable. If the material is strained to point  $c$  and then unloaded, it follows the path  $cd$  (a line parallel to the original elastic line  $ab$ ) rather than returning along  $cba$ . When the stress has been brought to zero (point  $d$ ), the plastic strain  $ad$  remains as a *residual* strain.

Plastic deformation can generate “residual” stresses in structures, internal stresses that remain even after the external loads are removed. To illustrate this, consider two rods having different stress-strain curves, connected in parallel (so their strains are always equal) as shown in Fig. 5.14. When the rods are strained up to the yield point of rod  $B$  (point  $a$  on the strain axis), rod  $A$  will have experienced an amount of permanent plastic deformation  $\epsilon^p$ . When the applied load is removed, rod  $B$  unloads along its original stress-strain curve, but rod  $A$  follows a path parallel to its original elastic line. When rod  $A$  reaches zero stress (point  $b$ ), rod  $B$  will still be in tension (point  $c$ ). In order for the load transmitted by the rods together to come to zero, rod  $B$  will pull rod  $A$  into compression until  $-\sigma_B = \sigma_A$  as indicated by points  $d$  and  $e$ . Residual stresses are left in the rods, and the assembly as a whole is left with a residual tensile strain.

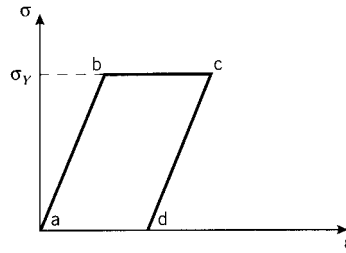


Figure 5.13: The elastic-perfectly plastic idealization of plastic deformation.

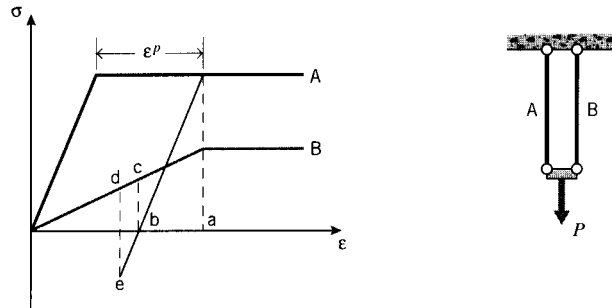


Figure 5.14: Plastic deformation of two-bar assembly.

Compressive residual stress can be valuable if the structure must bear tensile loads. Similarly to how rapid quenching can be used to make safety glass by putting the surfaces in compression, plastic deformation can be used to create favorable compressive stresses. One famous such technique is called “autofrettage;” this is a method used to strengthen cannon barrels against bursting by pressurizing them from the inside so as to bring the inner portion of the barrel into the plastic range. When the pressure is removed, the inner portions are left with a compressive residual stress just as with bar *A* in the above example.

## 5.5 The Dislocation Basis of Yield and Creep

Phenomenological treatments such those outlined earlier in this Chapter are very useful for engineering predictions, but they provide only limited insight to the molecular mechanisms underlying yield. Molecular understanding is a higher level of insight, and also guides processing adjustments that can optimize the material. As discussed in Chap. 2, the high level of order present in crystalline materials lead to good atomistic models for the stiffness. Early workers naturally sought an atomistic treatment of the yield process as well. This turned out to be a much more subtle problem than might have been anticipated, and required hypothesizing a type of crystalline defect — the “dislocation” — to explain the experimentally observed results. Dislocation theory permits a valuable intuitive understanding of yielding in crystalline materials, and explains how yielding can be controlled by alloying and heat treatment. It is one of the principal triumphs of the last century of materials science.

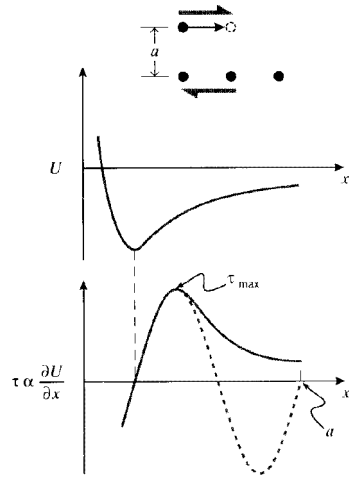


Figure 5.15: Atomistic energy and stress functions.

### 5.5.1 Theoretical yield strength

In yield, atoms slide tangentially from one equilibrium position to another. The forces required to bring this about are given by the bond energy function, which is the anharmonic curve resulting from the balance of attractive and repulsive atomic forces described in Chap. 2. The force needed to displace the atom from equilibrium is the derivative of the energy function, being zero at the equilibrium position (see Fig. 5.15). As a simplifying assumption, let us approximate the force function with a harmonic expression, and write

$$\tau = \tau_{max} \sin \left( 2\pi \frac{x}{a} \right)$$

where  $a$  is the interatomic spacing. The stress reaches a maximum a quarter of the distance between the two positions, dropping to zero at the metastable position midway between them. After that, the stress changes sign, meaning that force is required to hold the atom back as it tries to fall toward the new equilibrium position. Using  $\gamma = x/a$  as the shear strain, the maximum shear stress  $\tau_{max}$  can be related to the shear modulus  $G$  as

$$\begin{aligned} \frac{d\tau}{d\gamma} &= \frac{d\tau}{dx} \frac{dx}{d\gamma} = a \frac{d\tau}{dx} = a \tau_{max} \frac{2\pi}{a} \cos \frac{2\pi x}{a} \\ G &= \left. \frac{d\tau}{d\gamma} \right|_{\gamma \rightarrow 0} = \tau_{max} \cdot 2\pi \end{aligned}$$

This implies a shear stress at yield of  $\tau_{max} = G/2\pi \approx G/10$ , which would be on the order of 10 GPa. Measured values are 10–100 MPa, so the theoretical value is 2 to 3 orders of magnitude too large. More elaborate derivations give a somewhat smaller value for the theoretical yield stress, but still much larger than what is observed experimentally.

### 5.5.2 Edge, screw, and mixed dislocations

A rationale for the apparently low experimental values for the yield strengths of crystalline materials was proposed independently by Taylor, Polyani and Orowan in 1934. These workers realized that it

was not necessary to slip entire planes of atoms past one another to deform the material plastically, a process that would require breaking all the bonds connecting the planes simultaneously. The stress needed to do this would be very high, on the order of  $G/10$  as described above. But it isn't necessary to move all the atoms at once; only a few at a time need to move, requiring a much smaller stress. Analogously to the way an inchworm moves, only those atoms lying in a plane above a single line might be displaced one atomic spacing. This would force the plane of atoms previously there into a midway position as shown in Fig. 5.16, creating an "extra" plane of atoms halfway between the normal equilibrium positions. The termination of this plane then constitutes a line defect in the crystal known as a *dislocation*<sup>3</sup>.

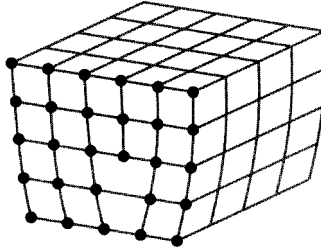


Figure 5.16: The edge dislocation.

Viewed end-on as seen in Fig. 5.17, it can be appreciated that the extra plane of atoms creates a region of compression near the plane but above the dislocation line, and a tensile region below it. In a "soft" crystal whose interatomic bonds are relatively compliant, the distortion extends an appreciable distance from the dislocation. Conversely, in "hard" crystals with stiffer bonds the distortion is confined to a smaller region near the dislocation. The face-centered cubic (fcc) metals such as copper and gold have close-packed planes (those with (111) Miller indices), which corresponds to large distances between those planes. This gives rise to relatively soft interplanar bonds, so that the dislocation width is large. The dislocation width is substantially smaller in the body centered cubic (bcc) metals such as iron and steel, smaller still in ionically bonded ceramics, and even smaller in covalently bonded ceramics.

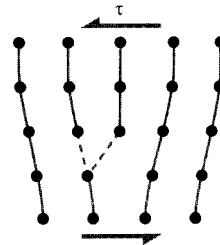


Figure 5.17: Dislocation motion.

The dislocation associated with this extra plane of atoms can be moved easily, since only a small adjustment in position is required to break the bonds on the next plane over and allow them to form on the originally "extra" plane. Now the third plane is the extra one, and the dislocation

---

<sup>3</sup>For an extended discussion of the geometrical aspects of crystal dislocations, see S.M. Allen and E.L. Thomas, *The Structure of Materials*, John Wiley & Sons, New York, 1999.

will have moved by one atomic position. Slip is obviously made much easier if dislocation motion is available to the material. In fact, it first appears the dislocation concept does *too* good a job in explaining crystal plasticity, since the dislocation is in a balanced metastable position and should be capable of being moved either left or right with a vanishingly small force. If this were true, the crystal would have essentially *no* shear strength.

However, as the dislocation moves it drags with it the regions of compressive and tensile distortion in the lattice around it. This is accompanied by a sort of frictional drag, giving rise to a resistance to dislocation motion known as the *Peierls* force. This force is dependent on such factors as the crystal type and the temperature, and this plays an important role in determining the material's yield stress. As seen in Table 5.1, materials with wide dislocations have low Peierls forces, since the distortion is spread out over a large volume and is much less intense at its core.

Table 5.1: Relationship between dislocation width and yield strength temperature sensitivity (from R.W. Hertzberg, *Deformation and Fracture Mechanics of Engineering Materials*, John Wiley & Sons, 1976).

Material	Crystal Type	Dislocation Width	Yield Strength	
			Peierls Stress	Temperature Sensitivity
Metal	fcc	wide	very small	negligible
Metal	bcc	narrow	moderate	strong
Ceramic	ionic	narrow	large	strong
Ceramic	covalent	very narrow	very large	strong

Table 5.1 also indicates that the effect of temperature on the Peierls force is low for fcc materials having wide dislocations, and this results in a small temperature dependency of the yield stress. Conversely, materials with narrow and intense dislocation fields have high Peierls forces with a large temperature sensitivity of the yield stress, with higher temperatures facilitating dislocation mobility and thus reducing the yield strength. Among the important consequences of these factors is the dangerous tendency of steel to become brittle at low temperatures; as the temperature is lowered, the yield stress can rise to such high levels that brittle fracture intervenes.

Dislocations can have geometries other than the simple edge dislocation shown in Fig. 5.17. A more general view is provided by considering displacing a portion of the atoms in a “slip plane”  $acfg$  a distance  $\bar{b}$ , as shown in Fig. 5.18. The vector  $\bar{b}$  is also a measure of the magnitude and direction of the crystal dislocation, and is known as the *Burgers' vector*. The boundary between slipped and unslipped atoms on the slip plane is the dislocation line, shown as a dotted line. At position  $e$ , the dislocation line is perpendicular to the Burgers' vector, so these two quantities lie in the slip plane. A dislocation so situated is called an *edge* dislocation, and is constrained to move only in the slip plane defined by the dislocation line and the Burgers' vector.

At position  $b$ , a spiral-like defect is formed such that a circular transit around the dislocation line ends on a plane a distance  $\bar{b}$  from the starting point. Now the defect is known as a *screw* dislocation. The dislocation line is now parallel to the Burgers' vector, so these two quantities do not define a unique slip plane the way an edge dislocation does. A screw dislocation can therefore *cross-slip* to another easy-glide plane passing through the dislocation line, and this mechanism enables screw dislocations to maneuver around obstacles that might otherwise impede their motion. Edge dislocations are more easily pinned, since they must “climb” by diffusion of vacancies to surmount obstacles as illustrated in Fig. 5.19.

As the curved dislocation line is traversed from point  $b$  to point  $e$ , the dislocation changes

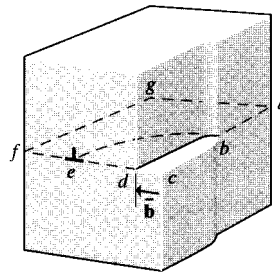


Figure 5.18: The mixed dislocation.

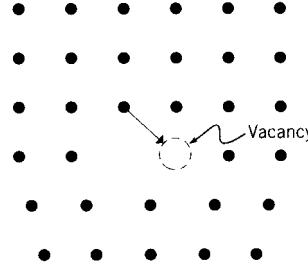


Figure 5.19: Dislocation climb by vacancy diffusion.

gradually from screw to edge character. At intermediate points the dislocation has both edge and screw character, and is known as a *mixed* dislocation.

### 5.5.3 Dislocation-Controlled Yield

Single crystals tend to slip on their most closely packed planes, and in directions of minimum atomic separation distance. The distances between planes is maximum for the close-packed planes, so these are the most loosely bonded. Slip in close-packed directions minimizes the distance the stresses need to displace the slipping atoms. Both of these act to minimize the energy needed for slip. There are 12 such slip systems in the face-centered cubic (fcc) systems; using Miller indices, these are the  $\{111\}$  planes and the  $\langle 110 \rangle$  directions. There are 4 independent nonparallel  $(111)$  planes, and 3 independent  $[110]$  directions in each plane.

Table 5.2: Critical resolved shear stress for single crystals of various materials.

Material	crystal type	slip system	$\tau_{crss}$ , MPa
Nickel	fcc	$\{111\} \langle 110 \rangle$	5.7
Copper	fcc	$\{111\} \langle 110 \rangle$	0.98
Gold	fcc	$\{111\} \langle 110 \rangle$	0.90
Silver	fcc	$\{111\} \langle 110 \rangle$	0.60
Magnesium	hcp	$\{1101\} \langle 001 \rangle$	0.81
NaCl	cubic	$\{110\} \langle 110 \rangle$	0.75

Slip occurs when the shear stress on the slip plane, and in the slip direction, reaches a value  $\tau_{crss}$ , the *critical resolved shear stress*; experimental values for  $\tau_{crss}$  are listed in Table 5.2 for a number of single crystal materials. The resolved shear stress corresponding to an arbitrary stress state can be computed using the transformation relations of Sect. 4.3. In a simple tension test it can be written by inspection of Fig. 5.20 as

$$\tau_{rss} = \frac{P \cos \theta}{A_s} = \frac{P \cos \theta}{A_0 / \cos \phi} = \sigma (\cos \theta \cos \phi) \equiv \frac{\sigma}{m}$$

where  $m$  is a structure factor dependent on the orientation of the slip system relative to the applied tensile stress. For single crystals of arbitrary alignment, the yield stress will then be of the form

$$\sigma_Y = \tau_{crss} \cdot m \quad (5.5)$$

This is known as “Schmid’s Law,” and  $m$  is the “Schmid factor.”

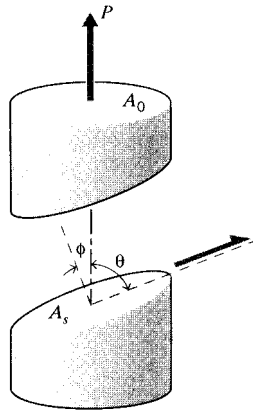


Figure 5.20: Critical resolved shear stress.

The yield stress will generally be higher in polycrystalline materials, since many of the grains will be oriented unfavorably (have high Schmid factors). Equation 5.5 can be modified for polycrystalline systems as

$$\sigma_Y = \tau_{crss} \cdot \bar{m}$$

where  $\bar{m}$  is an equivalent Schmid factor that is generally somewhat higher than a simple average over all the individual grains; for fcc and bcc systems  $\bar{m} \approx 3$ .

#### 5.5.4 Strain Energy in Dislocations

Many calculations in dislocation mechanics are done more easily with energy concepts than with Newtonian force-displacement approaches. As seen in Fig. 5.21, the shear strain associated with a screw dislocation is the deflection  $\bar{b}$  divided by the circumference of a circular path around the dislocation core:

$$\gamma = \frac{\bar{b}}{2\pi r} \quad (5.6)$$

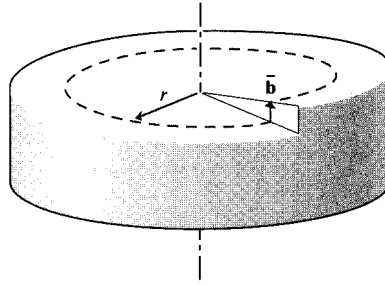


Figure 5.21: Shear strain associated with a screw dislocation.

where  $r$  is the distance from the dislocation core. Assuming Hookean elasticity, the corresponding strain energy per unit volume is

$$U = \int \tau d\gamma = \frac{1}{2} \tau \gamma = \frac{G\gamma^2}{2} = \frac{G\bar{b}^2}{8\pi^2 r^2}$$

The total strain energy associated with the screw dislocation is now obtained by integrating this over the volume around the dislocation:

$$U_{screw} = \int U dV = l \cdot \int_{r_0}^r \frac{G\bar{b}^2}{8\pi^2 r^2} 2\pi r dr$$

where here  $l$  is the length of the dislocation line and  $r_0$  is the radius of the dislocation “core” inside which the energy is neglected. (Mathematically, the energy density increases without bound inside the core; however its volume becomes very small.) Taking  $l = 1$  to obtain energy per unit length and carrying out the integration,

$$U_{screw} = \frac{G\bar{b}^2}{4\pi} \ln \frac{r}{r_0} \approx G\bar{b}^2$$

(5.7)

This last approximation should be read “scales as,” since it is arbitrary to select the limiting value  $r$  so that  $\ln \frac{r}{r_0} \approx 4\pi$ . The important conclusion is that the dislocation energy increases linearly with the shear modulus  $G$  and quadratically with the Burgers’ vector  $\bar{b}$ . A similar expression can be obtained for the strain energy per unit length of edge dislocation; it can be shown that

$$U_{edge} = \frac{G\bar{b}^2}{1 - \nu}$$

(5.8)

where  $\nu$  is the Poisson’s ratio.

The dislocation energy represents an increase in the total energy of the system, which the material will try to eliminate if possible. For instance, two dislocations of opposite sign will be attracted to one another, since their strain fields will tend to cancel and lower the energy. Conversely, two dislocations of same sign will repel one another. The force of this attraction or repulsion will scale as

$$F dr = dU \Rightarrow F_{screw} \approx \frac{G\bar{b}^2}{r}$$

where here  $r$  is the distance between dislocations.

### 5.5.5 Dislocation motion and hardening

The ductility of crystalline materials is determined by dislocation mobility, and factors that impede dislocation motion can produce dramatic increases in the material's yield strength. This increased resistance to plastic flow also raises the indentation hardness of the material, so strengthening of this sort is known as *hardening*. Alloying elements, grain boundaries, and even dislocations themselves can provide this impediment, and these provide the means by which the materials technologist controls yield. A thorough treatment of these important concepts must be left to subjects in physical metallurgy, but the following paragraphs will provide a brief introduction to some of them.

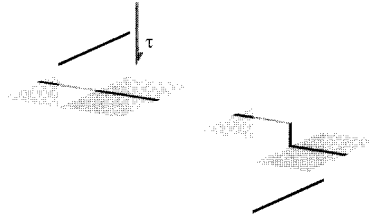


Figure 5.22: A dislocation jog.

When one dislocation, moving on its slip plane under the influence of a driving shear stress, passes through another a “jog” will be created in the second dislocation as shown in Fig. 5.22. The portion of the dislocation line in the jog is now no longer on its original glide plane, and is “pinned” in position. If the dislocation concentration is large, these jogs become a powerful impediment to plastic flow by dislocation motion. Paradoxically, the very dislocations that permit plastic flow in the first place can impede it if they become too numerous.



Figure 5.23: Dislocation bowing.

When a moving dislocation becomes pinned by jogs or other impediments, the shear stress  $\tau$  that had been driving the dislocation now causes the line segment between the obstacles to bow forward as shown in Fig. 5.23, with an angle  $\phi$  between adjacent segments. The extra length of the bowed line represents an increase in the strain energy of the dislocation, and if the shear stress were not present the line would straighten out to reduce this energy. The line acts similarly to an elastic band, with a “line tension”  $T$  that acts to return the line to a straight shortest-distance path between pinning points. The units of dislocation energy per unit length (N-m/m) are the same as simple tension, and we can write

$$T = \frac{\partial E}{\partial l} \approx Gb^2$$

As shown in Fig. 5.24, a free-body diagram of the line segment between two pinning points gives a force balance of the form

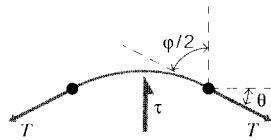


Figure 5.24: Force balance on dislocation segment.

$$2T \sin \frac{d\theta}{2} = \tau \bar{b} \cdot r d\theta$$

where here  $r$  is the radius of curvature of the line (not the distance from the dislocation, as in Eqn. 5.6). Rearranging and canceling the  $d\theta$  factor,

$$\tau = \frac{G\bar{b}}{r} \quad (5.9)$$

This relation gives the curvature of the dislocation in terms of the shear stress acting on it. The maximum shear stress is that needed to bend the dislocation into a semicircle (smallest  $r$ ), after which the dislocation expands spontaneously. When the loops meet, annihilation occurs at that point, spawning a new dislocation line embedded in a circular loop. The process can be repeated with the new dislocation as well, and by this mechanism a large number of dislocations can be spawned as shown in Fig. 5.25. This is the “Frank-Read” source, and is an important means by which dislocations can multiply during plastic deformation. The increasing number of dislocations leads to more and more entanglements, with jogs acting as pinning points.

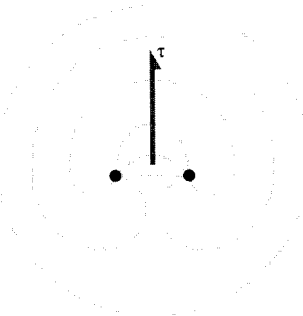


Figure 5.25: The Frank-Read dislocation source.

Equation 5.9 also provides an estimate of the influence of dislocation density on yield strength. If the obstacles pinning dislocation motion are “soft” the dislocation will be able to overcome them at relatively low driving stress, corresponding to a low critical angle  $\phi_c$ . But as the obstacle becomes “harder,” i.e. provides more resistance to dislocation motion, the angle approaches zero and the radius of curvature becomes on the order of the obstacle spacing  $L$ . The shear stress needed to overcome such obstacles is then

$$\tau \approx \frac{G\bar{b}}{L}$$

When the hard obstacles arise from jogs created by intersections with other dislocations, the obstacle spacing  $L$  can be written in terms of the dislocation density. If the number of dislocations passing through a unit area is  $\rho$ , the number of dislocations encountered in moving along a straight line will be proportional to  $\sqrt{\rho}$ . The spacing between them is proportional to the reciprocal of this, so  $\tau \propto G\bar{b}\sqrt{\rho}$ . The yield stress is then the stress  $\tau_0$  needed to move dislocations in the absence of interfering dislocations, plus that needed to break through the obstacles; this can be written as

$$\boxed{\tau_Y = \tau_0 + AG\bar{b}\sqrt{\rho}} \quad (5.10)$$

where  $A$  is a constant that has been found to vary between 0.3 and 0.6 for a number of fcc, bcc and polycrystalline metals as well as some ionic crystals. Experimental corroboration of this relation is provided in Fig. 5.26.

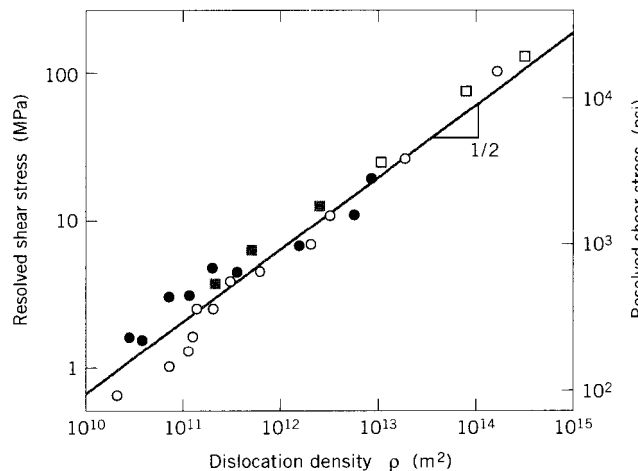


Figure 5.26: Effect of dislocation density  $\rho$  on critical resolved shear stress (for copper single and polycrystals, from T.H. Courtney, *Mechanical Behavior of Materials*, McGraw-Hill, 1990).

The action of plastic flow therefore creates new dislocations by Frank-Read and other sources, which makes the material harder and harder, i.e. increasingly resistant to further plastic flow. Eventually the yield stress for continued deformation becomes larger than the fracture stress, and the material will now break before it deforms further. If continued working of the material is desired, the number of dislocations must be reduced, for instance by thermal annealing. Annealing can produce *recovery* (dislocation climb around obstacles by vacancy diffusion) or recrystallization of new dislocation-free grains.

Grain boundaries act to impede dislocation motion, since the slip systems in adjoining grains will usually not line up; increases in yield strength arising from this mechanism are called *boundary strengthening*. Fine-grained metals have increased grain boundary area and thus have higher yield strengths than coarse-grained ones. The influence of grain size can often be described by the *Hall-Petch* formula

$$\boxed{\sigma_Y = \sigma_0 + k_Y d^{-1/2}} \quad (5.11)$$

where  $\sigma_0$  is the lattice friction stress needed to move dislocations and  $K$  is a constant. This relation is essentially empirical, but it can be rationalized by viewing the second term as being related to the stress needed to activate a new mobile dislocation in the unfavorably oriented grain.

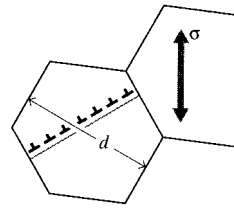


Figure 5.27: Dislocation pileup at a grain boundary.

As dislocations pile up against the boundary in the originally deforming grain, they act much like a crack whose length scales with the grain size  $d$  as shown in Fig. 5.27: the larger the grain, the more dislocations in the pileup, the larger the virtual crack. Since the stress in front of a sharp crack of length  $a$  scales as  $\sqrt{a}$ , the stress in front of the crack containing the dislocation pileup is increased by a factor that scales with  $\sqrt{d}$ . When this stress exceeds that needed to generate a new dislocation the unfavorably oriented grain begins to deform by dislocation motion. This stress diminishes according to  $d^{-1/2}$  as the size of the original grain is scaled down, thus strengthening the metal according to the Hall-Petch relationship. Grain size is determined by the balance between nucleation and growth rates as the metal is solidified, and these are in turn controllable by the cooling rates imposed. This is an important example of processing-structure-property control available to the materials technologist.

A related phenomenon accounts for the very high strengths ( $\approx 4$  GPa, or 600 kpsi) of piano wire, a eutectoid steel that has been drawn through a sequence of reducing dies to obtain a small final diameter. The “pearlitic” structure obtained on cooling this steel through the eutectoid temperature is a two-phase mixture of  $\text{Fe}_3\text{C}$  (“cementite”) in bcc iron (“ferrite”). As the diameter is reduced during drawing, the ferrite cells are reduced as well, forming a structure analogous to a fine-grained metal. The cell boundaries restrict dislocation motion, leading to the very high yield strengths.

Impurity atoms in solid solution can also serve to harden a crystalline material by impeding dislocation motion; this is called *solution strengthening*. An impurity atom smaller than the atoms of the host lattice will create an approximately spherical tensile field around itself which will attract the compressive regions around mobile dislocations, and a larger impurity atom will tend to trap the tensile region of nearby dislocations. On average, the population of dislocations will maneuver so as to lower their strain energies by associating with the nonuniform strain fields around impurities. This association impedes dislocation motion, which inhibits plastic flow and increases the yield stress.

Solution hardening is not usually an especially effective strengthening mechanism in commercial materials, largely because the solubility of impurity atoms is not sufficient to generate an appreciable number of obstacles. One important exception to this is the iron-carbon, or steel, system. If steel at approximately the eutectoid carbon composition (0.8% C) is cooled rapidly from above the eutectoid temperature of  $723^\circ\text{C}$ , the carbon atoms can become trapped in the iron lattice at much higher concentrations than bcc iron’s equilibrium carbon solubility would normally allow. (This tendency for trapping can be enhanced by alloying elements such as chromium and molybdenum, which have an affinity for carbon and thus reduce its ability to diffuse away.) To accommodate these metastable impurity atoms, the iron lattice transforms to a body-centered tetragonal form named *martensite* (see Fig. 5.28), with a strong nonspherical strain field around the carbon atoms. These tetragonal distortions are very effective impediments to dislocation motion, making martensite an

extremely hard phase. The periodic water quenches a blacksmith uses during metalworking is done (perhaps without the smith knowing why it works) to tailor the material's hardness by developing martensitic inclusions in the steel.

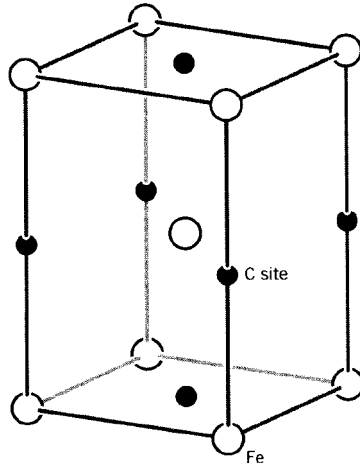


Figure 5.28: The body-centered tetragonal structure of martensite.

Martensite is so hard and brittle that the rapidly quenched steel must usually be *tempered* by heating it to approximately 400°C for an hour or so. This allows diffusion of carbon to take place, creating a dispersion of cementite inclusions; it also permits recovery of the dislocations present in the martensite. The resulting material is much tougher than the as-formed martensitic steel, but still retains a high strength level due to the strengthening effect of the carbide inclusions.

## 5.6 Kinetics of Creep in Crystalline Materials

“Creep” is the term used to describe the tendency of many materials to exhibit continuing deformation even though the stress is held constant. Viscoelastic polymers exhibit creep, as was discussed in Chap. 2. However, creep also occurs in polycrystalline metallic and ceramic systems, most importantly when the temperature is higher than approximately half their absolute melting temperature. This high-temperature creep can occur at stresses less than the yield stress, but is related to this chapter’s discussion of dislocation-controlled yield since dislocation motion often underlies the creep process as well.

High-temperature creep is of concern in such applications as jet engines or nuclear reactors. This form of creep often consists of three distinct regimes as seen in Fig. 5.29: *primary* creep, in which the material appears to harden so the creep rate diminishes with time; *secondary* or steady state creep, in which hardening and softening mechanisms appear to balance to produce a constant creep rate  $\dot{\epsilon}_{II}$ ; and *tertiary* creep in which the material softens until creep rupture occurs. The entire creep curve reflects a competition between hardening mechanisms such as dislocation pileup, and mechanisms such as dislocation climb and cross-slip which are termed *recovery* and which augment dislocation mobility.

In most applications the secondary regime consumes most of the time to failure, so much of the modeling effort has been directed to this stage. The secondary creep rate  $\dot{\epsilon}_{II}$  can often be described by a general nonlinear expression of the form

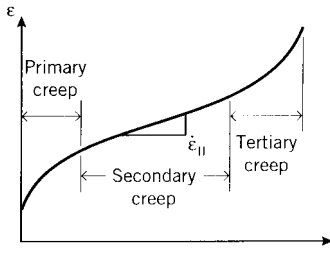


Figure 5.29: The three stages of creep.

$$\dot{\epsilon}_{II} = A\sigma^m \exp \frac{-E_c^*}{RT} \quad (5.12)$$

where  $A$  and  $m$  are adjustable constants,  $E_c^*$  is an apparent activation energy for creep,  $\sigma$  is the stress,  $R$  is the Gas Constant (to be replaced by Boltzman's constant if a molar basis is not used) and  $T$  is the absolute temperature. This is known as the *Weertman-Dorn equation*.

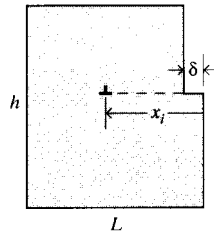


Figure 5.30: Dislocation motion and creep rate.

The plastic flow rate is related directly to dislocation velocity, which can be visualized by considering a section of material of height  $h$  and width  $L$  as shown in Fig. 5.30. A single dislocation, having traveled in the width direction for the full distance  $L$  will produce a transverse deformation of  $\delta_i = \bar{b}$ . If the dislocation has propagated through the crystal only a fraction  $x_i/L$  of the width, the deformation can be reduced by this same fraction:  $\delta_i = \bar{b}(x_i/L)$ . The total deformation in the crystal is then the sum of the deformations contributed by each dislocation:

$$\delta = \sum_i \delta_i = \sum_i \bar{b}(x_i/L)$$

The shear strain is the ratio of the transverse deformation to the height over which it is distributed:

$$\gamma = \frac{\delta}{h} = \frac{\bar{b}}{Lh} \sum_i x_i$$

The value  $\sum_i x_i$  can be replaced by the quantity  $N\bar{x}$ , where  $N$  is the number of dislocations in the crystal segment and  $\bar{x}$  is the average propagation distance. We can then write

$$\gamma = \rho \bar{b} \bar{x}$$

where  $\rho = N/Lh$  is the dislocation density in the crystal. The shear strain rate  $\dot{\gamma}$  is then obtained by differentiation:

$$\boxed{\dot{\gamma} = \rho \bar{v}} \quad (5.13)$$

where  $v = \dot{\bar{x}}$  is the average dislocation velocity. Hence the creep rate scales directly with the dislocation velocity.

To investigate the temperature and stress dependence of this velocity, we consider rate at which dislocations can overcome obstacles to be yet another example of a thermally activated, stress aided rate process and write an Eyring equation for the creep rate:

$$\dot{\epsilon} \propto v \propto \exp \frac{-(E_d^* - \sigma V^*)}{kT} - \exp \frac{-(E_d^* + \sigma V^*)}{kT}$$

where  $V^*$  is an apparent activation volume. The second term here indicates that the activation barrier for motion in the direction of stress is augmented by the stress, and diminished for motions in the opposite direction. When we discussed yielding the stress was sufficiently high that motion in the direction opposing flow could be neglected. Here we are interested in creep taking place at relatively low stresses and at high temperature, so that reverse flow can be appreciable. Factoring,

$$\dot{\epsilon} \propto \exp \frac{-E_d^*}{RT} \left( \exp \frac{+\sigma V^*}{RT} - \exp \frac{-\sigma V^*}{RT} \right)$$

Since  $\sigma V^* \ll RT$ , we can neglect quadratic and higher order terms in the series expansion  $e^x = 1 + x + (x^2/2!) + (x^3/3!) + \dots$  to give

$$\dot{\epsilon} = A \left( \frac{\sigma V^*}{RT} \right) \exp \frac{-(E_d^*)}{RT}$$

If now we neglect the temperature dependence in the preexponential factor in comparison with the much stronger temperature dependence of the exponential itself, this model predicts a creep rate in agreement with the Weertman-Dorn equation with  $m = 1$ .

Creep by dislocation glide occurs over the full range of temperatures from absolute zero to the melting temperature, although the specific equation developed above contains approximations valid only at higher temperature. The stresses needed to drive dislocation glide are on the order of a tenth the theoretical shear strength of  $G/10$ . At lower stresses the creep rate is lower, and becomes limited by the rate at which dislocations can climb over obstacles by vacancy diffusion. This is hinted at in the similarity of the activation energies for creep and self diffusion as shown in Fig. 5.31. (Note that these values also correlate with the tightness of the bond energy functions, as discussed in Sect. 2.1; diffusion is impeded in more tightly-bonded lattices.) Vacancy diffusion is another stress-aided thermally activated rate process, again leading to models in agreement with the Weertman-Dorn equation.

## 5.7 Problems

1. A steel plate is clad with a thin layer of aluminum on both sides at room temperature, and the temperature then raised. At what temperature increase  $\Delta T$  will the aluminum yield?
2. Yield stresses (in MPa) have been measured at various strain rates and temperatures as follows:

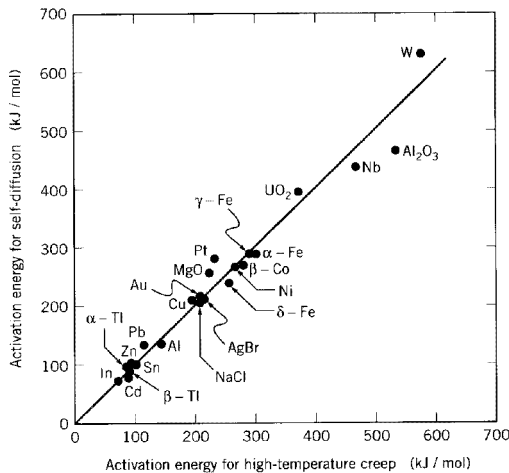
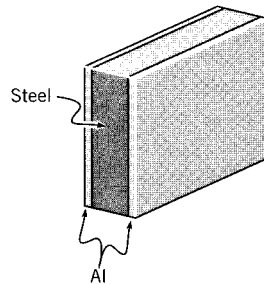


Figure 5.31: Correlation of activation energies for diffusion and creep.



*Prob. 1*

	$\dot{\epsilon} = 10^{-3} \text{ s}^{-1}$	$\dot{\epsilon} = 10^{-1} \text{ s}^{-1}$
$T = 0^\circ\text{C}$	54.1	62.7
$T = 40^\circ\text{C}$	42.3	52.1

Determine the activation volume for the yield process. What physical significance might this parameter have?

3. The yield stresses  $\sigma_Y$  have been measured using steel and aluminum specimens of various grain sizes, as follows:

Material	$d, \mu$	$\sigma_Y, \text{ MPa}$
steel	60.5	160
	136	130
aluminum	11.1	235
	100	225

- (a) Determine the coefficients  $\sigma_0$  and  $k_Y$  in the Hall-Petch relation (Eqn. 5.11) for these two materials.  
 (b) Determine the yield stress in each material for a grain size of  $d = 30\mu$ .



# Chapter 6

## Fracture

In 1983, the National Bureau of Standards (now the National Institute for Science and Technology) and Battelle Memorial Institute<sup>1</sup> estimated the costs for failure due to fracture to be \$119 billion per year in 1982 dollars. The dollars are important, but the cost of many failures in human life and injury is infinitely more so. This chapter will introduce several important means of understanding and dealing with fracture in stressed materials.

### 6.1 Atomistics of Creep Rupture

*Creep rupture* is a conceptually simple mode of failure in which a specimen is subjected to a constant uniaxial stress at constant temperature and humidity, and the time to fracture recorded. The fact that rupture can occur can occur later – perhaps much later – than the time of application of stress implies that fracture is a time-dependent process in which damage takes place within the specimen and accumulates until the specimen no longer has sufficient strength to prevent total rupture.

As a very simple approach to the damage accumulation process, we might propose a first-order mechanism in which the number of unbroken bonds decreases at a rate proportional to the number of unbroken bonds remaining:

$$\frac{dn}{dt} = -Kn \rightarrow \frac{dn}{n} = -K dt \rightarrow n = n_0 e^{-Kt}$$

where  $n$  is the fraction of unbroken bonds remaining and  $K$  is a rate constant for the process. In such a process the number of unbroken bonds goes to zero only at  $t \rightarrow \infty$ , and clearly fracture will occur well before that. Perhaps a reasonable scaling law would take the creep-rupture lifetime  $t_f$  to scale with the *average* time  $\langle t \rangle$  for a bond scission, which can be computed as

$$t_f \approx \langle t \rangle = \frac{\int n \cdot t dt}{\int n dt} = \frac{1}{K}$$

Following the approach used earlier in describing yield as a thermally-activated stress-aided rate process (Eqn. 5.4), we view the bond scission process similarly and write the rate constant  $K$  as

$$K = K_0 \exp \frac{-(E_f^* - \psi V^*)}{kT}$$

where  $E^*$  and  $V^*$  are an activation energy and volume, and  $\psi$  is the stress on the bond. Determining  $\psi$  is nontrivial, as  $\psi$  obviously varies over the distribution of bonds and is dependent on the

---

<sup>1</sup>R.P. Reed et al., NBS Special Publication 647-1, Washington, 1983.

material's microstructure. But as another approximation, we might take the atomic stress to scale with the externally applied stress, giving

$$\psi \approx \sigma \longrightarrow t_f = t_o \exp \frac{(E_f^* - \sigma V^*)}{kT} \quad (6.1)$$

where  $t_0 = 1/K_0$ . A relation similar to this was proposed by S.N. Zhurkov, who conducted a large number of important and innovative studies on the physics of fracture. He argued that fracture is in fact a thermal degradation process, in which an applied stress acts to lower the energy barrier to thermofluctuational bond dissociation. Fig. 6.1 shows this relation to describe creep rupture in a wide variety of materials, including ceramics, metals and polymers.

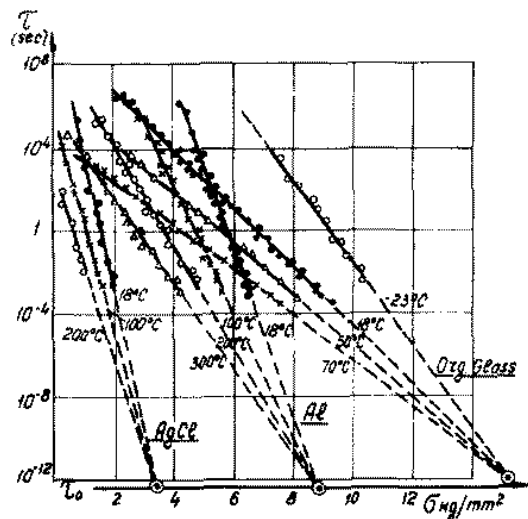


Figure 6.1: Time and temperature dependence of the creep-rupture lifetime of solids. (Org. Glass is PMMA.) From S.N. Zhurkov, "Kinetic Concept of the Strength of Solids," *Int. J. of Fracture Mechanics*, Vol. 1, No. 4, pp. 311–323, Dec. 1965.

## 6.2 Fracture Mechanics - the Energy-Balance Approach

Failures have occurred for many reasons, including uncertainties in the loading or environment, defects in the materials, inadequacies in design, and deficiencies in construction or maintenance. Design against fracture has a technology of its own, and this is a very active area of current research. This chapter will provide an introduction to an important aspect of this field, since without an understanding of fracture the elaborate methods in stress analysis now available would be of little use. We will focus on fractures due to simple tensile overstress, but the designer is cautioned about the need to consider absolutely as many factors as possible that might lead to failure, especially when life is at risk.

Chapter 5 showed how the strength of structural metals – particularly steel – can be increased to very high levels by manipulating the microstructure so as to inhibit dislocation motion. Unfortunately, this renders the material increasingly brittle, so that cracks can form and propagate catastrophically with very little warning. An unfortunate number of engineering disasters are re-

lated directly to this phenomenon, and engineers involved in structural design must be aware of the procedures now available to safeguard against brittle fracture.

The central difficulty in designing against fracture in high-strength materials is that the presence of cracks can modify the local stresses to such an extent that the elastic stress analyses done so carefully by the designers are insufficient. When a crack reaches a certain critical length, it can propagate catastrophically through the structure, *even though the gross stress is much less than would normally cause yield or failure in a tensile specimen*. The term “fracture mechanics” refers to a vital specialization within solid mechanics in which the presence of a crack is assumed, and we wish to find quantitative relations between the crack length, the material’s inherent resistance to crack growth, and the stress at which the crack propagates at high speed to cause structural failure.

When A.A. Griffith (1893–1963) began his pioneering studies of fracture in glass in the years just prior to 1920, he was aware of Inglis’ work<sup>2</sup> in calculating the stress concentrations around elliptical holes, and naturally considered how it might be used in developing a fundamental approach to predicting fracture strengths. However, the Inglis solution poses a mathematical difficulty: in the limit of a perfectly sharp crack, the stresses approach infinity at the crack tip. This is obviously nonphysical (actually the material generally undergoes some local yielding to blunt the cracktip), and using such a result would predict that materials would have near-zero strength: even for very small applied loads, the stresses near crack tips would become infinite, and the bonds there would rupture. Rather than focusing on the crack-tip stresses directly, Griffith employed an energy-balance approach that has become one of the most famous developments in materials science<sup>3</sup>.

The strain energy per unit volume of stressed material is

$$U^* = \frac{1}{V} \int f dx = \int \frac{f}{A} \frac{dx}{L} = \int \sigma d\epsilon$$

If the material is linear ( $\sigma = E\epsilon$ ), then the strain energy per unit volume is

$$U^* = \frac{E\epsilon^2}{2} = \frac{\sigma^2}{2E}$$

When a crack has grown into a solid to a depth  $a$ , a region of material adjacent to the free surfaces is unloaded, and its strain energy released. Using the Inglis solution, Griffith was able to compute just how much energy this is.

A simple way of visualizing this energy release, illustrated in Fig. 6.2, is to regard two triangular regions near the crack flanks, of width  $a$  and height  $\beta a$ , as being completely unloaded, while the remaining material continues to feel the full stress  $\sigma$ . The parameter  $\beta$  can be selected so as to agree with the Inglis solution, and it turns out that for plane stress loading  $\beta = \pi$ . The total strain energy  $U$  released is then the strain energy per unit volume times the volume in both triangular regions:

$$U = -\frac{\sigma^2}{2E} \cdot \pi a^2$$

Here the dimension normal to the  $x$ - $y$  plane is taken to be unity, so  $U$  is the strain energy released per unit thickness of specimen. This strain energy is *liberated* by crack growth. But in forming the

---

<sup>2</sup>C.E. Inglis, “Stresses in a Plate Due to the Presence of Cracks and Sharp Corners,” *Transactions of the Institution of Naval Architects*, Vol. 55, London, 1913, pp. 219–230.

<sup>3</sup>A.A. Griffith, *Philosophical Transactions*, Series A, Vol. 221, pp. 163–198, 1920. The importance of Griffith’s work in fracture was largely unrecognized until the 1950’s. See J.E. Gordon, *The Science of Structures and Materials*, Scientific American Library, 1988, for a personal account of the Griffith story.

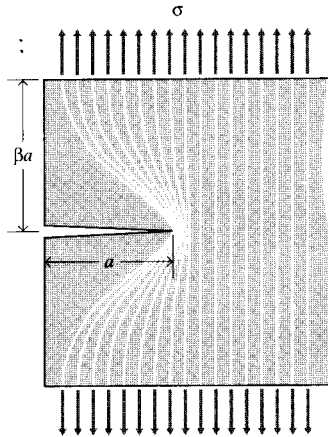


Figure 6.2: Idealization of unloaded region near crack flanks.

crack, bonds must be broken, and the requisite bond energy is in effect *absorbed* by the material. The surface energy  $S$  associated with a crack of length  $a$  (and unit depth) is:

$$S = 2\gamma a$$

where  $\gamma$  is the surface energy (e.g., Joules/meter<sup>2</sup>) and the factor 2 is needed since two free surfaces have been formed. As shown in Fig. 6.3, the total energy associated with the crack is then the sum of the (positive) energy absorbed to create the new surfaces, plus the (negative) strain energy liberated by allowing the regions near the crack flanks to become unloaded.

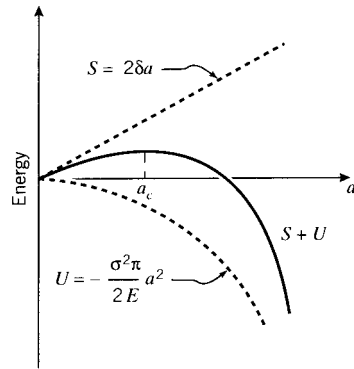


Figure 6.3: The fracture energy balance.

As the crack grows longer ( $a$  increases), the quadratic dependence of strain energy on  $a$  eventually dominates the surface energy, and beyond a critical crack length  $a_c$  the system can lower its energy by letting the crack grow still longer. Up to the point where  $a = a_c$ , the crack will grow only if the stress is increased. Beyond that point, crack growth is spontaneous and catastrophic.

The value of the critical crack length can be found by setting the derivative of the total energy  $S + U$  to zero:

$$\frac{\partial(S + U)}{\partial a} = 2\gamma - \frac{\sigma_f^2}{E}\pi a = 0$$

Since fast fracture is imminent when this condition is satisfied, we write the stress as  $\sigma_f$ . Solving,

$$\sigma_f = \sqrt{\frac{2E\gamma}{\pi a}}$$

Griffith's original work dealt with very brittle materials, specifically glass rods. When the material exhibits more ductility, consideration of the surface energy alone fails to provide an accurate model for fracture. This deficiency was later remedied, at least in part, independently by Irwin<sup>4</sup> and Orowan<sup>5</sup>. They suggested that in a ductile material a good deal – in fact the vast majority – of the released strain energy was absorbed not by creating new surfaces, but by energy dissipation due to plastic flow in the material near the crack tip. They suggested that catastrophic fracture occurs when the strain energy is released at a rate sufficient to satisfy the needs of all these energy “sinks,” and denoted this *critical strain energy release rate* by the parameter  $G_c$ ; the Griffith equation can then be rewritten in the form:

$$\sigma_f = \sqrt{\frac{EG_c}{\pi a}}$$

(6.2)

This expression describes, in a very succinct way, the interrelation between three important aspects of the fracture process: the *material*, as evidenced in the critical strain energy release rate  $G_c$ ; the *stress level*  $\sigma_f$ ; and the *size*,  $a$ , of the flaw. In a design situation, one might choose a value of  $a$  based on the smallest crack that could be easily detected. Then for a given material with its associated value of  $G_c$ , the safe level of stress  $\sigma_f$  could be determined. The structure would then be sized so as to keep the working stress comfortably below this critical value.

### Example 6.1

The story of the DeHavilland Comet aircraft of the early 1950's, in which at least two aircraft disintegrated in flight, provides a tragic but fascinating insight into the importance of fracture theory. It is an eerie story as well, having been all but predicted in a 1948 novel by Nevil Shute named *No Highway*. The book later became a movie starring James Stewart as a perseverant metallurgist convinced that his company's new aircraft (the “Reindeer”) was fatally prone to metal fatigue. When just a few years later the Comet was determined to have almost exactly this problem, both the book and the movie became rather famous in the materials engineering community.

The postmortem study of the Comet's problems was one of the most extensive in engineering history<sup>6</sup>. It required salvaging almost the entire aircraft from scattered wreckage on the ocean floor and also involved full-scale pressurization of an aircraft in a giant water tank. Although valuable lessons were learned, it is hard to overstate the damage done to the DeHavilland Company and to the British aircraft industry in general. It is sometimes argued that the long predominance of the United States in commercial aircraft is due at least in part to the Comet's misfortune.

The Comet aircraft had a fuselage of clad aluminum, with  $G_c \approx 300$  in-psi. The hoop stress due to relative cabin pressurization was 20,000 psi, and at that stress the length of crack that will propagate catastrophically is

<sup>4</sup>G.R. Irwin, “Fracture Dynamics,” *Fracturing of Metals*, American Society for Metals, Cleveland, 1948.

<sup>5</sup>E. Orowan, “Fracture and Strength of Solids,” Report of Progress in Physics, Vol. 12, 1949.

<sup>6</sup>T. Bishop, *Metal Progress*, Vol. 67, pp. 79–85, May 1955.

$$a = \frac{G_c E}{\pi \sigma^2} = \frac{(300)(11 \times 10^6)}{\pi(20 \times 10^3)^2} = 2.62''$$

A crack would presumably be detected in routine inspection long before it could grow to this length. But in the case of the Comet, the cracks were propagating from rivet holes near the cabin windows. When the crack reached the window, the size of the window opening was effectively added to the crack length, leading to disaster.

Modern aircraft are built with this failure mode in mind, and have “tear strips” that are supposedly able to stop any rapidly growing crack. But this remedy is not always effective, as was demonstrated in 1988 when a B737 operated by Aloha Airlines had the roof of the first-class cabin tear away.. That aircraft had stress-corrosion damage at a number of rivets in the fuselage lap splices, and this permitted multiple small cracks to link up to form a large crack. A great deal of attention is currently being directed to protection against this sort of “multi-site damage.”

It is important to realize that the critical crack length is an absolute number, not depending on the size of the structure containing it. Each time the crack jumps ahead, say by a small increment  $\delta a$ , an additional quantity of strain energy is released from the newly-unloaded material near the crack. Again using our simplistic picture of a triangular-shaped region that is at zero stress while the rest of the structure continues to feel the overall applied stress, it is easy to see in Fig. 6.4 that much more energy is released due to the jump at position 2 than at position 1. This is yet another reason why small things tend to be stronger: they simply aren’t large enough to contain a critical-length crack.

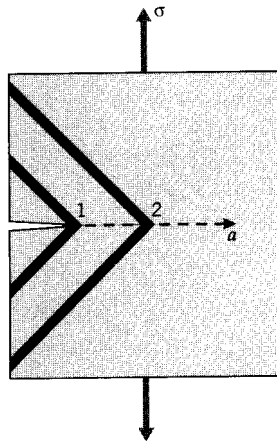


Figure 6.4: Energy released during an increment of crack growth, for two different crack lengths.

### Example 6.2

Gordon<sup>7</sup> tells of a ship’s cook who one day noticed a crack in the steel deck of his galley. His superiors assured him that it was nothing to worry about — the crack was certainly small compared with the vast bulk of the ship — but the cook began painting dates on the floor to mark the new length of the crack each time a bout of rough weather would cause it to grow longer. With each advance of the crack, additional decking material was unloaded, and the strain energy formerly contained in it released. But as the amount of energy released grows *quadratically* with the crack length, eventually enough was available to keep the crack

<sup>7</sup>J.E. Gordon, *Structures, or Why Things Don’t Fall Down*, Plenum, New York, 1978.

growing even with no further increase in the gross load. When this happened, the ship broke into two pieces; this seems amazing but there are a more than a few such occurrences that are very well documented. As it happened, the part of the ship with the marks showing the crack's growth was salvaged, and this has become one of the very best documented examples of slow crack growth followed by final catastrophic fracture.

---

### 6.2.1 Compliance calibration

A number of means are available by which the material property  $\mathcal{G}_c$  can be measured. One of these is known as *compliance calibration*, which employs the concept of compliance as a ratio of deformation to applied load:  $C = \delta/P$ . The total strain energy  $U$  can be written in terms of this compliance as:

$$U = \frac{1}{2}P\delta = \frac{1}{2}CP^2$$

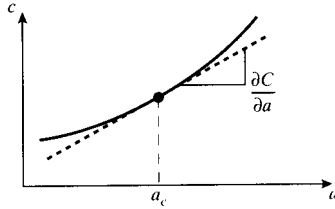


Figure 6.5: Compliance as a function of crack length.

The compliance of a suitable specimen, for instance a cantilevered beam, could be measured experimentally as a function of the length  $a$  of a crack that is grown into the specimen (see Fig. 6.5). The strain energy release rate can then be determined by differentiating the curve of compliance versus length:

$$\mathcal{G} = \frac{\partial U}{\partial a} = \frac{1}{2}P^2 \frac{\partial C}{\partial a} \quad (6.3)$$

The *critical* value of  $\mathcal{G}$ ,  $\mathcal{G}_c$ , is then found by measuring the critical load  $P_c$  needed to fracture a specimen containing a crack of length  $a_c$ , and using the slope of the compliance curve at this same value of  $a$ :

$$\mathcal{G}_c = \frac{1}{2}P_c^2 \frac{\partial C}{\partial a} \Big|_{a=a_c}$$

(6.4)

---

#### Example 6.3

For a double-cantilever beam (DCB) specimen such as that shown in Fig. 6.6, beam theory gives the deflection as

$$\frac{\delta}{2} = \frac{Pa^3}{3EI}$$

where  $I = bh^3/12$ . The elastic compliance is then

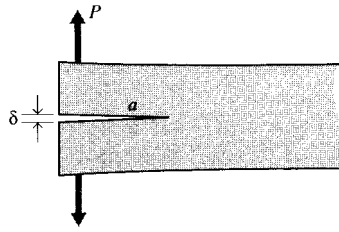


Figure 6.6: DCB fracture specimen.

$$C = \frac{\delta}{P} = \frac{2a^3}{3EI}$$

If the crack is observed to jump forward when  $P = P_c$ , Eqn. 6.4 can be used to compute the critical strain energy release rate as

$$\mathcal{G}_c = \frac{1}{2} P_c^2 \cdot \frac{2a^2}{EI} = \frac{12P_c^2 a^2}{b^2 h^3 E}$$


---

### 6.3 The Stress Intensity Approach

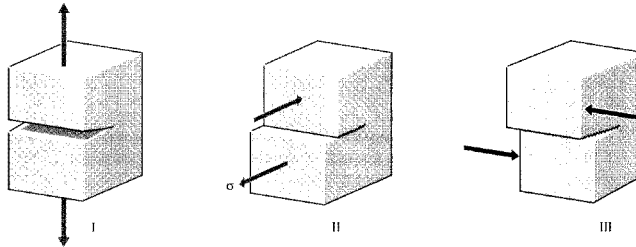


Figure 6.7: Fracture modes.

While the energy-balance approach provides a great deal of insight to the fracture process, an alternative method that examines the stress state near the tip of a sharp crack directly has proven more useful in engineering practice. The literature treats three types of cracks, termed mode I, II, and III as illustrated in Fig. 6.7. Mode I is a normal-opening mode and is the one we shall emphasize here, while modes II and III are shear sliding modes. The “semi-inverse” method developed by Westergaard<sup>8</sup> shows the opening-mode stresses to be:

$$\begin{aligned}\sigma_x &= \frac{K_I}{\sqrt{2\pi r}} \cos \frac{\theta}{2} \left( 1 - \sin \frac{\theta}{2} \sin \frac{3\theta}{2} \right) + \dots \\ \sigma_y &= \frac{K_I}{\sqrt{2\pi r}} \cos \frac{\theta}{2} \left( 1 + \sin \frac{\theta}{2} \sin \frac{3\theta}{2} \right) + \dots\end{aligned}\quad (6.5)$$

<sup>8</sup>Westergaard, H.M., “Bearing Pressures and Cracks,” *Transactions, Am. Soc. Mech. Engrs., Journal of Applied Mechanics*, Vol. 5, p. 49, 1939.

$$\tau_{xy} = \frac{K_I}{\sqrt{2\pi r}} \cos \frac{\theta}{2} \cos \frac{3\theta}{2} \sin \frac{\theta}{2} \dots$$

For distances close to the crack tip ( $r \leq 0.1a$ ), the second and higher order terms indicated by dots may be neglected. At large distances from the crack tip, these relations cease to apply and the stresses approach their far-field values that would obtain were the crack not present.

The  $K_I$  in Eqns. 6.5 is a very important parameter known as the *stress intensity factor*. The  $I$  subscript is used to denote the crack opening mode, but similar relations apply in modes II and III. The equations show three factors that taken together depict the stress state near the crack tip: the denominator factor  $(2\pi r)^{-1/2}$  shows the singular nature of the stress distribution;  $\sigma$  approaches infinity as the crack tip is approached, with a  $r^{-1/2}$  dependency. The angular dependence is separable as another factor; e.g.  $f_x = \cos \theta/2 \cdot (1 - \sin \theta/2 \sin 3\theta/2) + \dots$ . The factor  $K_I$  contains the dependence on applied stress  $\sigma_\infty$ , the crack length  $a$ , and the specimen geometry. The  $K_I$  factor gives the overall intensity of the stress distribution, hence its name.

For the specific case of a central crack of width  $2a$  or an edge crack of length  $2a$  in a large sheet,  $K_I = \sigma_\infty \sqrt{\pi a}$ , and  $K_I = 1.12 \sigma_\infty \sqrt{\pi a}$  for an edge crack of length  $a$  in the edge of a large sheet. (The factor  $\pi$  could obviously be canceled with the  $\pi$  in the denominator of Eqn. 6.5, but is commonly retained for consistency with earlier work.) Expressions for  $K_I$  for some additional geometries are given in Table 6.1. The literature contains expressions for  $K$  for a large number of crack and loading geometries, and both numerical and experimental procedures exist for determining the stress intensity factor for specific actual geometries.

Table 6.1: Stress intensity factors for several common geometries.

Type of Crack	Stress Intensity Factor, $K_I$
Center crack, length $2a$ , in an infinite plate	$\sigma_\infty \sqrt{\pi a}$
Edge crack, length $a$ , in a semi-infinite plate	$1.12 \sigma_\infty \sqrt{\pi a}$
Central penny-shaped crack, radius $a$ , in an infinite body	$2 \sigma_\infty \sqrt{\frac{a}{\pi}}$
Center crack, length $2a$ in plate of width $W$	$\sigma_\infty \sqrt{W \tan(\frac{\pi a}{W})}$
2 symmetrical edge cracks, each length $a$ , in plate of total width $W$	$\sigma_\infty \sqrt{W \left[ \tan\left(\frac{\pi a}{W}\right) + 0.1 \sin\left(\frac{2\pi a}{W}\right) \right]}$

These stress intensity factors are used in design and analysis by arguing that the material can withstand crack tip stresses up to a critical value of stress intensity, termed  $K_{Ic}$ , beyond which the crack propagates rapidly. This *critical stress intensity factor* is then a measure of material toughness. The failure stress  $\sigma_f$  is then related to the crack length  $a$  and the fracture toughness by

$$\boxed{\sigma_f = \frac{K_{Ic}}{\alpha \sqrt{\pi a}}} \quad (6.6)$$

where  $\alpha$  is a geometrical parameter equal to 1 for edge cracks and generally on the order of unity for other situations. Expressions for  $\alpha$  are tabulated for a wide variety of specimen and crack geometries, and specialty finite element methods are available to compute it for new situations.

The stress intensity and energy viewpoints are interrelated, as can be seen by comparing Eqns. 6.2 and 6.6 (with  $\alpha = 1$ ):

$$\sigma_f = \sqrt{\frac{EG_c}{\pi a}} = \frac{K_{Ic}}{\sqrt{\pi a}} \rightarrow K_{Ic}^2 = EG_c$$

This relation applies in plane stress; it is slightly different in plane strain:

$$K_{Ic}^2 = EG_c(1 - \nu^2)$$

For metals with  $\nu = .3$ ,  $(1 - \nu^2) = 0.91$ . This is not a big change; however, the numerical values of  $G_c$  or  $K_{Ic}$  are very different in plane stress or plane strain situations, as will be described below.

Typical values of  $G_{Ic}$  and  $K_{Ic}$  for various materials are listed in Table 6.2, and it is seen that they vary over a very wide range from material to material. Some polymers can be very tough, especially when rated on a per-pound bases, but steel alloys are hard to beat in terms of absolute resistance to crack propagation.

Table 6.2: Fracture toughness of materials.

Material	$G_{Ic}(\text{kJm}^{-2})$	$K_{Ic}(\text{MPam}^{1/2})$	$E(\text{GPa})$
Steel alloy	107	150	210
Aluminum alloy	20	37	69
Polyethylene	20 ( $J_{Ic}$ )	—	0.15
High-impact polystyrene	15.8 ( $J_{Ic}$ )	—	2.1
Steel — mild	12	50	210
Rubber	13	—	0.001
Glass-reinforced thermoset	7	7	7
Rubber-toughened epoxy	2	2.2	2.4
PMMA	0.5	1.1	2.5
Polystyrene	0.4	1.1	3
Wood	0.12	0.5	2.1
Glass	0.007	0.7	70

---

#### Example 6.4

Equation 6.6 provides a design relation among the applied stress  $\sigma$ , the material's toughness  $K_{Ic}$ , and the crack length  $a$ . Any one of these parameters can be calculated once the other two are known. To illustrate one application of the process, say we wish to determine the safe operating pressure in an aluminum pressure vessel 0.25 m in diameter and with a 5 mm wall thickness. First assuming failure by yield when the hoop

stress reaches the yield stress (330 MPa) and using a safety factor of 0.75, we can compute the maximum pressure as

$$p = \frac{0.75\sigma t}{r} = \frac{0.75 \times 330 \times 10^6}{0.25/2} = 9.9 \text{ MPa} = 1400 \text{ psi}$$

To insure against failure by rapid crack growth, we now calculate the maximum crack length permissible at the operating stress, using a toughness value of  $K_{Ic} = 41 \text{ MPa}\sqrt{\text{m}}$ :

$$a = \frac{K_{Ic}^2}{\pi\sigma^2} = \frac{(41 \times 10^6)^2}{\pi(0.75 \times 330 \times 10^6)^2} = 0.01 \text{ m} = 0.4 \text{ in}$$

Here an edge crack with  $\alpha = 1$  has been assumed. An inspection schedule must be implemented that is capable of detecting cracks before they reach this size.

---

### 6.3.1 Effect of specimen geometry

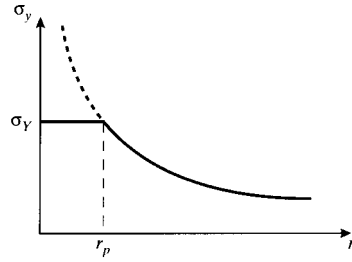


Figure 6.8: Stress limited by yield within zone  $r_p$ .

The toughness, or resistance to crack growth, of a material is governed by the energy absorbed as the crack moves forward. In an extremely brittle material such as window glass, this energy is primarily just that of rupturing the chemical bonds along the crack plane. But as already mentioned, in tougher materials bond rupture plays a relatively small role in resisting crack growth, with by far the largest part of the fracture energy being associated with plastic flow near the crack tip. A “plastic zone” is present near the crack tip within which the stresses as predicted by Eqn. 6.5 would be above the material’s yield stress  $\sigma_Y$ . Since the stress cannot rise above  $\sigma_Y$ , the stress in this zone is  $\sigma_Y$  rather than that given by Eqn. 6.5. To a first approximation, the distance  $r_p$  this zone extends along the  $x$ -axis can be found by using Eqn. 6.5 with  $\theta = 0$  to find the distance at which the crack tip stress reduces to  $\sigma_Y$ :

$$\begin{aligned} \sigma_y &= \sigma_Y = \frac{K_I}{\sqrt{2\pi r_p}} \\ r_p &= \frac{K_I^2}{2\pi\sigma_Y^2} \end{aligned} \tag{6.7}$$

This relation is illustrated in Fig. 6.8. As the stress intensity is increased either by raising the imposed stress or by crack lengthening, the plastic zone size will increase as well. But the extent of plastic flow is ultimately limited by the material’s molecular or microstructural mobility, and the zone can become only so large. When the zone can grow no larger, the crack can no longer be

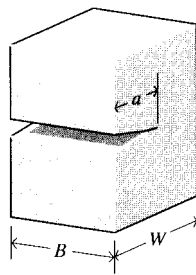


Figure 6.9: Dimensions of fracture toughness specimen.

constrained and unstable propagation ensues. The value of  $K_I$  at which this occurs can then be considered a materials property, named  $K_{Ic}$ .

In order for the measured value of  $K_{Ic}$  to be valid, the plastic zone size should not be so large as to interact with the specimen's free boundaries or to destroy the basic nature of the singular stress distribution. The ASTM specification for fracture toughness testing<sup>9</sup> specifies the specimen geometry to insure that the specimen is large compared to the crack length and the plastic zone size (see Fig. 6.9):

$$a, B, (W - a) \geq 2.5 \left( \frac{K_I}{\sigma_Y} \right)^2$$

A great deal of attention has been paid to the important case in which enough ductility exists to make it impossible to satisfy the above criteria. In these cases the stress intensity view must be abandoned and alternative techniques such as the J-integral or the crack tip opening displacement method used instead. The reader is referred to the references listed at the end of the chapter for discussion of these approaches.

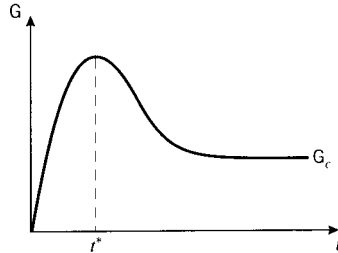


Figure 6.10: Effect of specimen thickness on toughness.

The fracture toughness as measured by  $K_c$  or  $G_c$  is essentially a measure of the extent of plastic deformation associated with crack extension. The quantity of plastic flow would be expected to scale linearly with the specimen thickness, since reducing the thickness by half would naturally cut the volume of plastically deformed material approximately in half as well. The toughness therefore rises linearly, at least initially, with the specimen thickness as seen in Fig. 6.10. Eventually, however, the toughness is observed to go through a maximum and fall thereafter to a lower value. This loss of toughness beyond a certain critical thickness  $t^*$  is extremely important in design against fracture,

---

<sup>9</sup>E 399-83, "Standard Test Method for Plane-Strain Fracture Toughness of Metallic Materials," ASTM, 1983.

since using too thin a specimen in measuring toughness will yield an unrealistically optimistic value for  $\mathcal{G}_C$ . The specimen size requirements for valid fracture toughness testing are such that the most conservative value is measured.

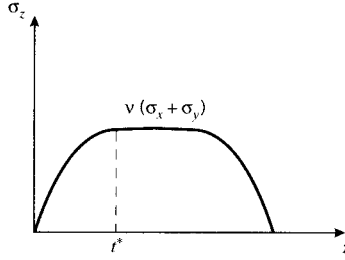


Figure 6.11: Transverse stress at crack tip.

The critical thickness is that which causes the specimen to be dominated by a state of *plane strain*, as opposed to *plane stress*. The stress in the through-thickness  $z$  direction must become zero at the sides of the specimen since no traction is applied there, and in a thin specimen the stress will not have room to rise to appreciable values within the material. The *strain* in the  $z$  direction is not zero, of course, and the specimen will experience a Poisson contraction given by  $\epsilon_z = \nu(\sigma_x + \sigma_y)$ . But when the specimen is thicker, material near the center will be unable to contract laterally due to the constraint of adjacent material. Now the  $z$ -direction strain is zero, so a tensile stress will arise as the material tries to contract but is prevented from doing so. The value of  $\sigma_z$  rises from zero at the outer surface and approaches a maximum value given by  $\sigma_z \approx \nu(\sigma_x + \sigma_y)$  in a distance  $t^*$  as seen in Fig. 6.11. To guarantee that plane strain conditions dominate, the specimen thickness  $t$  must be such that  $t \gg 2t^*$ .

The triaxial stress state set up near the center of a thick specimen near the crack tip *reduces* the maximum shear stress available to drive plastic flow, since the maximum shear stress is equal to one half the difference of the largest and smallest principal stress, and the smallest is now greater than zero. Or equivalently, we can state that the mobility of the material is constrained by the inability to contract laterally. From either a stress or a strain viewpoint, the extent of available plasticity is reduced by making the specimen thick.

### Example 6.5

The plastic zone sizes for the plane stress and plane strain cases can be visualized by using a suitable yield criterion along with the expressions for stress near the crack tip. The v. Mises yield criterion was given in terms of principal stresses in Chap. 5 as

$$2\sigma_Y^2 = (\sigma_1 - \sigma_2)^2 + (\sigma_1 - \sigma_3)^2 + (\sigma_2 - \sigma_3)^2$$

The principal stresses can be obtained from Eqns. 6.5 as

$$\begin{aligned}\sigma_1 &= \frac{K_I}{\sqrt{2\pi r}} \cos \frac{\theta}{2} \left( 1 + \sin \frac{\theta}{2} \right) \\ \sigma_2 &= \frac{K_I}{\sqrt{2\pi r}} \cos \frac{\theta}{2} \left( 1 - \sin \frac{\theta}{2} \right)\end{aligned}$$

The third principal stress is

$$\sigma_3 = \begin{cases} 0, & \text{plane stress} \\ \nu(\sigma_1 + \sigma_2), & \text{plane strain} \end{cases}$$

These stresses can be substituted into the yield criterion, which is then solved for the radius  $r$  at which yield occurs. It is convenient to normalize this radius by the radius of the plastic zone along the  $x$ -axis, given by Eqn. 6.7. Maple commands to carry out these substitutions and plot the result are:

```
# Radius of plastic zone along x-axis
> rp:=K[I]^2/(2*Pi*sigma[Y]^2):

# v. Mises yield criterion in terms of principal stresses
> v_mises:=2*sigma[Y]^2= (sigma[1]-sigma[2])^2 + (sigma[1]-sigma[3])^2
+ (sigma[2]-sigma[3])^2:

# Principal stresses in crack-tip region
> sigma[1]:=(K[I]/sqrt(2*Pi*r))*cos(theta/2)*(1+sin(theta/2)):
> sigma[2]:=(K[I]/sqrt(2*Pi*r))*cos(theta/2)*(1-sin(theta/2));

# Evaluate v. Mises for plane stress (v_strs) and plane strain (v_strn)
# Take nu = 0.3
> v_strs:=subs(sigma[3]=0,v_mises):
> v_strn:=subs(sigma[3]=.3*(sigma[1]+sigma[2]),v_mises):

# Solve for plastic zone radius, normalize by rp
# pl_strs for plane stress case, pl_strn for plane strain
> pl_strs:=solve(v_strs,r)/rp:
> pl_strn:=solve(v_strn,r)/rp:

# Plot normalized plastic zones for plane stress and plane strain
> plot({pl_strs,pl_strn},theta=0..2*Pi,coords=polar);
```

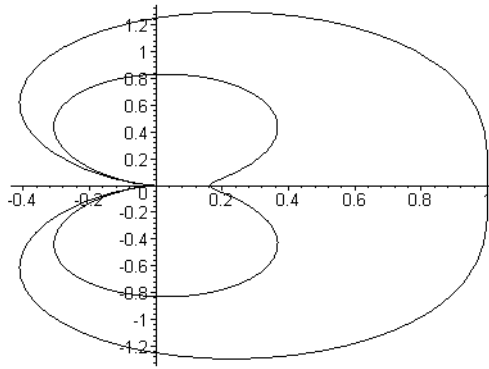


Figure 6.12: Normalized plastic zone shapes for plane strain (inner contour) and plane stress (outer contour).

---

Even in a thick specimen, the  $z$ -direction stress must approach zero at the side surfaces. Regions near the surface are therefore free of the triaxial stress constraint, and exhibit greater shear-driven plastic flow. After a cracked specimen has been tested to failure, a flat “thumbnail” pattern will often be visible as illustrated in Fig. 6.13. This is the region of slow crack growth, where the crack is able to maintain its preferred orientation transverse to the  $y$ -direction stress. The crack growth near the edges is retarded by the additional plastic flow there, so the crack line bows inward. When

the stress is increased enough to cause the crack to grow catastrophically, it typically does so at speeds high enough that the transverse orientation is not always maintained. The region of rapid fracture is thus faceted and rough, leading some backyard mechanics to claim the material failed because it “crystallized.”

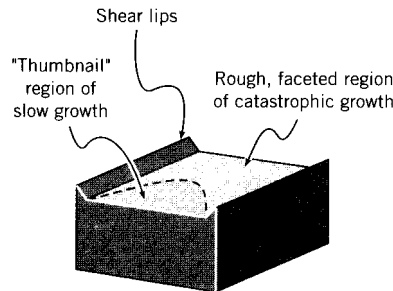


Figure 6.13: Fracture surface topography.

Along the edges of the specimen, “shear lips” can often be found on which the crack has developed by shear flow and with intensive plastic deformation. The lips will be near a  $45^\circ$  angle, the orientation of the maximum shear planes.

### 6.3.2 Grain size and temperature

Steel is such an important and widely used structural material that it is easy to forget that steel is a fairly recent technological innovation. Well into the nineteenth century, wood was the dominant material for many bridges, buildings, and ships. As the use of iron and steel became more widespread in the latter part of that century and the first part of the present one, a number of disasters took place that can be traced to the then-incomplete state of understanding of these materials, especially concerning their tendency to become brittle at low temperatures. Many of these failures have been described and analyzed in a fascinating book by Parker<sup>10</sup>.

One of these brittle failures is perhaps the most famous disaster of the last several centuries, the sinking of the transatlantic ocean liner *Titanic* on April 15, 1912, with a loss of some 1,500 people and only 705 survivors. Until very recently, the tragedy was thought to be caused by a long gash torn through the ship’s hull by an iceberg. However, when the wreckage of the ship was finally discovered in 1985 using undersea robots, no evidence of such a gash was found. Further, the robots were later able to return samples of the ship’s steel whose analysis has given rise to an alternative explanation.

It is now well known that lesser grades of steel, especially those having large concentrations of impurities such as interstitial carbon inclusions, are subject to embrittlement at low temperatures. William Garzke, a naval architect with the New York firm of Gibbs & Cox, and his colleagues have argued that the steel in the *Titanic* was indeed brittle in the  $31^\circ\text{F}$  waters of the Atlantic that night, and that the 22-knot collision with the iceberg generated not a gash but extensive cracking through which water could enter the hull. Had the steel remained tough at this temperature, these authors feel, the cracking may have been much less extensive. This would have slowed the flooding and allowed more time for rescue vessels to reach the scene, which could have increased greatly the number of survivors.

---

<sup>10</sup>E.R. Parker, *Brittle Behavior of Engineering Structures*, John Wiley & Sons, 1957.

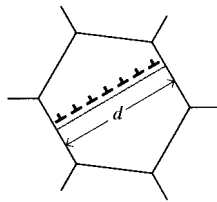


Figure 6.14: Dislocation pileup within a grain.

In the bcc transition metals such as iron and carbon steel, brittle failure can be initiated by dislocation glide within a crystalline grain. The slip takes place at the yield stress  $\sigma_Y$ , which varies with grain size according to the Hall-Petch law as described in Chap. 5:

$$\sigma_Y = \sigma_0 + k_Y d^{-1/2}$$

Dislocations are not able to propagate beyond the boundaries of the grain, since adjoining grains will not in general have their slip planes suitably oriented. The dislocations then “pile up” against the grain boundaries as illustrated in Fig. 6.14. The dislocation pileup acts similarly to an internal crack with a length that scales with the grain size  $d$ , intensifying the stress in the surrounding grains. Replacing  $a$  by  $d$  in the modified Griffith equation (Eqn. 6.2), the applied stress needed to cause fracture in adjacent grains is related to the grain size as

$$\sigma_f = k_f d^{-1/2}, \quad k_f \propto \sqrt{\frac{E\mathcal{G}_c}{\pi}}$$

The above two relations for yielding and fracture are plotted in Fig. 6.15 against inverse root grain size (so grain size increases to the left), with the slopes being  $k_Y$  and  $k_f$  respectively. When  $k_f > k_Y$ , fracture will not occur until  $\sigma = \sigma_Y$  for values of  $d$  to the left of point A, since yielding and slip is a prerequisite for cleavage. In this region the yielding and fracture stresses are the same, and the failure appears brittle since large-scale yielding will not have a chance to occur. To the right of point A, yielding takes place prior to fracture and the material appears ductile. The point A therefore defines a critical grain size  $d^*$  at which a “nil-ductility” transition from ductile (grains smaller than  $d^*$ ) to brittle failure will take place.

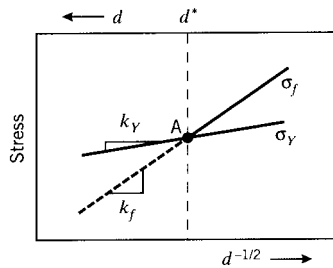


Figure 6.15: Effect of grain size on yield and fracture stress.

As the temperature is lowered, the yield stress  $\sigma_Y$  will increase as described in Chap. 5, and the fracture stress  $\sigma_f$  will decrease (since atomic mobility and thus  $\mathcal{G}_C$  decrease). Therefore, point A

shifts to the right as temperature is lowered. The critical grain size for nil ductility now occurs at a smaller value; i.e. the grains must be smaller to avoid embrittling the material. Equivalently, refining the grain size has the effect of lowering the ductile-brittle transition temperature. Hence grain-size refinement raises both the yield and fracture stress, lowers the ductile-brittle transition temperature, and promotes toughness as well. This is a singularly useful strengthening mechanism, since other techniques such as strain hardening and solid-solution hardening tend to achieve strengthening at the expense of toughness.

Factors other than temperature can also embrittle steel. Inclusions such as carbon and phosphorus act to immobilize slip systems that might otherwise relieve the stresses associated with dislocation pileups, and these inclusions can raise the yield stress and thus the ductile-brittle transition temperature markedly. Similar effects can be induced by damage from high-energy radiation, so embrittlement of nuclear reactor components is of great concern. Embrittlement is also facilitated by the presence of notches, since they generate triaxial stresses that constrain plastic flow. High strain rates promote brittleness because the flow stress needed to accommodate the strain rate is higher, and improper welding can lead to brittleness both by altering the steel's microstructure and by generating residual internal stresses.

## 6.4 Fatigue

The concept of "fatigue" arose several times in this chapter, as in the growth of cracks in the Comet aircraft that led to disaster when they became large enough to propagate catastrophically as predicted by the Griffith criterion. Fatigue, as understood by materials technologists, is a process in which damage accumulates due to the repetitive application of loads that may be well below the yield point. The process is dangerous because a single application of the load would not produce any ill effects, and a conventional stress analysis might lead to a assumption of safety that does not exist.

In one popular view of fatigue in metals, the fatigue process is thought to begin at an internal or surface flaw where the stresses are concentrated, and consists initially of shear flow along slip planes. Over a number of cycles, this slip generates intrusions and extrusions that begin to resemble a crack. A true crack running inward from an intrusion region may propagate initially along one of the original slip planes, but eventually turns to propagate transversely to the principal normal stress as seen in Fig. 6.16.

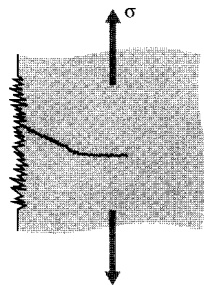


Figure 6.16: Intrusion-extrusion model of fatigue crack initiation.

When the failure surface of a fatigued specimen is examined, a region of slow crack growth is usually evident in the form of a "clamshell" concentric around the location of the initial flaw. (See Fig. 6.17.) The clamshell region often contains concentric "beach marks" at which the crack was

arrested for some number of cycles before resuming its growth. Eventually, the crack may become large enough to satisfy the energy or stress intensity criteria for rapid propagation, following the previous expressions for fracture mechanics. This final phase produces the rough surface typical of fast fracture. In postmortem examination of failed parts, it is often possible to correlate the beach marks with specific instances of overstress, and to estimate the applied stress at failure from the size of the crack just before rapid propagation and the fracture toughness of the material.



Figure 6.17: Typical fatigue-failure surfaces. From B. Chalmers, *Physical Metallurgy*, Wiley, p. 212, 1959.

The modern study of fatigue is generally dated from the work of A. Wöhler, a technologist in the German railroad system in the mid-nineteenth century. Wöhler was concerned by the failure of axles after various times in service, at loads considerably less than expected. A railcar axle is essentially a round beam in four-point bending, which produces a compressive stress along the top surface and a tensile stress along the bottom (see Fig. 6.18). After the axle has rotated a half turn, the bottom becomes the top and vice versa, so the stresses on a particular region of material at the surface varies sinusoidally from tension to compression and back again. This is now known as *fully reversed* fatigue loading.

#### 6.4.1 S-N curves

Well before a microstructural understanding of fatigue processes was developed, engineers had developed empirical means of quantifying the fatigue process and designing against it. Perhaps the most important concept is the *S-N diagram*, such as those shown in Fig. 6.19<sup>11</sup>, in which a constant cyclic stress amplitude  $S$  is applied to a specimen and the number of loading cycles  $N$  until the specimen fails is determined. Millions of cycles might be required to cause failure at lower loading levels, so the abscissa is usually plotted logarithmically.

In some materials, notably ferrous alloys, the  $S - N$  curve flattens out eventually, so that below a certain *endurance limit*  $\sigma_e$  failure does not occur no matter how long the loads are cycled. Obviously, the designer will size the structure to keep the stresses below  $\sigma_e$  by a suitable safety factor if cyclic loads are to be withstood. For some other materials such as aluminum, no endurance

---

<sup>11</sup>H.W. Hayden, W.G. Moffatt, and J. Wulff, *The Structure and Properties of Materials*, Vol. III, John Wiley & Sons, 1965.

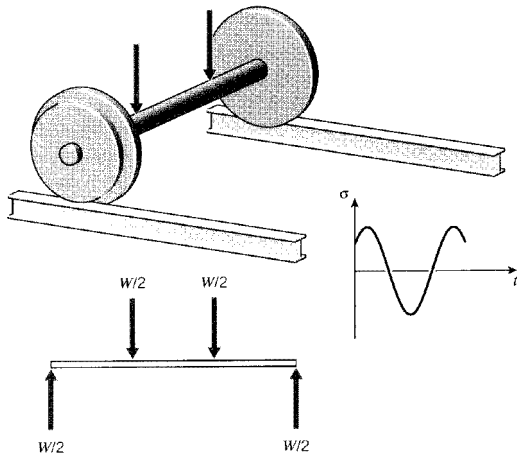


Figure 6.18: Fatigue in a railcar axle.

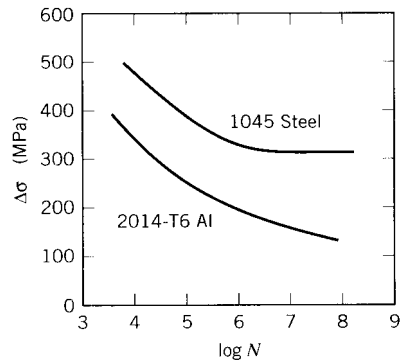


Figure 6.19:  $S - N$  curves for aluminum and low-carbon steel.

limit exists and the designer must arrange for the planned lifetime of the structure to be less than the failure point on the  $S - N$  curve.

Statistical variability is troublesome in fatigue testing; it is necessary to measure the lifetimes of perhaps twenty specimens at each of ten or so load levels to define the  $S - N$  curve with statistical confidence<sup>12</sup>. It is generally impossible to cycle the specimen at more than approximately 10Hz (inertia in components of the testing machine and heating of the specimen often become problematic at higher speeds) and at that speed it takes 11.6 days to reach  $10^7$  cycles of loading. Obtaining a full  $S - N$  curve is obviously a tedious and expensive procedure.

At first glance, the scatter in measured lifetimes seems enormous, especially given the logarithmic scale of the abscissa. If the coefficient of variability in conventional tensile testing is usually only a few percent, why do the fatigue lifetimes vary over orders of magnitude? It must be remembered that in tensile testing, we are measuring the variability in stress at a given number of *cycles* (one), while in fatigue we are measuring the variability in cycles at a given *stress*. Stated differently, in tensile testing we are generating vertical scatter bars, but in fatigue they are horizontal (see Fig. 6.20). Note that we must expect more variability in the lifetimes as the  $S - N$  curve becomes

<sup>12</sup>A Guide for Fatigue Testing and the Statistical Analysis of Fatigue Data, ASTM STP-91-A, 1963.

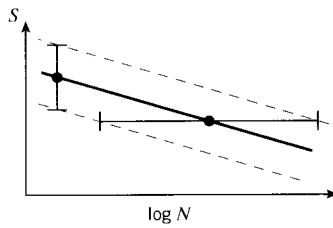


Figure 6.20: Variability in fatigue lifetimes and fracture strengths.

flatter, so that materials that are less prone to fatigue damage require more specimens to provide a given confidence limit on lifetime.

#### 6.4.2 Effect of mean load

Of course, not all actual loading applications involve fully reversed stress cycling. A more general sort of fatigue testing adds a *mean stress*  $\sigma_m$  on which a sinusoidal cycle is superimposed, as shown in Fig. 6.21. Such a cycle can be phrased in several ways, a common one being to state the alternating stress  $\sigma_{alt}$  and the *stress ratio*  $R = \sigma_{min}/\sigma_{max}$ . For fully reversed loading,  $R = -1$ . A stress cycle of  $R = 0.1$  is often used in aircraft component testing, and corresponds to a tension-tension cycle in which  $\sigma_{min} = 0.1\sigma_{max}$ .

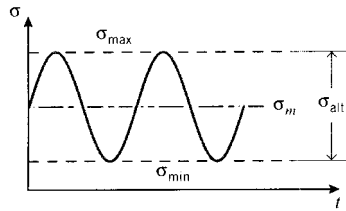


Figure 6.21: Simultaneous mean and cyclic loading.

A very substantial amount of testing is required to obtain an  $S - N$  curve for the simple case of fully reversed loading, and it will usually be impractical to determine whole families of curves for every combination of mean and alternating stress. There are a number of strategems for finesseing this difficulty, one common one being the *Goodman diagram*, shown in Fig. 6.22. Here a graph is constructed with mean stress as the abscissa and alternating stress as the ordinate, and a straight “lifeline” is drawn from  $\sigma_e$  on the  $\sigma_{alt}$  axis to the ultimate tensile stress  $\sigma_f$  on the  $\sigma_m$  axis. Then for any given mean stress, the endurance limit — the value of alternating stress at which fatigue fracture never occurs — can be read directly as the ordinate of the lifeline at that value of  $\sigma_m$ . Alternatively, if the design application dictates a given ratio of  $\sigma_m$  to  $\sigma_{alt}$ , a line is drawn from the origin with a slope equal to that ratio. Its intersection with the lifeline then gives the effective endurance limit for that combination of  $\sigma_f$  and  $\sigma_m$ .

#### 6.4.3 Miner's law for cumulative damage

When the cyclic load level varies during the fatigue process, a *cumulative damage* model is often hypothesized. To illustrate, take the lifetime to be  $N_1$  cycles at a stress level  $\sigma_1$  and  $N_2$  at  $\sigma_2$ . If

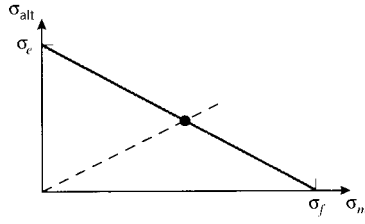


Figure 6.22: The Goodman diagram.

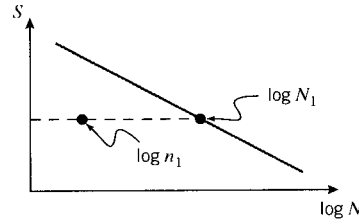


Figure 6.23: The concept of fractional lifetime.

damage is assumed to accumulate at a constant rate during fatigue and a number of cycles  $n_1$  is applied at stress  $\sigma_1$ , where  $n_1 < N_1$  as shown in Fig. 6.23, then the fraction of lifetime consumed will be  $n_1/N_1$ . To determine how many additional cycles the specimen will survive at stress  $\sigma_2$ , an additional fraction of life will be available such that the sum of the two fractions equals one:

$$\frac{n_1}{N_1} + \frac{n_2}{N_2} = 1$$

Note that absolute cycles and not log cycles are used here. Solving for the remaining cycles permissible at  $\sigma_2$ :

$$n_2 = N_2 \left( 1 - \frac{n_1}{N_1} \right)$$

The generalization of this approach is called *Miner's Law*, and can be written

$$\sum \frac{n_j}{N_j} = 1$$

(6.8)

where  $n_j$  is the number of cycles applied at a load corresponding to a lifetime of  $N_j$ .

### Example 6.6

Consider a hypothetical material in which the  $S$ - $N$  curve is linear from a value equal to the fracture stress  $\sigma_f$  at one cycle ( $\log N = 0$ ), falling to a value of  $\sigma_f/2$  at  $\log N = 7$  as shown in Fig. 6.24. This behavior can be described by the relation

$$\log N = 14 \left( 1 - \frac{S}{\sigma_f} \right)$$

The material has been subjected to  $n_1 = 10^5$  load cycles at a level  $S = 0.6\sigma_f$ , and we wish to estimate how many cycles  $n_2$  the material can now withstand if we raise the load to  $S = 0.7\sigma_f$ . From the  $S$ - $N$

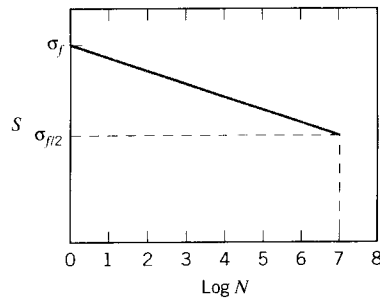


Figure 6.24: Linear  $S$ - $N$  curve.

relationship, we know the lifetime at  $S = 0.6\sigma_f = \text{constant}$  would be  $N_1 = 3.98 \times 10^5$  and the lifetime at  $S = 0.7\sigma_f = \text{constant}$  would be  $N_2 = 1.58 \times 10^4$ . Now applying Eqn. 6.8:

$$\frac{n_1}{N_1} + \frac{n_2}{N_2} = \frac{1 \times 10^5}{3.98 \times 10^5} + \frac{n_2}{1.58 \times 10^4} = 1$$

$$n_2 = 1.18 \times 10^4$$

Miner's "law" should be viewed like many other material "laws," a useful approximation, quite easy to apply, that *might* be accurate enough to use in design. But damage accumulation in fatigue is usually a complicated mixture of several different mechanisms, and the assumption of linear damage accumulation inherent in Miner's law should be viewed skeptically. If portions of the material's microstructure become unable to bear load as fatigue progresses, the stress must be carried by the surviving microstructural elements. The rate of damage accumulation in these elements then increases, so that the material suffers damage much more rapidly in the last portions of its fatigue lifetime. If on the other hand cyclic loads induce strengthening mechanisms such as molecular orientation or crack blunting, the rate of damage accumulation could drop during some part of the material's lifetime. Miner's law ignores such effects, and often fails to capture the essential physics of the fatigue process.

#### 6.4.4 Crack growth rates

Certainly in aircraft, but also in other structures as well, it is vital that engineers be able to predict the rate of crack growth during load cycling, so that the part in question be replaced or repaired before the crack reaches a critical length. A great deal of experimental evidence supports the view that the crack growth rate can be correlated with the cyclic variation in the stress intensity factor:

$$\boxed{\frac{da}{dN} = A \Delta K^m} \quad (6.9)$$

where  $da/dN$  is the fatigue crack growth rate per cycle,  $\Delta K = K_{max} - K_{min}$  is the stress intensity factor range during the cycle, and  $A$  and  $m$  are parameters that depend the material, environment, frequency, temperature and stress ratio. This is sometimes known as the "Paris law," and leads to plots similar to that shown in Fig. 6.25.

The exponent  $m$  is often near 4 for metallic systems, which might be rationalized as the damage accumulation being related to the volume  $V_p$  of the plastic zone: since the volume  $V_p$  of the zone

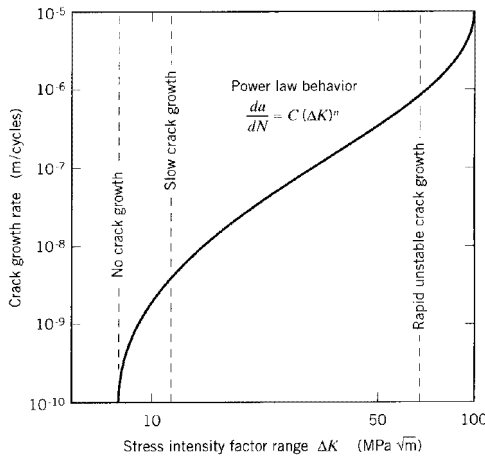


Figure 6.25: The Paris law for fatigue crack growth rates.

scales with  $r_p^2$  and  $r_p \propto K_I^2$ , then  $da/dn \propto \Delta K^4$ . Some specific values of the constants  $m$  and  $A$  for various alloys are given in Table 6.3.

Table 6.3: Numerical parameters in the Paris equation.

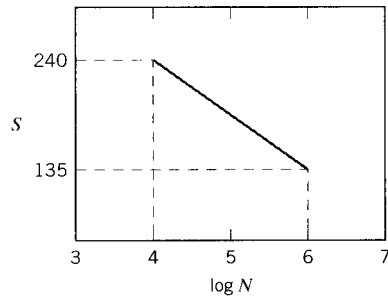
alloy	$m$	$A$
Steel	3	$10^{-11}$
Aluminum	3	$10^{-12}$
Nickel	3.3	$4 \times 10^{-12}$
Titanium	5	$10^{-11}$

## References

1. Anderson, T.L., *Fracture Mechanics: Fundamentals and Applications*, CRC Press, Boca Raton, 1991.
2. Gordon, J.E., *The New Science of Strong Materials, or Why You Don't Fall Through the Floor*, Princeton University Press, 1976.
3. Hertzberg, R.W., *Deformation and Fracture Mechanics of Engineering Materials*, Wiley, New York, 1976.
4. Knott, J.F., *Fundamentals of Fracture Mechanics*, John Wiley – Halsted Press, New York, 1973.
5. Strawley, J.E., and W.F. Brown, *Fracture Toughness Testing, ASTM STP 381*, 133, 1965.

## 6.5 Problems

- Using data from Fig. 6.1, determine numerical values for the parameters  $t_0$ ,  $E^*$  and  $V^*$  for PMMA in Eqn. 6.1 and comment on their atomistic significance.
  - Using a development analogous to that employed in Chap. 5 for the theoretical yield stress, show that the theoretical ultimate tensile strength is  $\sigma_{th} \approx E/10$  (much larger than that observed experimentally). Assume a harmonic atomic force function  $\sigma = \sigma_{th} \sin(2\pi x/\lambda)$ , where  $x$  is the displacement of an atom from its equilibrium position and  $\lambda \approx a_0$  is the interatomic spacing. The maximum stress  $\sigma_{th}$  can then be found by using
- $$E = \left( \frac{d\sigma}{d\epsilon} \right)_{x \rightarrow 0} \quad \text{and} \quad \epsilon = \frac{x}{a_0}$$
- A pressure vessel is constructed with a diameter of  $d = 18''$  and a length of  $L = 6'$ . The vessel is to be capable of withstanding an internal pressure of  $p = 1000$  psi, and the wall thickness is such as to keep the nominal hoop stress under 2500 psi. However, the vessel bursts at an internal pressure of only 500 psi, and a micrographic investigation reveals the fracture to have been initiated by an internal crack 0.1" in length. Calculate the fracture toughness ( $K_{Ic}$ ) of the material.
  - A steel alloy has an S-N curve that falls linearly from 240 kpsi at  $10^4$  cycles to 135 kpsi at  $10^6$  cycles. A specimen is loaded at 160 kpsi alternating stress for  $10^5$  cycles, after which the alternating stress is raised to 180 kpsi. How many additional cycles at this higher stress would the specimen be expected to survive?



Prob. 4

- Integrate the crack growth law (Eqn. 6.9) from an initial crack of dimension  $a_0$  to the critical crack size  $a_f$  (Eqn. 6.6) to give the number of cycles to failure  $N_f$  under an alternating stress  $\Delta\sigma$  as

$$N_f = \frac{2m}{2-m} \left( a_f^{1-\frac{m}{2}} - a_0^{1-\frac{m}{2}} \right) \cdot \frac{1}{A \cdot \Delta\sigma^m \pi^m / 2}$$